USING LIGHT EMITTING DIODES FOR INACTIVATING FOODBORNE PATHOGENIC BACTERIA IN FOOD PROCESSING ENVIRONMENTS

A Thesis

Presented to the Faculty of the Graduate School

Of Cornell University

In Partial Fulfillment of the Requirements for the Degree of

Master of Science in Food Science & Technology

by

Hanyu Chen

December 2019

ABSTRACT

Nonthermal treatments are increasingly used in food processing due to their potential of microbial inactivation with minimal physicochemical and sensorial quality damage to the food products. Recent advances in Light Emitting Diodes (LED) technology have shown great potential in food preservation, due the lower energy consumption and higher flexibility in design than traditional mercury or gas discharge lamps. This study investigates the use of LED technology in both Ultraviolet (UV) and visible range for inactivation of foodborne bacteria, under lower temperature conditions.

One strategy of inactivating bacteria in foods and food processing environment is by using germicidal short-wave UV-C light (200 to 280 nm), which is typically emitted by mercury or amalgam lamps. UV-C LEDs were recently developed as a chemical-free, energy-efficient alternative to deliver germicidal UV and mitigate microbial contamination on material surfaces, but their effectiveness has not been fully explored. One of the objectives of this work was to gain a better understanding of the antimicrobial effectiveness of UV-C LEDs. Specifically, the inactivation kinetics of *Escherichia coli* ATCC 25922 and *Listeria innocua* FSL C2-0008 was studied by exposing them to a custom-made UV-C LED array (λ max =280 nm) under a variety of substrate conditions commonly encountered in food processing and handling environment. UV-C resulted in over 5-log reduction of both bacterial strains after 600 s in thin liquid films (thickness $\leq$ 0.6mm), and on all stainless steel (SS) surfaces. The fastest initial inactivation was achieved on dry SS surfaces for both bacteria, but maximum inactivation was similar for the dry and wet conditions. The results of this work can help end users design effective and efficient UV-C LED disinfection strategies for various surface conditions.

Another approach for eliminating undesirable bacteria in food processing environments is by using antimicrobial blue light in the wavelength spectrum of 400-470 nm. Previous work suggested that 405 nm light has maximum antimicrobial effects in this range, but the effectiveness of the treatment has not been fully explored. In this work, the efficacy of 405 nm LED against *Escherichia coli* O157:H7*, Listeria monocytogenes, Pseudomonas aeruginosa, Salmonella* Typhimurium*,* and *Staphylococcus aureus*, and the

effect of substrate on inactivation kinetics were investigated. Additionally, the influence of nanoscale surface topography on the inactivation behavior of pathogenic *E. coli*, *L. monocytogenes,* and *S. aureus* was evaluated. Exposure to 405nm LED resulted in over 5-log reduction for *P. aeruginosa* and *S. aureus* in liquid films after 48 h. Maximum inactivation was observed for *E. coli* on stainless steel (SS) surfaces; the highest rate of inactivation was observed on small nanopore anodic aluminum oxide (AAO) for *L. monocytogenes* and *S. aureus*, with over 5-log reduction achieved after 12 h, suggesting potential inactivation enhancing properties of nanoscale topography. The results suggest that 405 nm LEDs have great potential for antimicrobial treatments in the food industry, but disinfection success depends on bacterial species, substrate, and environmental conditions. Additionally, surfaces with nanoscale topography may offer additional inactivation enhancing properties.

Overall, these approaches can have positive impacts on food safety and quality. This study demonstrates that LED technology can play an important role in combating foodborne bacteria in food processing and handling environments, clinical environments, as well as other areas relevant to human health.

BIOGRAPHICAL SKETCH

Hanyu Chen was born and raised in Anhui, China. She is the only child of Guofeng Jin and Jiaxuan Chen. Hanyu attended Hefei No.1 High School at the age of 15, where she developed a strong interest in math and chemistry. Having lived all her growing years in the East, Hanyu thought it would be a good idea to experience Western culture. Thus, she decided to pursue her undergraduate education at Rensselaer Polytechnic Institute (RPI), where she discovered the beautiful fall colors of upstate New York. Under the unique mentorship of Dr. Sufei Shi and Dr. Joel Plawsky, Hanyu started exploring the world of scientific research, and learned many things proved to be useful during her M.S. She was also an active member of Alpha Phi Omega Service Fraternity. Hanyu earned a Bachelor of Science degree in Chemical Engineering from RPI in 2018.

Upon graduation from RPI, Hanyu began wondering what the next step for her is. Combining her interest in engineering and snacking, food science seemed like the perfect choice. Hanyu began her journey as a M.S. student in food science with Dr. Carmen Moraru on a sunny, beautiful Ithaca day (very deceiving) in August 2018. Hanyu's understanding of food deepened with the help of her research projects. Over the course of one year and a half, the graduate program in food science offered her invaluable opportunities for academic, professional, and personal growth for which she will always be grateful.

After the conclusion of her M.S., Hanyu will be continuing her research in food engineering and safety as a PhD student in the Moraru lab.

This work is dedicated to my family, for their love, patience,

and support through every season of my life.

ACKNOWLEDGEMENTS

First and foremost, I would like to acknowledge my advisor and committee chair, Dr. Carmen Moraru, for believing in my potential, taking me into her lab, and trusting me with the tasks of a M.S. student. She is the kindest and most supportive supervisor a student can ask for, and she has fostered an environment where all of us in her lab truly feel like family. I could not have asked for a better lab group to be a part of. Thank you for your generous guidance and encouragement, and for inspiring me to become a better person every day. And her black forest cake is the best (sorry Joseph). I would also like to thank my minor advisor Dr. Andrew Novaković from Applied Economics and Management for his intellectual input and contribution over time.

I am grateful for the research funds provided by the USDA-NIFA. I am also grateful for the help I received at the Cornell Center for Materials Research (CCMR) and the Cornell Graduate School. In addition, I would like to thank all the amazing staff at the Department of Food Science, namely Erin Atkins, Janette Robins, and Karen Barry, for always being there to support students with basically anything and everything.

I would like to thank all of the Moraru lab members past and present: Yifan Cheng, Shaun Sim, Pedro Menchik, Linran Wang, Kyle Kriner, Joyce Cao, Daniela Buosi, Allie Hall, Huijuan Zheng, and Andreea Beldie. Special thanks to Yifan Cheng for his endless patience for all the questions I had and being such a great mentor. Finally, thank you to all the lab members who assisted me in research, either as undergraduate students, summer scholars, or research associates.

Finally, I am grateful for the support of all my friends and family. Special thanks to Fred for always being there for me. All these individuals have my most sincere thanks, for without their assistance, guidance, and support, this dissertation would not have been possible.

Table of Contents

LIST OF FIGURES

LIST OF TABLES

CHAPTER 1

Light emitting diode (LED) technology in processing and preservation of foods: a review

1.1 Abstract

As negative consumer reaction grew in recent years against the addition of chemical preservatives to foods, and concerns grew regarding the development of resistance to disinfectants used in processing environments, nonthermal processing technologies are increasingly adopted by industry to meet the needs of ensuring food safety while maintaining the nutritional and sensory value of foods. In this context, utilization of non-ionizing light-based electromagnetic irradiation methods have shown great potential for disinfection, and their potential has also been boosted by recent advances in the science and engineering of light emitting diode (LED) technologies. Currently, LED sources include ultraviolet light LED (UV-LED) and visible LED systems. This chapter will give an overall introduction to the current LED technology, and the different LED light-based irradiation treatments used in food processing. Topics covered include the mechanism of microbial inactivation for each treatment, factors affecting their efficacy, as well as advantages and limitations associated with each treatment. Examples of food applications of each treatment will be given, including discussions on microbial inactivation and the effects on food components.

1.2 Introduction: general aspects of LED technology

The sterilizing capabilities of ultraviolet (UV) radiation are well known and investigated; more recently, visible light has been shown to have bactericidal effects under certain conditions, hence suggesting potential for food safety applications. Traditionally, mercury and amalgam lamps and high-intensity discharge (HID) light sources, such as xenon lamps, are used as light sources for these applications (D'Souza, Yuk, Khoo, & Zhou, 2015). However, such light sources are characterized by excessive heating, broad spectral power distribution, with limited control over the emission of irradiation. Moreover, traditional UV lamps contain mercury, and therefore need to be handled carefully to prevent damage and leakage of this toxic heavy metal (Giuseppina, et al., 2019).

In recent years, significant developments have occurred in the area of light emitting diodes (LED), which can avoid some of the drawbacks of the light sources mentioned above. A LED is a semiconductor light source that emits light when current flows through it. Electrons in the semiconductor recombine with electron holes, releasing energy in the form of photons (Branas, Azcondo, & Alonso, 2013). The color of the light emitted, corresponding to the energy of the photons, is determined by the energy required for electrons to cross the band gap of the semiconductor. By selecting different semiconductor materials, single-color LEDs can emit light within a very narrow wavelength spectrum, from near-infrared through the visible spectrum and into the ultraviolet range (Held, 2009). This is an advantage over other traditional light sources as they are not able to produce monochromatic wavelength. Other advantages of LEDs include high photoelectric efficiency and photon flux or irradiance, low thermal output, temporal setting of the light produced and high durability (Gupta & Jatothu, 2013) (Richardson, 2008). The compact size of LEDs allows flexible designs and easy implementation into existing systems, without requiring special disposal methods at the end of their usage.

The development of LEDs began when the British radio engineer Henry Josef Round of Marconi Labs accidentally observed that a light was being emitted from a man-made SiC crystal when a current flowed through the material (Gupta & Jatothu, 2013). This was the very first demonstration of a solid-state light source. Current LED technology uses solid-state semiconductor diodes to produce light through electroluminescence. The semiconductor comprises a p-side and an n-side, with an interface termed the p-n junction. Current only flows from the p-side (anode) to the n-side (cathode), resulting in electrons and holes flowing toward the junction when a voltage is applied (Branas, Azcondo, & Alonso, 2013). Electron luminescence occurs when an electron-hole interaction causes an electron to fall to a lower energy level, thereby releasing a photon and resulting the emission of light of a distinct wavelength (Branas, Azcondo, & Alonso, 2013). The color of the emitted light depends on the band gap energy of the semiconductor material. Gallium arsenide is used for red and IR light; indium gallium aluminum phosphide for green, yellow, orange, and red lights; gallium nitride and silicon carbide for blue lights. UV-LEDs are typically

composed of aluminum gallium nitride or indium gallium nitride, with a wavelength as low as 210 nm (D'Souza, Yuk, Khoo, & Zhou, 2015).

The key structure of an LED setup consists of the light-emitting semiconductor material, a lead frame with both cathode and anode onto where the die is in place. An epoxy encapsulation covers and protects the die (Fig 1.1) (Gupta & Jatothu, 2013). The design of LED circuits can be quite flexible to allow both parallel and in series positions. Several LEDs can be connected at the same time in series, lit with the same current (D'Souza, Yuk, Khoo, & Zhou, 2015). In a situation of LEDs with different voltage requirements, only the lowest voltage LED will emit light, hence LEDs used in series must have the same forward voltage or at least not differ greatly (D'Souza, Yuk, Khoo, & Zhou, 2015). When the LEDs are mounted in parallel, it is important to place one resister per LED chip to prevent high current damage (Richardson, 2008).

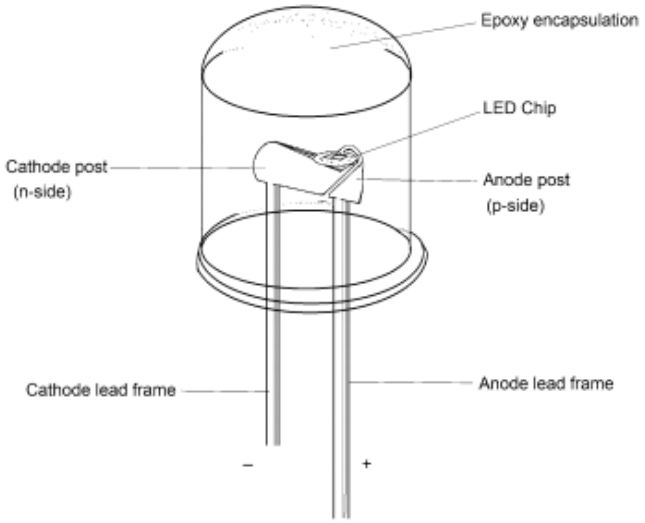

Figure 1.1. Basic structure of an LED *(Gupta & Jatothu, 2013)*

In May 2018, the Lighting Research Center at Rensselaer Polytechnic Institute (RPI) published a report on the testing performance with various lighting fixtures. The current luminous efficacy and the photon efficacy of LED luminaries surpassed fluorescent and HID luminaries (Radetsky, 2018). Another means of evaluating LED performance is through measuring electrical efficiency, which represents the percentage of

output power in the light form per unit of input electrical power. Currently, blue LEDs have reached electrical efficiencies of above 60%, while the electrical efficiency of UV-LEDs is still limited, at an estimated average of 10% (Radetsky, 2018). The overall efficacy of LEDs has steadily improved over recent years, and the trend is expected to continue with the help of novel semiconductor materials, new configurations, and better manufacturing processes (Radetsky, 2018).

The properties of LED that are useful in food processing environments include nontoxicity, the ability to control the light wavelength, light quality, the amount of heat generated, as well as the ease of installation to give a better control over the emitted light. Moreover, recent modifications of the microstructured surfaces of semiconductor materials are proven to increase the light extraction efficiency (LEE) of LEDs from 50% to 90%, expanding the advantage of UV-LEDs compared to traditional UV sources (Chen, et al., 2019).

1.3 UV-LEDs

1.3.1 Microbial Inactivation by UV-LEDs

UV light refers to a part of electromagnetic spectrum that has wavelengths ranging from 200 nm to 400 nm. There are three regions of UV light depending on the wavelength: long wave UV-A, from 320 to 400 nm; medium wave UV-B, from 280 to 320 nm, and short-wave UV-C, from 200 to 280 nm. Short wavelength UV-C light is responsible for most of the germicidal effects of UV, with maximum microbial inactivation effectiveness peak around 240-260 nm, corresponding to the maximum DNA absorption (Kim, Kim, & Kang, 2017). UV-LEDs of various wavelengths can be manufactured using different semiconductor materials. The most frequently used materials are III-nitride, including gallium nitride (GaN), aluminum gallium nitride (AlGaN), and aluminum nitride (AIN) (Khan, 2005). AIN UV-LEDs are reported to emit the shortest wavelength at 210 nm, while AlGaN UV-LEDs are able emit light with wavelength ranging from 210 to 365 nm. The wavelength of GaN-based UV-LEDs is around 365 nm (Khan, 2005).

The critical factor affecting the efficiency of UV-LED treatments is their light transmittance through the treated products, which limits the treatment efficiency in opaque fluids. The efficacy of UV-LED inactivation also depends largely on the effective exposure of the treated microorganisms to UV photons. Therefore, commercial UV chambers are designed to have thin streams of fluid with turbulence to ensure the even exposure of the treated products to UV light.

Mechanisms of microbial inactivation by UV has been intensely studied. The DNA damage from the UV photons is recognized as the main lethal effect on microorganisms. When the microorganism's DNA is exposed to UV light, the absorbed photons lead to the formation of covalent linkages between adjacent bases on a single DNA strand in the vicinity of their carbon-carbon double bonds, thus producing cyclobutane pyrimidine dimers (CPDs) and 6-4 photoproducts (6-4PPs). These premutagenic lesions can alter the DNA double-helix structure in that region and prevent the normal base-pairings (Gayán, Condón, & Álvarez, 2014). These CPDs and 6-4PPs can inhibit DNA polymerase, which has a significant role in terminating the synthesis of new DNA, and thus can inhibit the growth of microorganisms. The proportion of 6-4PPs is much smaller compared to CPDs, comprising about 25% of the total UV-induced DNA damage. UV can also generate reactive oxygen species, which also react with DNA and proteins (Li & Farid, 2016). Although UV light has little effect on spores, it can sensitize spores and improve lethal effects of subsequent thermal treatments (Li & Farid, 2016).

Many factors can affect the UV-C treatment efficiency, some of which are microorganism related (gram-positive vs gram-negative, DNA repair ability, and the physiological state of microorganisms), while others depend on the substrate (i.e. presence of turbulence in liquid substrates, presence of light absorbers or particle size in the medium).

As shown in Figure 1.2, the shape of microbial inactivation curves by UV treatments is sigmoidal. The initial plateau is due to sublethal injury of the UV treated microorganisms. After a critical level of injury has been surpassed, minimal additional UV exposure is lethal for microorganisms, and the number of

survivors declines rapidly. The rapid inactivation phase is followed by a tail phase, which is due to UV resistance of microorganisms and the presence of suspended particles that might block the UV light. Gram-positive bacteria tend to have higher resistance in response of UV treatments, which caused a more visible sigmoidal shape in inactivation curves than the Gram-negative ones (Kim, Kim, & Kang, 2017). The non-linear Weibull model is commonly used for describing the nonlinear inactivation curves for single bacteria populations, since it can incorporate the shoulder and the tailing effects, along with the linear range (SUDHIR K. SASTRY, 2000). Many prior studies have focused on the UV inactivation of microorganisms in water, while much less literature exists on UV inactivation in various food products (Bintsis, Litopoulou-Tzanetaki, & Robinson, 2000) (Li G. W., 2017). Due to the complexities inherent to food products, UV inactivation kinetics for different products should be explored individually to design effective applications.

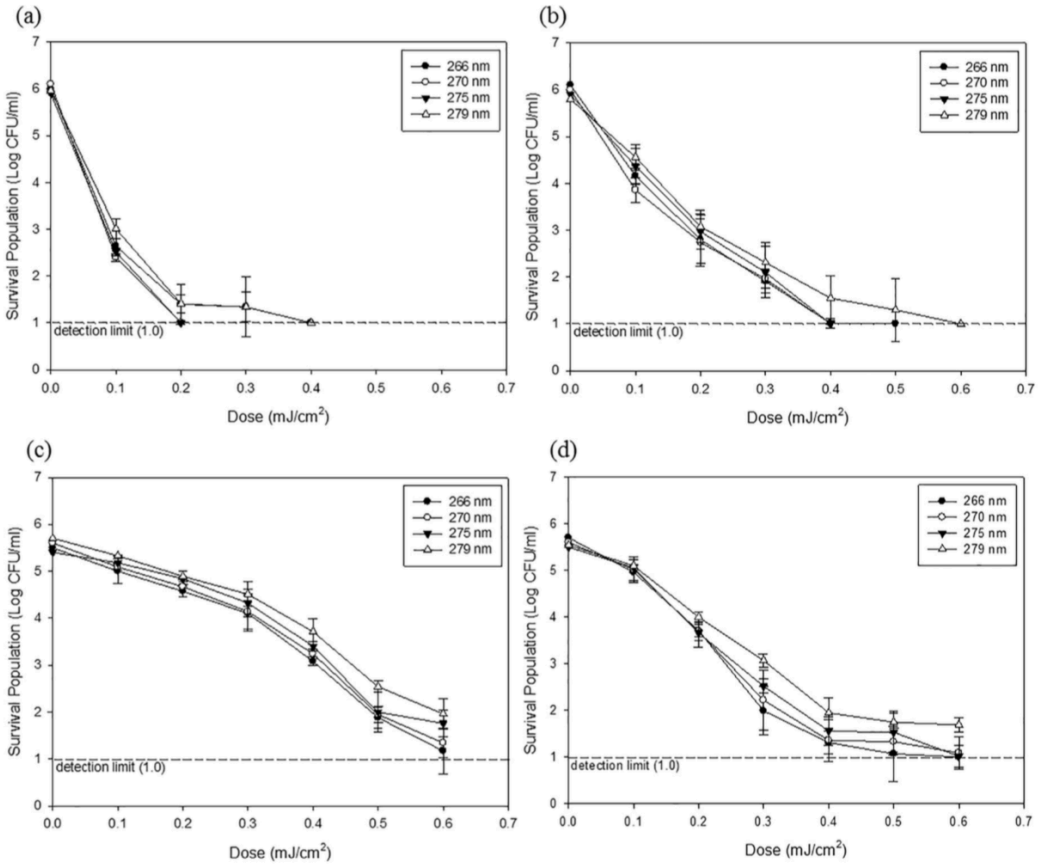

Figure 1.2. UV reduction (Log CFU/mL) of selective Gram-negative bacteria: (a) *E. coli* O157:H7, (b)*Salmonella* spp., and selective Gram-positive bacteria: (c) *L. monocytogenes*, (d) *S. aureus* after UVC-LED irradiation *(Kim, Kim, & Kang, 2017)*.

Compared to the traditional mercury UV lamps, UV-C LEDs can achieve much higher levels of microbial inactivation. According to Kim et al., 266 nm UV-C LEDs demonstrated over 5-log reduction in *E. coli* O157:H7 and *S*. Typhimurium, while 1–2-log reductions were achieved using UV lamp intensity attenuated to the levels of UV-C LEDs (Kim, Kim, & Kang, 2015). Another advantage of UV-C LEDs is the flexibility in configuring to specific wavelengths rather than having a peak wavelength of 254 nm like in the case of Low Pressure (LP) mercury lamps. A previous study has shown that inactivation efficiencies by UV-C LEDs with wavelengths ranging from 254 nm to 280 nm were not significantly different (Kim, Kim, & Kang, 2017). It was shown by Kim et al. that the DNA damage caused by 280 nm UV-C LEDs were 5-8 times greater compared to those of 260 nm in major food pathogens (*E. coli* O157:H7, *Salmonella* spp., *L.*

monocytogenes, *Staphylococcus aureus*) and spoilage yeasts (*Saccharomyces pastorianus*, *Pichia membranaefaciens*) (Kim, Kim, & Kang, 2017). It is also well established that 280 nm is the peak absorbance wavelength for aromatic amino acids such as Tryptophan and Tyrosine (Pace, 1995), which allows UV-C light with 280 nm peak wavelength to be absorbed by proteins, increase the protein vulnerability, and eventually induce a higher level of deterioration of membrane proteins in response to the light treatment. It was also shown that protein damage induced by UV exposure plays an important role in virus inactivation (Eischeid & Linden, 2011).

1.3.2 DNA repair mechanisms

One of the key factors affecting the microbial survivability post UV treatment is the cell's ability to repair the DNA damage. The main DNA UV damage repair pathways are: (1) nucleotide excision repair; (2) photoreactivation. The nucleotide excision repair (NER) mechanism can repair the damaged DNA by resynthesizing the damaged nucleotides (Gayán, Condón, & Álvarez, 2014). In eukaryotes, NER is carried out by at least 18 protein complexes via four steps: detection of damage; excision of the section of DNA that includes the damaged sequence; filling out the gap by DNA polymerase; and sealing of the nick between the newly synthesized and the older DNA fragments. In bacteria, the process of NER is completed by only 3 proteins: UvrA, UvrB, and UvrC (Clancy, 2014). NER is considered an error-free mechanism and can remove a broad spectrum of DNA lesions through multiple cascade reactions carried out by UvrABC excinuclease. NER carried out by UvrABC is often referred as "dark repair", because UV-irradiated cells are able to repair their DNA damage without the presence of light (Gayán, Condón, & Álvarez, 2014).

The photoreactivation repair mechanism is often referred as "light repair" because it is dependent on the presence of blue or near UV light energy. This reactivation mechanism is followed if UV treated products are exposed to light post treatment. In photoreactivation, CPD lyase, also known as photolyase, binds the pyrimidine dimer lesions; in addition, a second molecule, called chromophore, converts light energy into

the chemical energy required to directly revert the affected area of DNA to its undamaged form. Energy from visible light (350-500 nm) is needed to activate the CPD lyase. These CPD lyases are found in numerous organisms, including fungi, plants, invertebrates such as fruit flies, and vertebrates such as frogs (Clancy, 2014). Another DNA lyase in some bacteria species that is involved in some reverse damage repair mechanisms is the spore photoproduct (SP) lyase, which is the main enzyme of SP repair in spores and does not require visible light to activate. SP can also be removed by excision repair mechanisms (Gayán, Condón, & Álvarez, 2014).

Hu and Quek found that the photolyase activity decreased by 20% by exposure to a dose of 2 mJ/cm^2 of medium pressure (MP) UV wavelengths between 220-300 nm, but was unaffected by LP UV exposure (Hu & Quek, 2008). Figure 1.3 shows that 280 nm UV-C LEDs had a repression effect on DNA repair of *E. coli* after UV treatments. This is likely because photolyase of *E. coli* also has an absorption peak around 280 nm, like most proteins (Pace, 1995). Hence, it is worth investigating whether UV-C LEDs of 280 nm could repress DNA repair in other microorganisms. However, results from different studies often demonstrate that the extent of photoreactivation may vary significantly with the lighting conditions (wavelength, intensity), temperature, substrate, and potential genetic diversity. The lack of standardized procedure for quantifying photoreactivation makes it rather difficult to make comparisons between studies. More microorganisms and wavelengths should be tested to obtain a comprehensive understanding of post UV treatment repair mechanisms.

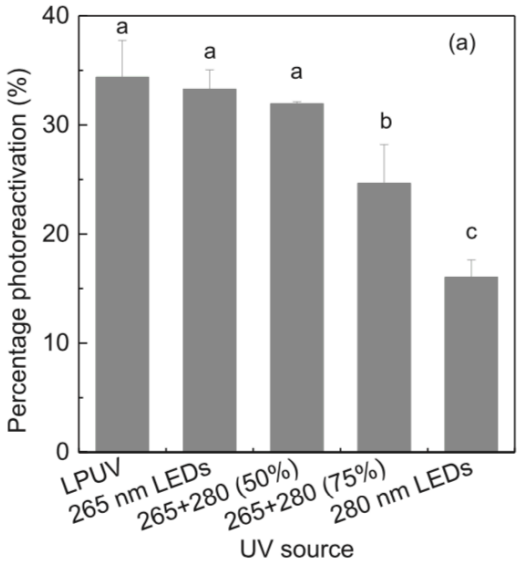

Figure 1.3. Percentage photoreactivation of *E. coli* after 3.0 log reduction was achieved in UV inactivation from different UV sources. *(Li G. W., 2017)*.

1.3.3 Effects of UV-LED on food components

The exposure of food products to UV-LED light can initiate free radical oxidation and catalyze other stages of oxidation processes. The superoxide radicals (SOR) produced can further induce carbohydrate cross-linkage, protein fragmentation, peroxidation of unsaturated fatty acids, and the loss of membrane fluidity function. Denaturation of proteins and enzymes in milk may occur after UV irradiation, thereby also bringing potential textural changes (Choudhary & Bandla, 2012). It has also been reported that under high dose of UV light exposure, there are changes in the chemical composition of food components and obvious deteriorations in product quality (Choudhary & Bandla, 2012) (Bintsis, Litopoulou-Tzanetaki, & Robinson, 2000).

On the other hand, it has been shown that UV-C LED treatments can enhance the anthocyanin level and the antioxidant capacity in strawberries in the postharvest period (D'Souza, Yuk, Khoo, & Zhou, 2015). Other studies have shown that exposure to UV-LED can increase the vitamin D2 content in edible mushrooms,

and increase the phenolic stilbenes in grapes, which led to the development of “functional table grapes” in early 2000s (Nigro & Ippolito, 2016).

Controlled exposure to UV light of tomatoes (pre-harvest) showed increases in phenolic acids content, particularly caffeic acid and p-coumaric acid (Figure 1.4) (D. L. Luthria, 2006).

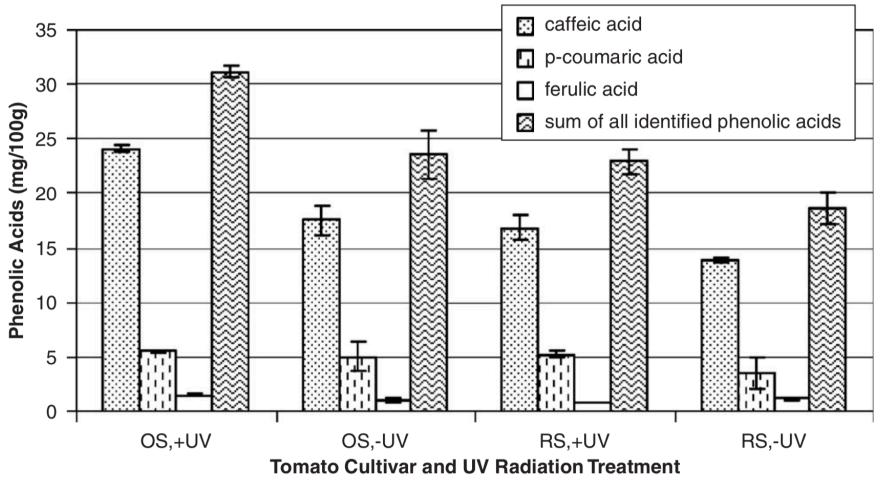

Figure 1.4. Phenolic acid content in ‘‘Oregon Spring’’ (OS) and ‘‘Red Sun’’ (RS) tomato fruits. Fruits collected from plants grown under ambient solar radiation in high tunnels covered with a UV-transmitting (+UV) or a UV-blocking (-UV) material. *(D. L. Luthria, 2006)*

The increase in antioxidant concentration in fresh produce is possibly due to the increased level of photosynthesis and self-protecting mechanism in plants in response to the generation of reactive oxygen species (ROS) induced by the exposure of UV-LED light (Lobo, 2010). The types of bioactive compounds activated by the UV exposure depend on the species, as well as the radiation dose and intensity. The increase of health-promoting compounds induced by UV treatments is also plant-, organ-, tissue- and age-specific, and varies depending on the season for postharvest fruits and vegetables (Venditti & D'hallewin, 2014). Therefore, it is necessary to optimize the UV treatment process parameters so that the treated products are maintained safe and nutritious for human consumption.

In general, UV treatment of food products has not been found to have any adverse effects, especially if the exposure is moderate and short-term. Moreover, UV treatments using LED technology may allow better optimization of the treatments so that antimicrobial effects are maximized, while the negative effects on product quality are minimized.

1.3.4 Current applications of UV LED and main limitations

Current applications of UV-LED treatments in the food industry predominantly focus on their germicidal effects and fall into two general categories: (a) inactivation of microorganisms on surfaces; (b) antimicrobial treatment of liquid products.

The first category of application of UV include decontamination of food packaging materials such as bottle caps, wrappings, and containers by arranging several lamps above the conveyors in packaging lines. Studies have shown that UV-C treatment of fruit yogurt packaging extended the shelf life for about 2 weeks at 5-7 °C (D'Souza, Yuk, Khoo, & Zhou, 2015). Short-wave UV-LEDs have also been employed in the treatment of food product surfaces, although, due to the limited penetration depth of UV light, uneven surface of some food products can protect bacteria from being inactivated effectively. UV-LEDs have been used to control food spoilage microorganisms such as *Bacillus stearothermophilus* in thin layers of sugar or *Pseudomonas* spp. on the surface of meat and vegetables (Choudhary & Bandla, 2012). However, due to generation of ozone and absorption by nitrogen oxides, in combination with the photochemical effects on the lipid fraction, meat that has been exposed directly to UV light can develop off-flavors, and a similar problem has been encountered with milk (Choudhary & Bandla, 2012). A combination of UV-C irradiation and heat treatments has been suggested for producing high-quality meat product while mitigating the side-effects of each individual treatment (Bintsis, Litopoulou-Tzanetaki, & Robinson, 2000). Synergistic effect of combining different wavelengths of UV light in one treatment is also worthy of investigation since difference in DNA repair was observed after exposure to different UV wavelengths (Figure 3).

UV-LED treatments were also used to prolong the shelf life of liquid products. However, studies have shown that the effect of treatments strongly depend on the amount of light absorbed by the treated liquid (Bintsis, Litopoulou-Tzanetaki, & Robinson, 2000). One of the simplest and most widely used UV treatments of liquids is the treatment of water. In fruit and vegetable juice applications, the effectiveness of UV-LED might be hindered for several reasons: blockage of light and limited penetration in colored products due to absorption, scattering of light and bacteria shielding effects due to the suspended particles in turbid liquid foods and beverages. Another limitation is the potential sensorial change in the products after exposure to continuous UV. Due to these limitations of UV-C, this treatment is often combined with other processing techniques (i.e. hurdle technologies) to achieve maximal benefits in microbial reduction and retention of product quality (Abdul Karim Shah, Shamsudin, Abdul Rahman, & Adzahan, 2016).

1.4 Blue LEDs

1.4.1 Mechanism of Microbial Inactivation by blue LEDs

Blue LED, combined with red and green LED, can produce tunable colored light, and is currently used as a replacement of incandescent light source for its energy efficiency. Blue LEDs are also widely used in digital displays on electronics such as smartphones, televisions, and laptops.

Recently, LED technology in the visible light spectrum is gaining significance for food treatment despite its relatively low microbial inactivation efficacy compared to UV-LEDs. UV treatments have limitations in use due to their harmful effects on humans as well as the potential detrimental side-effect on the quality of treated food. Visible light can also induce cell damage, injury, and death in microorganisms through photodynamic inactivation (PDI). Blue light, particularly in the wavelength range between 405nm and 470 nm, has higher inactivation effect on microorganisms compared to other regions of visible light (Ghate, et al., 2013). Blue LEDs are also much less detrimental to mammalian cells compared to UV irradiation.

Different from UV irradiation, inactivation of microorganisms by blue LED illumination is attributed to the production of reactive oxygen species (ROS) by intracellular photosensitizer excitation. Blue light excites endogenous intracellular porphyrins, and this photon absorption leads to energy transfer and ultimately the production of highly cytotoxic ROS, particularly singlet oxygen ($^1O_2$); ROS may attack cellular components such as DNA, lipids, and proteins, ultimately leading to bacterial death (Dai, et al., 2012). ROS might preferentially oxidize DNA rather than lipids in cell membrane and cause damage to DNA by targeting guanine bases, forming 8-hydroxy-deoxyguanosine (8-OHdG), an oxidized derivative. Transmission microscopy (TM) imaging revealed apparent steps of blue LED inactivation of *P. aeruginosa* cells (Figure 1.5). These TEM images show that damage to *P. aeruginosa* cells begins with development of vacuoles within the cell cytoplasm (Figure 1.5B), followed by the release of cytoplasm materials into surrounding environment (Figure 1.5C), and eventually a significant disruption of the cytoplasm (Figure 1.5D). The cytoplasm damage suggests that blue LED excites the intracellular chromophores, particularly uroporphyrin III and coproporphyrin III in *P. aeruginosa*, in the inactivation mechanisms (Dai, et al., 2012).

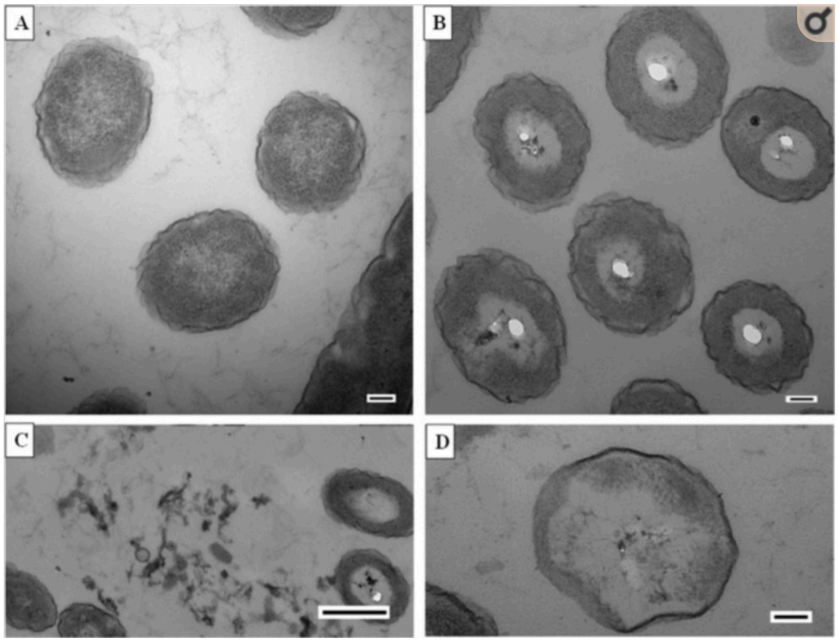

Figure 1.5. Transmission electron microscopy of *P. aeruginosa* cells. (A) Untreated *P. aeruginosa* cells. Bar = 100 nm. (B to D) *P. aeruginosa* cells after being exposed to 109.9 J/cm^2 blue light: development of

vacuoles within the cytoplasm (B) (bar = 100 nm), release of cytoplasmic material to the surrounding environment (C) (bar = 500 nm), and disappearance of cytoplasm (D) (bar = 100 nm) *(Dai T, 2013)*.

It has been found that blue light can mediate a broad-spectrum antimicrobial effect for both Gram-negative and Gram-positive bacteria, with a general trend showing Gram-positive species to be more susceptible than Gram-negative bacteria. Treatment of Gram-positive *L. monocytogenes* reached 5-$\log_{10}$ reduction at light dosage of 108 J/cm^2, while the Gram-negative *E. coli* reached similar reduction at a significantly higher light dosage of 288 J/cm^2 (Figure 1.6). The intra-species variation in susceptibility is likely due to the inherent differences in endogenous porphyrin concentrations within species (Amin, Bhayana, Hamblin, & Dai, 2016).

As seen in Figure 1.6, a sigmoidal shape was observed from inactivation curves of *S. enterica* and *M. terrae*, but not obvious in the other species treated. However, data on microbial inactivation kinetics for blue light LED treatments are scarce, and more studies in this area need to be conducted.

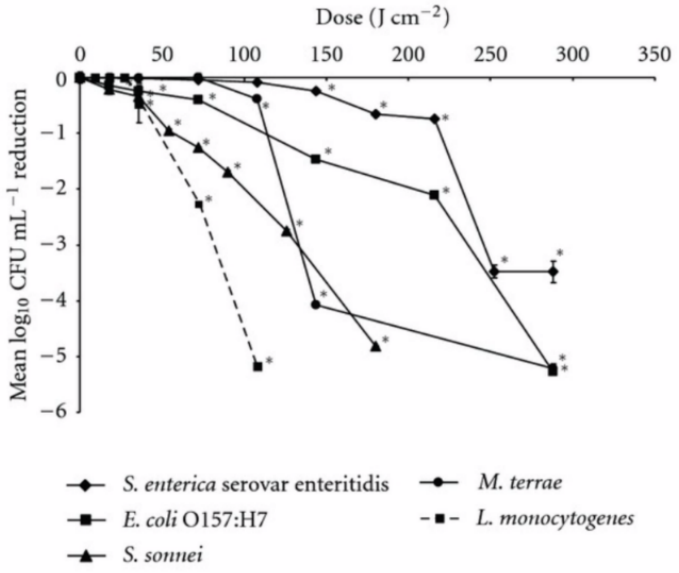

Figure 1. 6. Inactivation of *S. sonnei*, *E. coli*, *S. enterica*, *L. monocytogenes*, and *M. terrae* in liquid suspension, by exposure to high-intensity 405 nm light of an irradiance of approximately 10 mW/cm^2 *(Murdoch LE, 2012)*

The wavelength range of 402-420 nm has been reported as the most effective range of the spectrum, while 455-470 nm have also been found to have antimicrobial potential for some bacterial species (*e.g., S. aureus*) (Bhavya & Hebbar, 2018). The antimicrobial efficacy of blue light varies significantly between studies. This might due to the different experimental conditions, including light source (wavelength spectrum, laser or LED, *etc*.), bacteria species and strain, culture conditions, temperature, and light exposure. It is important to note that much longer exposure time (7 to 48 h) is required to achieve similar inactivation of foodborne pathogens by blue LEDs compared to Pulsed Light (PL) and continuous UV treatments (Bhavya & Hebbar, 2018).

Blue light can be sensed by numerous bacteria and can induce physiological responses elicited by the blue light receptors. As a result of this, blue light can regulate bacterial motility, suppress biofilm formation, and inactivate bacteria (Dai, et al., 2012). On the other hand, the presence of blue light may also activate or increase bacterial virulence (Dai, et al., 2012). A large number of publications on the antimicrobial effect of blue light focus on clinical treatments for wounds or dental complications (Guffey, 2006) (Enwemeka, 2009), while the studies on food applications are rather limited. Therefore, further studies are needed to answer the following questions: to what extent does blue light affect biofilm formation and dispersal, whether or not microbes will develop resistance to antimicrobial blue light, through what mechanism blue light can activate virulence factors and modulate pathogenesis, *etc.*

1.4.2 Effects of blue LED treatments *in vivo*

When applied *in vivo*, LED light can stimulate the production of various nutrients, antioxidants, and secondary metabolites in plants, which function to provide defense against ROS produced during photosynthesis and light stress. Thus, blue light has potential for enhancing the nutritional quality of plant crops. Studies have shown that various blue and red LED light treatments result in the accumulation of bioactive compounds and antioxidants in crops such as various lettuces, pea seedlings, Chinese cabbage, and other plants (D'Souza, Yuk, Khoo, & Zhou, 2015). The use of blue LED light in the production of

broccoli microgreens resulted in greater accumulation of K, P, Ca, Mg, and Fe in leaf tissues as compared to plants grown without blue LED exposure, which was related to the increased transpirational fluxes and stomatal conductance under blue LED (Giuseppina, et al., 2019). The nutritional quality of other plant parts such as fruits can also be enhanced. The skin of grape berries that was irradiated by blue LED additional to the exposure of daylight had shown greater content of anthocyanins and sugars (Kondo, et al., 2014). Moreover, because the minimal radiant heat emitted, blue LEDs cause little increase in the temperature on the surface or interior of the treated foods, which is beneficial in preserving the sensory and general acceptability of LED treated foods to consumers.

The exact biological mechanisms of how these nutritional compounds are enhanced through exposure to blue LED are not fully understood yet. More recent research appears to be moving towards tracking the changes in nutrition with gene expression when tuning the spectral compositions of LED light for food crops. This could allow food producers and manufacturers to manipulate the lighting regimens in order to increase the nutritional quality of their products in the future (D'Souza, Yuk, Khoo, & Zhou, 2015).

1.4.3 Current applications of blue LED in food processing and main limitations

In areas related to food production, the most popular current application of antimicrobial blue LED is water disinfection. The rise of blue LEDs in disinfecting drinking water came from their energy saving properties, which makes them more cost efficient compared to mercury lamps. Decontamination of fluids such as milk and orange juices at refrigerated temperature by blue LED has also been explored. After about 14 h of irradiation at 92 mW/cm^2, more than 3-log_{10} CFU reduction in bacteria was observed in orange juice at a temperature of 4 °C, suggesting potential for the implementations of blue LED light during refrigerated storage (Wang, et al., 2017).

While LEDs are already more energy efficient than mercury or gas discharge lamps, there is significant ongoing work aiming to further increase their energy efficiency. For example, a recent study showed that

the light extraction efficiency of LEDs can be improved significantly by incorporating asymmetric microstructured surfaces to increase the light interaction surface area and improve randomization of light effects (Chen, et al., 2019). With further progress in LED technology, there may be potential to utilize antimicrobial blue LEDs in developing countries where the safe and hygienic storage and distribution of foods are critical issues. It is encouraging also that LEDs can harness energy from the sun to provide supplementary light for crop growth, so photovoltaic-powered LEDs can also be applicable in postharvest preservation of foods and in sanitary maintenance of food wastage (Wang, et al., 2017).

Overall, blue LEDs have much potential to become useful in food industry in the future.

1.5 Conclusions

The research data available in the scientific literature and discussed in this chapter clearly demonstrates the potential of LED technology for use in food processing. Besides having longer life expectancy than conventional UV sources, LEDs are of comparable, or of higher photon efficiency to conventional lighting systems, and are more durable. Their monochromatic nature allows for the exclusion of undesired wavelengths, preventing degradation of food quality. A notable benefit of adopting LED technology in food processing is its lack of toxic metals, which reduces the need for special disposal. Hence, LEDs can be economically and environmentally beneficial. UV-LEDs have shown great potential for sterilization on liquid food and food contacting surfaces; blue LED provides promising lightning approach for food preservation and storage. The low penetration depth of light still limits the use of such treatments to smooth surfaces or liquids with low optical density, like in traditional light-based treatments. One interesting prospect is the use of these light treatments as terminal, post-process treatment for surface decontamination of various products, such as fresh fruit, vegetables, and ready to eat meats or cheeses.

With the development of more energy efficient LEDs, this non-conventional technology could have a substantial market value in the future. Although nonthermal light treatments using LED technology is

attracting attention from scientists and the food industry, much work still needs to be done in this area, both in terms of inactivation potential, as well as their effect on the nutritional and sensory properties of foods.

1.6 References

Abdul Karim Shah, N., Shamsudin, R., Abdul Rahman, R., & Adzahan, N. (2016). Fruit Juice Production Using Ultraviolet Pasteurization: A Review. *Beverages*, 3-22.

Akgün, M. P., & Ünlütürk, S. (2017). Effects of ultraviolet light emitting diodes (LEDs) on microbial and enzyme inactivation of apple juice. *Int. J. Food Microbiol.* , 65-74.

Amin, R., Bhayana, B., Hamblin, M., & Dai, T. (2016). Antimicrobial blue light inactivation of Pseudomonas aeruginosa by photo-excitation of endogenous porphyrins: In vitro and in vivo studies. *Lasers in Surgery and Medicine*, 562-568.

Bánáti, D. (2014). European perspectives of food safety. *Journal of the Science of Food and Agriculture*, 1941-1946.

Barnes, L.-M., Lo, M., Adams, M., & Chamberlain, A. (1999). Effect of milk proteins on adhesion of bacteria to stainless steel surfaces. *Applied and Environmental Microbiology*, 4543-4548.

Bhavya, M., & Hebbar, U. (2018). Efficacy of blue LED in microbial inactivation: Effect of photosensitization and process parameters. *International Journal of Food Microbiology*, 296-304.

Bintsis, T., Litopoulou-Tzanetaki, E., & Robinson, R. (2000). Existing and potential applications of ultraviolet light in the food industry - a critical review. . *Journal of the Science of Food and Agriculture*, 637-645.

Bjerkan, G., Witso, E., & Bergh, K. (2009). Sonication is superior to scraping for retrieval of bacteria in biofilm on titanium and steel surfaces in vitro. *Acta Orthop.*, 245-250.

Bower, C., McGuire, J., & Daeschel, M. (1996). The adhesion and detachment of bacteria and spores on food-contact surfaces. *Trends in Food Science & Technology*, 152-157.

Branas, C., Azcondo, F., & Alonso, J. (2013). Solid-state lighting: a system. *Industrial Electronics Magazine*, 6-14.

Chatterley, C., & Linden, K. (2010). Demonstration and evaluation of germicidal UV-LEDs for point-of-use water disinfection. . *J. Water Health* , 479–486 .

Chen, C.-J., Yao, J., Zhu, W., Chao, J.-H., Shang, A., Lee, Y.-G., & Yin, S. (2019). Ultrahigh light extraction efficiency light emitting diodes by harnessing asymmetric obtuse angle microstructured surfaces. *Optik*, 400-407.

Chen, C.-J., Yao, J., Zhu, W., Chao, J.-H., Shang, A., Lee, Y.-G., & Yin, S. (2019). Ultrahigh light extraction efficiency light emitting diodes by harnessing asymmetric obtuse angle microstructured surfaces. *Optik*, 400-407.

Cheng, Y., & Moraru, C. I. (2018). Long-range interactions keep bacterial cells from liquid-solid interfaces: Evidence of a bacteria exclusion zone near Nafion surfaces and possible implications for bacterial attachment. . *Colloids Surfaces B Biointerfaces* , 16-24.

Chmielewski, R. a., & Frank, J. F. (2003). Biofilm Formation and Control in Food Processing Facilities. . *Compr. Rev. Food Sci. Food Saf.*, 22-32.

Choudhary, R., & Bandla, S. (2012). Ultraviolet Pasteurization for Food Industry. *International Journal of Food Science and Nutrition Engineering*, 12-15.

Clancy, S. (2014). *DNA Damage & Repair: Mechanisms for Maintaining DNA Integrity*. Retrieved from Scitable by Nature Education: https://www.nature.com/scitable/topicpage/dna-damage-repair-mechanisms-for-maintaining-dna-344

D. L. Luthria, e. a. (2006). Content of total phenolics and phenolic acids in tomato (Lycopersicon esculentum Mill.) fruits as influenced by cultivar and solar UV radiation. *Journal of Food Composition and Analysis*, 771-777.

Dai T, G. A. (2013). Blue light rescues mice from potentially fatal Pseudomonas aeruginosa burn infection: efficacy, safety, and mechanism of action. *Antimicrobial Agents and Chemotherapy*, 1238–1245.

Dai, T., Gupta, A., Murray, C., Vrahas, M., Tegos, G., & Hamblin, M. (2012). Blue light for infectious diseases: Propionibacterium acnes, Helicobacter pylori, and beyond? *Drug resistance updates : reviews and commentaries in antimicrobial and anticancer chemotherapy*, 223-236.

Das, J. R., Bhakoo, M., Jones, M. V., & Gilbert, P. (1998). Changes in the biocide susceptibility of Staphylococcus epidermidis and Escherichia coli cells associated with rapid attachment to plastic surfaces. . *J. Appl. Microbiol.* , 852-858.

Donlan, R., & Costerton, J. (2002). Biofilms: Survival Mechanisms of Clinically Relevant Microorganisms. *Clinical Microbiology Review*, 167-193.

D'Souza, C., Yuk, H., Khoo, G. H., & Zhou, W. (2015). Application of Light-Emitting Diodes in Food Production, Postharvest Preservation, and Microbiological Food Safety. *COMPREHENSIVE REVIEWS IN FOOD SCIENCE AND FOOD SAFETY*, 719-740.

Eischeid, A., & Linden, K. (2011). Molecular indication of protein damage in adenoviruses after UV disinfection. *Applied Environmental Microbiology*, 1145-1147.

Enwemeka, C. W. (2009). Blue 470-nm light kills methicillin-resistant Staphylococcus aureus (MRSA) in vitro. *Photomedicine and Laser Surgery*, 221–226.

Faille, C. e. (2000). Influence of physicochemical properties on the hygienic status of stainless steel with various finishes. *Biofouling*, 261-274.

Felix Vajdos, ’. C., Fee, ’. L., Grimsley, ’. A., & Gray’, T. (1995). How to measure and predict the molar absorption coefficient of a protein. *Prorein Science* .

Feng, G., Cheng, Y., Wang, S.-y., Borca-Tasciuc, D. A., Worobo, R. W., & Moraru, C. (2015). Bacterial attachment and biofilm formation on surfaces are reduced by small-diameter nanoscale pores: how small is small enough? *npj Biofilms and Microbiomes*.

Feng, G., Cheng, Y., Wang, S.-Y., Hsu, L. C., Feliz, Y., Borca-Tasciuc, D. A., . . . Moraru, C. (2014). Alumina surfaces with nanoscale topography reduce attachment and biofilm formation by Escherichia coli and Listeria spp. *Biofouling: The Journal of Bioadhesion and Biofilm Research*, 1253-1268 .

Freitag, N., Port, G., & Miner, M. (2009). Listeria monocytogenes—from saprophyte to intracellular pathogen. *Nature Reviews Microbiology*, 623-628.

Ganz, R. A., Viveiros, Ahmad, Ahmadi, Khalil, Tolkoff, . . . Hamblin. (2005). Helicobacter pylori in patients can be killed by visible light. . *Lasers in Surgery and Medicine*, 260-265.

Gayán, E., Condón, S., & Álvarez, I. (2014). Biological Aspects in Food Preservation by Ultraviolet Light: a Review. *Food and Bioprocess Technology*, 1-20.

Ghate, V., Siang Ng, K., Zhou, W., Yang, H., Hoon Khoo, G., Yoon, W. B., & Yuk, H.-G. (2013). Antibacterial effect of light emitting diodes of visible wavelengths on selected foodborne pathogens at different illumination temperatures. *International journal of food microbiology*, 399-406.

Giuseppina, P., Sonia, B., Antonio, C., Lorenzo, M., Andrea, C., Ilaria, B., . . . Giorgio, G. (2019). Unraveling the Role of Red:Blue LED Lights on Resource Use Efficiency and Nutritional Properties of Indoor Grown Sweet Basil. *Frontiers in Plant Science* , 305.

Guffey, J. W. (2006). In vitro bactericidal effects of 405-nm and 470-nm blue light. . *Photomedicine and Laser Surgery*, 684–688.

Gupta, S. D., & Jatothu, B. (2013). Fundamentals and applications of light-emitting diodes (LEDs). *Plant Biotechnol Reports*, 211-220.

Hamblin, M. R., & Hasan, T. (2004). Photodynamic therapy: a new antimicrobial approach to infectious disease? *Photochemical & Photobiological Sciences*, 436-450.

Harris, G. D., Dean Adams, V., Sorensen, D. L., & Curtis, M. S. (1987). ULTRAVIOLET INACTIVATION OF SELECTED BACTERIA AND VIRUSES WITH PHOTOREACTIVATION OF THE BACTERIA. *Wat. Res* .

Held, G. (2009). Chapter 1: Introduction to LEDs. In: Introduction to Light Emitting Diode Technology and Applications. *Taylor & Francis Group, LLC*.

Hu, J., & Quek, P. (2008). Effects of UV radiation on photolyase and implications with regards to photoreactivation following low-and medium-pressure UV disinfection. . *Applied Environmental Microbiology*, 327-328.

Khan, M. S. (2005). III-nitride UV devices. *Janapense Journal of Applied Physics*, 7191-7206.

Kim, D., & Dong-hyun, K. (2018). Elevated Inactivation Efficacy of a Pulsed UVC Light-Emitting Diode System for Foodborne Pathogens on Selective Media and Food Surfaces. . *Food Microbiol.* , 1-14.

Kim, D., Kim, S., & Kang, D. (2017). Bactericidal effect of 266 to 279nm wavelength UVC-LEDs for inactivation of Gram positive and Gram negative foodborne pathogenic bacteria and yeasts. *Food research international*, 280-287.

Kim, S.-J., Kim, D.-K., & Kang, D.-H. (2015). Using UVC Light-Emitting Diodes at Wavelengths of 266 to 279 Nanometers To Inactivate Foodborne Pathogens and Pasteurize Sliced Cheese. *Applied and Environmental Microbiology*, 11-17.

Kondo, S., Tomiyama, H., Rodyoung, A., Okawa, K., Ohara, H., Sugaya, S., . . . Hirai, N. (2014). Abscisic acid metabolism and anthocyanin synthesis in grape skin are affected by light emitting diode (LED) irradiation at night. *Journal of plant physiology* , 823-829.

Koutchma, T., Keller, S., Chirtel, S., & Parisi, B. (2004). Ultraviolet disinfection of juice products in laminar and turbulent flow reactors. *Innov. Food Sci. Emerg. Technol.* , 179-189.

Li, G. W. (2017). Comparison of UV-LED and low pressure UV for water disinfection: Photoreactivation and dark repair of Escherichia coli. *Water Research*, 134-143.

Li, X., & Farid, M. (2016). A review on recent development in non-conventional food sterilization technologies. *Journal of Food Engineering*, 33-45.

Lobo, V. e. (2010). Free radicals, antioxidants and functional foods: Impact on human health. *Pharmacognosy reviews*, 118-126.

Maclean, M., MacGregor, S. J., Anderson, J. G., & Woolsey, G. (2008). High-intensity narrow-spectrum ligh inactivation and wavelength sensitivity of Staphylococcus aureus. *FEMS Microbiology Letters*, 227-232.

Maclean, M., MacGregor, S. J., Anderson, J. G., & Woolsey, G. (2009). Inactivation of Bacterial Pathogens following Exposure to Light from a 405-Nanometer Light-Emitting Diode Array. *APPLIED AND ENVIRONMENTAL MICROBIOLOGY*, 1932-1937.

Maclean, M., MacGregor, S., A. J., & Woolsey, G. (2008). The role of oxygen in the visible-light inactivation of Staphylococcus aureus . *Journal of Photochemistry and Photobiology B*, 180-184.

Minamata Convention on Mercury. . (2019, March 28). Retrieved from http://www.mercuryconvention.org/.

Moraru, C. I. (2009). Reduction of Listeria on Ready-to-Eat Sausages after Exposure to a Combination of Pulsed Light and Nisin. *AND*, 347-353.

Murdoch LE, M. M. (2012). Bactericidal effects of 405 nm light exposure demonstrated by inactivation of Escherichia, Salmonella, Shigella, Listeria, and Mycobacterium species in liquid suspensions and on exposed surfaces. *Scientific World Journal*, 1-14.

Nigro, F., & Ippolito, A. (2016). UV-C light to reduce decay and improve quality of stored fruit and vegetables: a short review. *Acta Horticulturae*, 293-298.

Nitzan, Y. M., Salmon-Divon, Shporen, E., & Malik, Z. (2004). ALA induced photodynamic effects on gram positive and negative bacteria. *Photochemical & Photobiological Sciences*, 430-435.

Nyangaresi, P. e. (2018). Effects of single and combined UV-LEDs on inactivation and subsequent reactivation of E . coli in water disinfection. *Water Research*, 331-341.

Pace, C. V. (1995). How to measure and predict the molar absorption coefficient of a protein. *Protein Science*, 2411-2423.

Park, S., & Kang, D. (2017). Influence of surface properties of produce and food contact surfaces on the efficacy of chlorine dioxide gas for the inactivation of foodborne pathogens. *Food Control*, 88-95.

Peleg, M., & Cole, M. B. (1998). Reinterpretation of microbial survival curves. . *Crit. Rev. Food Sci. Nutr.*, 353-380.

Proulx, J., Hsu, L., Miller, B., Sullivan, G., Paradis, K., & Moraru, C. (2015). Pulsed-light inactivation of pathogenic and spoilage bacteria on cheese surface. *Journal of Dairy Science*, 5890-5898.

Radetsky, L. C. (2018). *LED and HID Horticultural.* Troy: Lighting Research Center, Rensselaer Polytechnic Institute.

Rattanakul, S., & Oguma, K. (2018). Inactivation kinetics and efficiencies of UV-LEDs against Pseudomonas aeruginosa, Legionella pneumophila, and surrogate microorganisms. . *Water Research*, 31-37.

Richardson, C. (2008). Driving high-power LEDs in series-parallel. *National Semiconductor*, 45-49.

Sauer, A., & Moraru, C. I. (2009). Inactivation of Escherichia coli ATCC 25922 and Escherichia coli O157 : H7 in Apple Juice and Apple Cider , Using Pulsed Light Treatment. . *Journal of Food Protection*.

Shin, J., Kim, S., Kim, D., & Kang, D. (2016). Fundamental Characteristics of Deep-UV Light-Emitting Diodes and Their Application To Control Foodborne Pathogens. . *Appl. Environ. Microbiol.*, 2-10.

Sommers, C. H., Cooke, P. H., Fan, X., & Sites, J. E. (2009). Ultraviolet light (254 nm) inactivation of Listeria monocytogenes on frankfurters that contain potassium lactate and sodium diacetate. *J. Food Sci.* , 114-119.

Stoscheck, C. M. (1990). 50 GENERAL MEHODS FOR HANDLING PROTEINS AND ENZYMES. In *Quantitation of Protein.* .

SUDHIR K. SASTRY, A. K. (2000). Ultraviolet Light. In *Kinetics of Microbial Inactivation for Alternative Food Processing Technologies* (pp. 90-93). Journal of Food Science.

Takayoshi, T. e. (2017). Deep-ultraviolet light-emitting diodes with external quantum efficiency higher than 20% at 275 nm achieved by improving light-extraction efficiency. . *Appl. Phys. Express* .

Uesugi, A., Woodling, S., & Moraru, C. (2007). Inactivation kinetics and Factors of Variability in the Pulsed Light Treatment of Listeria innocua Cells. *Journal of Food Protection*, 2518-2525.

Venditti, T., & D'hallewin, G. (2014). Use of ultraviolet radiation to increase the health-promoting properties of fruits and vegetables. *Stewart Postharvest Review*, 10-13.

Vogler, E. (1998). Structure and reactivity of water at biomaterial surfaces. *Advances in Colloid and Interface Science*, 69-117.

Wang, Y., Wang, Y., Wang, Y., Murray, C., Hamblin, M., Hooper, D., & Dai, T. (2017). Antimicrobial blue light inactivation of pathogenic microbes: State of the art. . *Drug Resistance Updates*, 1-22.

Wong, H.-C., Chung, Y.-C., & Yu, J.-A. (2002). Attachment and inactivation of Vibrio parahaemolyticus on stainless steel and glass surface. . *Food Microbiol.* , 341-350.

Woodling, S. E., & Moraru, C. I. (2005). Influence of Surface Topography on the Effectiveness of Pulsed Light Treatment for the Inactivation of Listeria innocua on Stainless-steel Surfaces. . *J Food Sci* , 345-351.

World Health Organisation (WHO) Initiative for vaccine research. (2019). Retrieved from https://www.who.int/immunization/research/en/

Young, A. R. (2006). Acute effects of UVR on human eyes and skin. *Progress in Biophysics & Molecular Biology*, 80-85.

CHAPTER 2

The effect of substrate on inactivation of bacteria by UVC-LEDs*

2.1 Abstract

Irradiation with UV-C light-emitting diodes (LED) is emerging as a low energy, chemical-free approach to mitigate microbial contamination, but the effect of surface conditions on treatment effectiveness is not well understood. Here, inactivation of *L. innocua* and *E. coli* ATCC25922, as examples of Gram-positive and Gram-negative bacteria, respectively, by UV-C LED of 280 nm wavelength was studied. Surface scenarios commonly encountered in environmental, clinical or food processing environments were used: nutrient rich surfaces, thin liquid films (TLF), and stainless-steel surfaces (SS). UV-C LED exposure achieved 5-log reduction for both strains within 10 min in most scenarios, except for TLF thicker than 0.6 mm. Inactivation kinetics in TLF and on dry SS followed the Weibull model ($0.96 \leq R^2 \leq 0.99$), but the model overestimated inactivation by small-dose UV-C on wet SS. Confocal microscopy revealed *in situ* that bacteria formed a dense outer layer at the liquid-air interface of the liquid droplet, protecting the cells inside the droplet from the bactericidal UV-C. This resulted in lower than anticipated inactivation on wet SS at small UV-C doses, and deviation from the Weibull model. These findings can be used to design effective UV-C LED disinfection strategies for various surface conditions and applications.

---

* This chapter is part of the paper "*Inactivation of Listeria and E. coli by UV-C LED: effect of substrate on inactivation kinetics*" by Yifan Cheng, Hanyu Chen, Albert Sánchez Basurto, Vladimir V. Protasenko, Shyam Bharadwaj, Moududul Islam, and Carmen I. Moraru. HC performed a large part of the inactivation experiments and the measurements associated with these, performed data analyses and interpretation, and contributed to the writing of the manuscript. This chapter only presents results of work in which HC was directly involved.

2.2 Introduction

Persistence of pathogens on material surfaces often causes severe consequences, including infections in dental offices and hospitals (Donlan & Costerton, 2002), or transfer of pathogenic or spoilage microorganisms from food contact surfaces to food products in food processing facilities and food service environments (Chmielewski & Frank, 2003). Exposing surfaces contaminated by microorganisms to ultraviolet C light (UV-C), with wavelength 100-280 nm, has been established as an effective disinfection method, often used as an alternative to or in tandem with chemical disinfection methods. Mercury lamps are currently the most commonly used source of UV light. Yet, according to the Minamata Convention on Mercury, a global legally binding agreement participated by 127 states and one reginal economic integration organization in 2013, manufacturing and trading of mercury-containing lamps for general lighting purposes will be disallowed after 2020, in order to reduce and eliminate the adverse effect of mercury on human health and the environment (Minamata Convention on Mercury. , 2019). This agreement accelerated the efforts for the development of alternatives to mercury lamps.

UV-C light-emitting diodes (LEDs) present several advantages compared to mercury lamps, including the lack of toxic mercury, device compactness and flexible designs, zero warm-up time (Chatterley & Linden, 2010) (Shin, Kim, Kim, & Kang, 2016), high durability, monochromatic light emission at specific wavelength (Kim, Kim, & Kang, 2015), wavelength diversity, possibility of pulsed illumination, and the capability of maintaining relatively high activity at cold temperatures (e.g. refrigeration) (Shin, Kim, Kim, & Kang, 2016). UV LEDs are also known for their lower heat emission in the form of IR radiation (D'Souza, Yuk, Khoo, & Zhou, 2015), which enables applications that demand high UV fluence and proximal LED configurations, while preventing heating over long periods of time. Recent progress in improving the light-extraction efficiency of UV LEDs in the range 200-300 nm has increased the external quantum efficiency beyond 20%, approaching the 30-40% efficiency range of low-pressure UV lamps (Takayoshi, 2017).

This also resulted in an increasing interest in substituting mercury lamp with UV LEDs for bacteria inactivation purposes. Successful applications of UV-C LEDs have emerged in the healthcare industry (e.g. disinfection of endoscopes, breathing circuits, and respirators), agriculture (e.g. disinfection of irrigation and feed water), packaging plants (e.g. air disinfection), food service (e.g. food contact surfaces disinfection), and homes (e.g. disinfection of cell phone surfaces and drinking water).

One limitation of using UV-C LED as a bactericidal technology is the short penetration depth of UV light, which impairs its effectiveness in inactivating bacteria that reside deeper than the surface of solid or liquid media. To mitigate this drawback, previous work on liquid disinfection via UV-C adopted stirring (Shin, Kim, Kim, & Kang, 2016) (Nyangaresi, 2018) (Rattanakul & Oguma, 2018) (Li G. W., 2017) or turbulent flow (Sauer & Moraru, 2009) (Koutchma, Keller, Chirtel, & Parisi, 2004), to facilitate access of UV-C to the target microorganisms. Notwithstanding its limited penetration depth, UV-C LED radiation is well-suited for disinfecting surface microbial contaminations, either in dry conditions or in the presence of static or undisturbed surface liquids, such as droplets or thin liquid films. Both scenarios are ubiquitous in environmental applications, the food industry and healthcare industry, yet knowledge on the effectiveness of UV-C LED inactivation kinetics of bacteria under such conditions is limited.

Another important aspect that must be considered is the potential reactivation of UV-injured bacterial cells that can occur post UV-C LED treatment, which has tremendous safety implications, as it can diminish the overall effectiveness of the treatment.

To address the current knowledge gaps in the area of bactericidal effectiveness of UV-C LEDs, in the present study the germicidal effectiveness and post-UV repair of bacterial cells treated with 280 nm wavelength UV-C LEDs was evaluated, for various substrate scenarios. A custom-made UV-C LED treatment panel with a peak emission wavelength at 280 nm was used in this study, both because 280 nm has higher electrical efficiency than the shorter wavelengths typically used in UV disinfection (e.g. 254 nm), and because it was shown to have higher germicidal efficiency at the same energy expenditure, without

excessive heat generation during the operation (Kim, Kim, & Kang, 2017). *Escherichia coli* ATCC 25922 and *Listeria innocua* were selected as challenge microorganisms because they were proven surrogates for UV-based treatments for pathogenic *E. coli* O157:H7 (Sauer & Moraru, 2009) and *L. monocytogenes* (Moraru, 2009), respectively.

The findings of this study provide insights into the kinetics and factors of influence for microbial inactivation by UV-C, which could be used to design effective and efficient UV-C LED surface disinfection applications.

2.3 Materials and Methods

2.3.1 Bacterial Cultures

Listeria innocua FSL C2-008 (environmental isolate from a smoked fish plant) and *Escherichia coli* ATCC 25922 (American Type Culture Collection, Manassas, VA) were stored in glycerol stock solution at -80 °C prior to use. Culture reactivation was conducted by first streaking the frozen culture on Trypticase Soy Agar (TSA; BD Difco™, Franklin Lakes, NJ) and incubate (37 °C, 24 h) to obtain isolated colonies, followed by loop-inoculation in 3 mL Tryptic Soy Broth (TSB; BD Difco™, Franklin Lakes, NJ) for passage one (37 °C, 24 h), and passing 30 µL of grown passage one culture to fresh 3mL TSB for passage two (37 °C, 16 h). To replace TSB with UV-transmitting phosphate buffer (Supplementary Fig. S1), the resulting early stationary phase culture were centrifuged (5000 RPM, 10 min, 21 °C) and resuspended in sterile Butterfield Phosphate Buffer (BPB, pH = 7.2). This wash step was repeated two more times to ensure minimal remnants of TSB in the final bacteria suspension. The final concentration of bacteria suspended in the BPB was about 10^9 CFU/mL for both strains.

2.3.2 UV-C LED Treatment Chamber

A custom-made UV-C LED chamber was used to perform all inactivation experiments. The apparatus delivers UV-C light via 16 individual UV-C LEDs (SMD3535, TaoYuan Electron Ltd., Shenzhen, China) arranged as shown in Fig. 1A. These LEDs produce a monochromatic emission spectrum with the peak at

280 nm (Fig. 2.1B). To determine an appropriate separation distance between the UV-C LED panel and target surfaces, spatial distribution of 280 nm irradiation maps at the target surfaces were simulated for separation distances of 10 mm (Fig. 2.1C), 45 mm (Fig. 2.1D), and 75 mm (Fig. 2.1E). A separation distance of 45 mm was selected for all UV-C exposure experiments because it provided a good balance between the intensity of the irradiance and the homogeneity of the distribution. At this distance, when the power source was operated under CV mode, with the potential set to 5.30 V, resulting in a current of ~320 mA, the fluence rate below the middle of the panel was 40 $\mu W/cm^2$ .The entire apparatus was covered with aluminum foil to isolate the UV-C treatment from any potential disturbance by ambient light. The following treatment durations were chosen to deliver different UV doses: 60 s, 180 s, 300 s, 600 s, 1000 s, corresponding to cumulative UV fluence of 2.38 mJ/cm^2, 7.13 mJ/cm^2, 11.88 mJ/cm^2, 23.76 mJ/cm^2, and 39.60 mJ/cm^2.

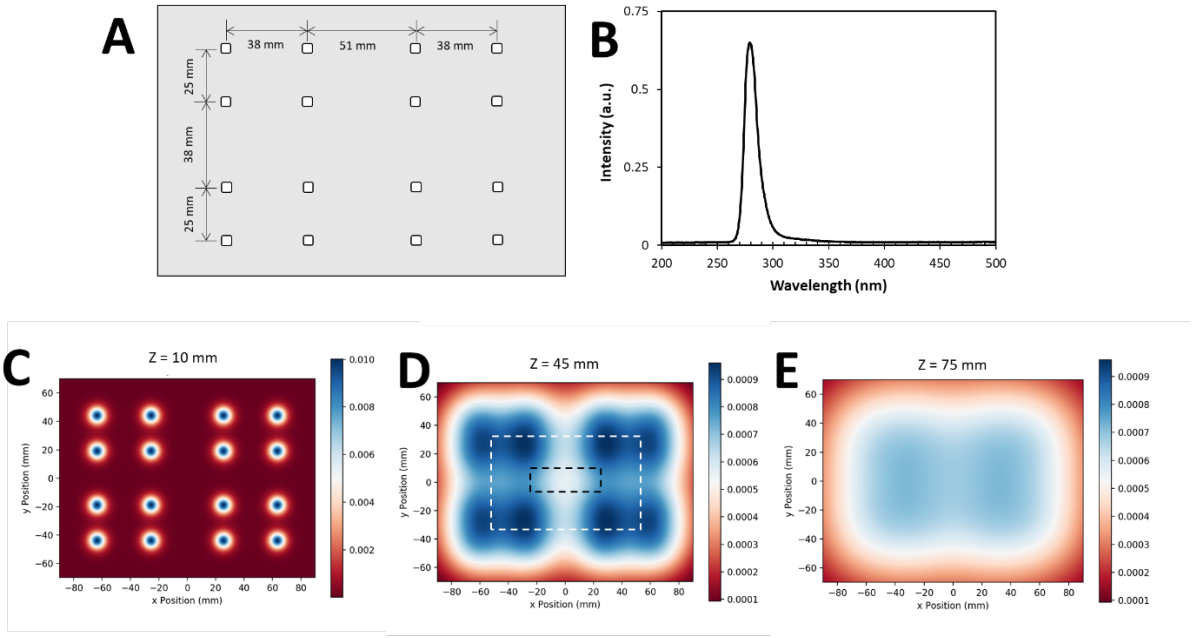

Figure 2.1. The custom-made UV-C LED panel and its performance characteristics. (A) Arrangement of UV-C LEDs on the panel. (B) Typical emission spectrum of the UV-C LEDs. (C-E) Simulation of the distribution of UV-C irradiance received by a flat surface located at 10 mm, 45 mm, 75 mm away from the light source, respectively. A larger intensity scale was used for (C) than (D) and (E), to capture the details of the distribution. The dashed-line rectangles illustrate the position of a liquid chamber or a SS coupon, respectively, in the UV-C energy field.

2.3.3 Bacteria Inactivation by UV-C LED on Various Substrates

2.3.3.1 Nutritive agar plates

Both the *E. coli* and *L. innocua* cultures were streaked in two parallel lines on TSA plates of 100 mm in diameter. Half of each plate was covered with aluminum foil, to divide the surface of the plate and the bacterial streaks into a 'Exposed' section and a 'Covered' section (Fig. 2.2A), followed by exposure to UV-C for a specified duration (10 s to 25 min). After UV-C treatment, the plates were incubated at 37 °C for 24 h for qualitative evaluation of bacteria inactivation.

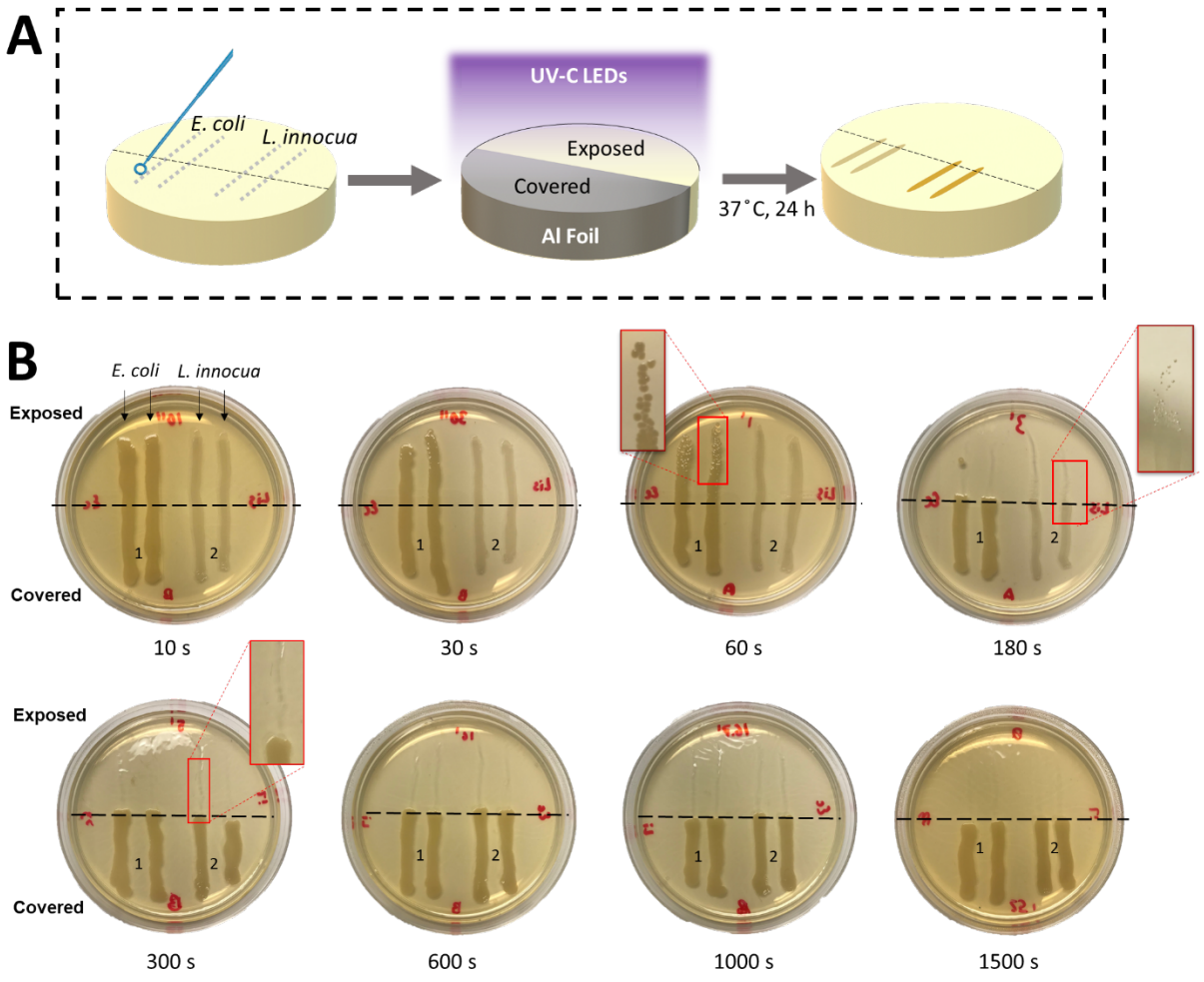

Figure 2.2. Qualitative evaluation of UV-C LED inactivation of *E. coli* and *L. innocua* on TSA agar plates, which mimic nutrient-rich surfaces. (A) Schematic flow chart of the experimental steps. (B) Photos of the agar plates after 24 h incubation, showing the differential growth patterns of bacteria streaks

with and without exposure to UV-C LEDs. The agar area below the black dashed-line was protected from exposure to UV-C.

2.3.3.2 Thin liquid films

Liquid chambers (Lab-Tek™ II Chamber Slide™ chamber, 17 mm × 48 mm; Fisher Scientific, Rochester, NY) were used to hold *E. coli* or *L. innocua* suspensions in the form of TLFs to mimic contaminated standing water. Before the experiment, the liquid chambers were decontaminated by soaking in 70% ethyl alcohol (Fisher Scientific, Rochester, NY) for 24 h, followed by drying in a biosafety cabinet for 2 h to evaporate the remaining ethyl alcohol. After that, bacteria suspensions were pipetted into the liquid chambers and allowed to equilibrate for 3 min before starting the UV-C exposure. The effect of strains on UV-C inactivation kinetics was investigated by exposing 1 mL of liquid film (thickness = 1.2 mm) containing either *L. innocua* or *E. coli*, for the durations specified previously. To determine the effect of thin film thickness on inactivation kinetics, 0.5 mL, 1 mL, 1.5 mL, and 2 mL of *L. innocua* suspension was aliquoted into a liquid chamber, resulting in liquid film thickness of 0.6 mm, 1.2 mm, 1.8 mm, and 2.4 mm, respectively, followed by 3-min equilibration and subsequent UV-C LED treatment for various durations. Due to the concave meniscus exhibited by the liquid films at the liquid chamber walls, the average thickness of the bacteria containing liquid films was calculated by dividing the volume of bacteria suspension by the bottom area of the liquid chamber instead of being measured directly. The bacteria suspension from both UV-treated and non-treated control samples were serially diluted with BPB and enumerated using standard plate counting method on TSA agar. Total bacteria reduction was calculated using the following equation:

$$Log\ Reduction = \mathrm{Log}_{10}(\frac{N}{N_0}) \qquad \text{Eq 2.1}$$

Where N_0 and N are the bacteria counts (in colony forming units per mL of suspension, CFU / mL) before and after UV-C treatment, respectively. The detection limit of the inactivation experiments in TLF is 10 cells per mL of bacteria suspension, for both *E. coli* and *L. innocua*.

All UV-C LED treatments were performed in triplicate, with independently grown bacterial cultures used in each replicate.

Transmittance spectra of UV-C through TLFs of thickness of 0.6 mm, 1.2 mm, 1.8 mm, and 2.4 mm were determined using an HR2000CG-UV-NIR spectrometer equipped with a DH-2000-BAL UV-VIS-NIR light source (Ocean Optics Inc, Largo, FL, USA). Briefly, *E. coli* and *L. innocua* suspensions (prepared as described above) were aliquoted into a space of desired thickness, as specified above, which was created by inserting polyethylene spacers between two clean UV-C transmitting fused quartz slides (Grade GE124, Technical Glass Products, WA, USA), placed horizontally on a metal stand. The optical fiber outlet (connected to light emitter) and the receiver inlet (connected to the detector) were perpendicularly affixed to the top and bottom quartz slide, respectively. An illustration of the setup is shown in Supplementary Fig. S3. The volume of the suspensions was adjusted to ensure that it covered the entire cross-section of the beam emitted by the fiber outlet (about 4 cm^2 surface area). All transmittance measurements were taken immediately after the suspensions were aliquoted, to minimize the potential interference by bacterial attachment onto the slides. Technical duplicates were performed on each sample to account for potential variation caused by the positioning of the suspension with respect to the beam.

2.3.3.3 Stainless-Steel Coupons

Food-grade stainless steel (SS) coupons (50 mm ×100 mm) with a glass bead blasted finish (R_a = 0.78 μm) were used to simulate polished SS surfaces commonly encountered in food handling and medical environments (Woodling & Moraru, 2005). To remove any surface chemical contaminants, the SS coupons were sequentially submerged in a rotating bath (100 RPM) of acetone (95%; Fisher Scientific, Rochester, NY), ethyl alcohol (95%) and deionized water, for 10 min at each step. The coupons were then autoclaved (15 min, 121℃) in individually sealed sterilization pouches to kill any potential microbial contaminants. The SS coupons prepared as described here exhibited a mean water contact angle of 62.2 ± 3.3°, as determined by a static sessile drop method with a Rame-Hart 500 goniometer (Rame-Hart Inc., Succasunna, NJ, USA).

For inoculation, a total of 1 mL bacteria suspension was deposited on the SS surfaces as 20 evenly spaced droplets of 50 µL each. The inoculated coupons were then divided into two treatment groups, as follows: 1) for the wet condition, inoculated coupons were left to equilibrate in the laminar flow hood (23 °C, relative humidity = 17%) for 3 min; 2) for the dry condition, the inoculated coupons were left to dry under the hood for about 3 h, until they reached a constant weight, without excessive drying (Supplementary Fig. S4).

The SS coupons prepared as described above were subjected to UV-C LED treatments, as described in section 2.3.3.1, after which they were individually placed in sterile Whirl-Pak bags with 100 mL BPB and sonicated for 5 min at 40 kHz (Branson 1210 Ultrasonic Cleaner, Branson Ultrasonics, Danbury, CT). This method of recovery was used since Bjerkan et al. showed that ultrasonication (>20 kHz) for 5 min achieved the highest recovery of bacteria from metal plates compared to other commonly used methods such as manual scraping (Bjerkan, Witso, & Bergh, 2009). Preliminary experiments conducted as part of the present study also showed no effect of ultrasonication for 5 min on bacterial viability (data not shown). After sonication, the BPB that contained recovered cells was subjected to serial ten-fold dilutions with sterile BPB, spread plating on TSA plates, and enumeration of CFUs after incubation at 37 ºC for 24 h. The control followed the same recovery and enumeration procedures except for the UV-C LED treatment. The detection limit of the inactivation experiments on SS surfaces was 100 cells per SS coupon (50 cm^2) for both *E. coli* and *L. innocua*. Inactivation effectiveness, expressed in Log reduction, was determined using Eq.2.1. All UV-C LED treatments were performed in triplicate, with independently grown bacterial cultures.

2.3.4 Modelling of inactivation kinetics

Microbial inactivation by UV-C LED was modelled by the non-linear Weibull model (Uesugi, Woodling, & Moraru, 2007):

$$\log_{10}(N/N_0) = \alpha t^{\beta} \qquad \text{Eq 2.2}$$

Where N/N_0 represents the ratio of survivors after treatment (N) over the initial population (N_0), α is the scale parameter and β is the shape factor. The non-linear regression was performed using the statistical software R (R Foundation for Statistical Computing, version 1.1.463).

2.3.5 Confocal Laser Scanning Microscopy (CLSM)

The distribution of *E. coli* and *L. innocua* cells within liquid droplets and dried pellets on the stainless steel coupons was visualized using a Zeiss LSM 710 equipped with inverted immersion objectives (Carl Zeiss, Jena, Germany), as described elsewhere (Feng G. , et al., 2014) (Cheng & Moraru, 2018). Briefly, to image a bacteria-containing liquid droplet, 5 µL bacteria-BPB suspension (prepared as described above), stained with a LIVE/DEAD™ *Bac*Light™ fluorescent dye (ThermoFisher Scientific, Waltham, MA, USA), was aliquoted onto the glass bottom of a confocal-compatible dish (Mat-Tek Corporation, Ashland, MA, USA). The scanning process was performed *in situ*, with minimal mechanical disturbance on bacterial movement and distribution. Apochromat 10 × and 40 × water immersion objective lenses were used for capturing the overall distribution and the details at the liquid-air interfaces, respectively. The Z-scan mode was deployed to capture the cell distributions in the three-dimensional space.

To image a dried bacteria pellet, 50 µL of bacterial suspension was aliquoted onto a smaller version (1 in × 2 in) of the SS coupon used in the inactivation experiments, followed by drying for 3 h. After drying, diluted fluorescent dye (5 µL in 3 mL BPB) was pipetted onto the dry bacteria pellet, incubated for 20 min in the dark at 21 °C, and the unbound dye was rinsed off gently with a 0.15 M NaCl solution. Next, the SS coupon was inverted and placed on the glass bottom of the dish, with the pellet side facing downward and immersed in *Bac*Light™ mounting oil. Z-scans were performed throughout the entire thickness of the pellet.

Considering that sample preparation procedures for confocal microscopy could result in biased conclusions on bacterial viability, only the signal from the green fluorescent channel, which accounts for all cells, regardless of their viability, was shown and discussed in the paper.

2.3.6 Reactivation of UV-C treated bacteria

To evaluate potential reactivation of UV-C treated bacteria under conditions mimicking real-world applications, *L. innocua* was spot-inoculated onto the SS coupons, exposed to UV-C under the wet condition for 600 s (or 23.76 mJ/cm^2), and then subjected to a 6-h reactivation step under four different lighting conditions: 1) Dark; 2) white ambient light (60W, GreybaR Electrics, Philadelphia, PA), labeled 'Amb'; 3) low luminance flux (260-290 μW/cm^2) and 4) high luminance flux (490-610 μW/cm^2) 405 nm LEDs (Vital Vio, Troy, NY), labeled '405 L' and '405 H', respectively. A 6-h reactivation period was used because previous studies showed that the post-UV bacterial reactivation plateaus around this time (Nyangaresi, 2018). Reactivation under each lighting condition was also tested under the 'DRY' or the 'WET' condition ('DRY' and 'WET' were capitalized to be differentiated from the dry and the wet conditions used in the kinetics study). For reactivation under 'DRY' conditions, the UV-C treated bacterial inoculum was allowed to dry on the SS coupons in a laminar flow hood for 6 h, followed by the same recovery and enumeration steps described in 2.3.

For the 'WET' condition, the UV-treated bacteria on the SS coupons were first transferred into BPB following the same procedures as for recovery. To conduct the 'Dark' reactivation under the 'WET' condition, 1mL of the resulting suspension was added to opaque 1.5 mL Eppendorf tubes (Eppendorf® Flex-Tubes®, Hauppauge, NY). To conduct the 'Amb', '405 L, and '405 H' reactivation, 1mL of the suspension was added to a custom-made chamber covered with an UV-transmitting quartz window lid, and all sides sealed with Parafilm® to prevent evaporation of the liquid during reactivation. All 'WET' samples were kept at 21 °C for 6 h under the specified lighting conditions before enumeration.

For each of the 8 reactivation conditions tested (2 wetness conditions × 4 lighting conditions), the bacterial concentration at the end of the UV treatment (N_{UV}) and post-reactivation (N_{PR}) were determined by standard plate counting on TSA plates after incubation for 24 h at 37 °C. The percent post-reactivation survival ratio (*PRS*) for each individual biological replicate was calculated using the equation:

$$PRS = \left(\frac{N_{PR}}{N_{UV}}\right) \cdot 100\% \qquad \text{Eq 2.3}$$

PRS greater than 100% represents an increase in survivor counts due to reactivation of injured cells, while PRS equal to or less than 100% represents no change, or a further decrease in counts during the resuscitation process. To account for potential genetic diversity within the strain, a larger number of biological replicates ($6 \leq n \leq 11$) were included than in the previous experiments, in order to acquire representative, unbiased reactivation results.

2.3.7 Statistical analysis

Analysis of variance and post hoc Tukey's HSD were used to compare experimental and Weibull calculated inactivation data. Non-parametric statistics were used to analyze the reactivation results because *PRS* data did not follow a Gaussian distribution. Specifically, the Kruskal-Wallis rank sum test was used to compare the *PRS* from the eight reactivation conditions and the Wilcoxon signed-rank test (two-sided) was used to evaluate the significance of the change in *PRS* before and after reactivation under each of the eight conditions. The False Discovery Rate method was used to determine the adjusted *p*-value for multiple comparisons (n = 8). A confidence level of 95% is adopted for all statistical tests. All statistical tests were performed using the statistical software R (version 1.1.463).

2.4 Results

2.4.1 Inactivation of bacteria streaked on nutritive agar

The qualitative results showed a significant reduction in the culturable population of *E. coli* and *L. innocua* cells on nutrient-rich surfaces exposed to UV-C LED treatments. A gradual decrease in viable bacterial cells was achieved within 1 min of UV-C LED exposure for both strains, as revealed by the gradual decrease in the density of colonies comprising the streaks after incubation (Fig. 2.2B). After 3 min of continuous UV-C LED exposure, no visible *E. coli* colonies were observed on the exposed area (not covered by aluminum foil). Scattered *L. innocua* colonies were observed near the border between exposed and covered areas, possibly due to partial blockage of UV-C radiation by the aluminum foil. After 5 min, no visible

colonies could be found along the streaking traces for either strains on the exposed area. Meanwhile, on the areas covered with aluminum foil, both strains grew into dense, continuous stripes along the streaking traces. Their growth was unaffected even for the longest treatment time tested. It should also be noted that the 24-h incubation on nutrient-rich agar surfaces at optimal growth temperature (37 °C) provided an ideal condition for post-UV reactivation of damaged cells to occur[23], yet no reactivation was observed beyond 5 min of UV-C exposure (corresponding to 11.88 mJ/cm^2).

2.4.2 Inactivation of bacteria in thin liquid films of various thickness

For all TLF thicknesses tested, survivor counts decreased nonlinearly with increasing UV-C dose emitted by the LEDs. The inactivation kinetics of *E. coli* and *L. innocua* with TLF thickness of 1.2 mm were determined, which allowed a direct comparison of the responses of the two strains to UV-C. Fig. 2.3A shows that overall there were no significant differences in inactivation between the two strains ($p > 0.05$, Fig. 2.3A).

To explore the effect of TLF thickness on UV-C LED inactivation, *L. innocua* suspensions with thickness ranging from 0.6 mm to 2.4 mm were exposed to UV-C with increasing fluence. The inactivation curves indicate that UV-C LED had a much higher efficiency against *L. innocua* in the 0.6 mm liquid film than in the thicker TLFs, particularly at higher UV-C fluence (>11.88 mJ/cm^2). For the TLFs with thickness above 1.2 mm, the inactivation curves are largely overlapped (Fig. 2.3B) and no significant difference was found among the log reduction values ($p > 0.05$). This result is further corroborated by the Weibull model parameters (Table 2.1), which indicate that the scale and shape of the inactivation curves for cells suspended in 0.6 mm thin film are significantly different from the rest ($p < 0.05$). To rule out the possible effect of water evaporation from the TLF on the inactivation results, the percent weight loss due to evaporation was determined. For the 0.6 mm, 1.2 mm, 1.8 mm, and 2.4 mm films, the weight losses over 1200 s of UVC-LED exposure were determined to be 9.1%, 4.2%, 3.0%, and 2.0%, respectively (see Supplementary Fig. S2). This indicates that water evaporation was rather insignificant during the UV-C LED treatment, and excessive drying can be excluded as a possible reason for cell death.

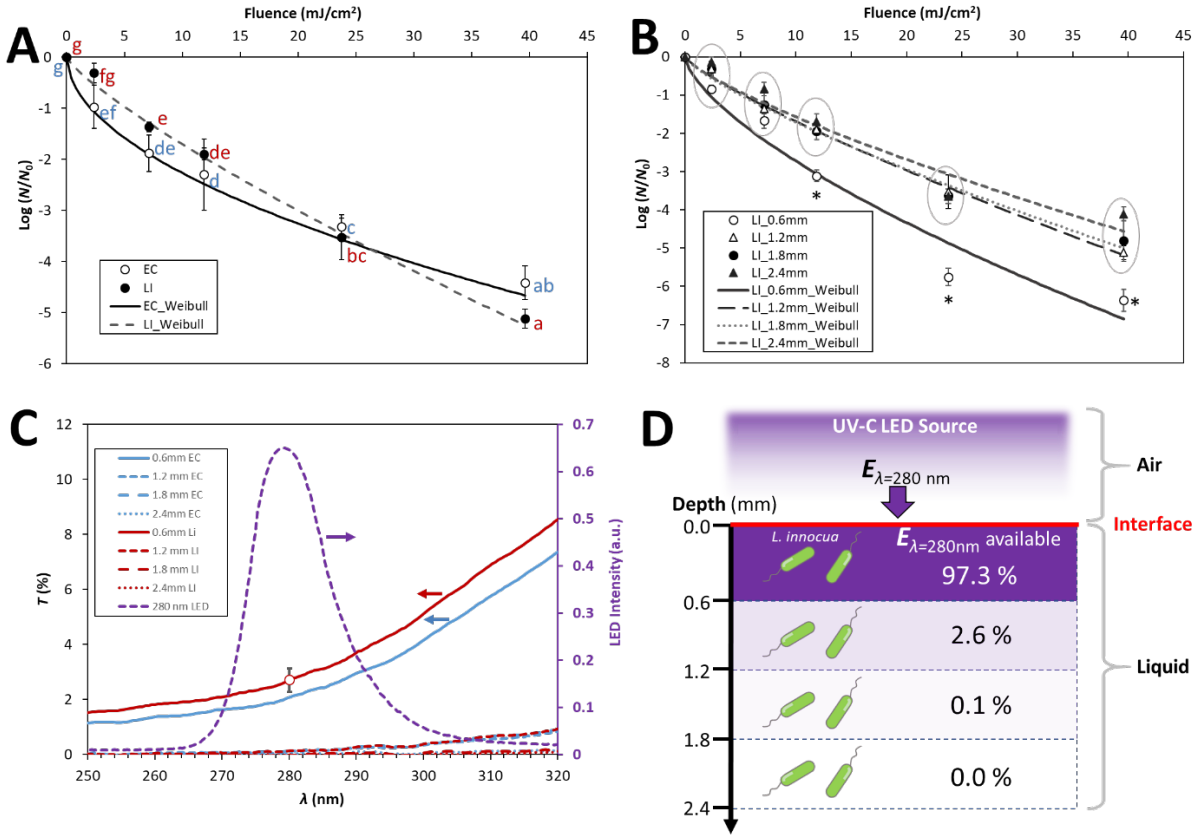

Figure 2.3. UV-C LED inactivation kinetics of *E. coli* (EC) and *L. innocua* (LI) suspended in thin liquid films. (A) Comparison between the inactivation kinetics of *E. coli* and *L. innocua* suspended in 1.2 mm thick BPB buffer. Disconnected letters denote significant differences ($p < 0.05$); EC (blue) and LI (red) were analyzed together. (B) Effect of film thickness on the inactivation kinetics of *L. innocua* suspended in BPB buffer of various thickness. Asterisks denote significant differences ($p < 0.05$), whereas circles denote insignificant differences ($p > 0.05$). (C) Transmittance (T%, left axis) of the spectrum emitted by the UV-C LEDs (intensity, right axis) through *E. coli* and *L. innocua* suspensions of various thickness. The horizontal arrows point to the relevant axes for the curves. (D) Percentage of the incident 280 nm energy ($E_{\lambda=280}$) available for inactivation at different depth of a *L. innocua* suspension. Error bars in (A), (B), and (C) represent standard deviations.

Table 2.1. Weibull model parameters for the UV-C LED inactivation kinetics of *L. innocua* suspended in liquid film of various thickness

Liquid Film Thickness (mm)	Scale Parameter α	Shape Parameter β	R^2
0.6	-0.58 ± 0.05 **a**	0.67 ± 0.03 **A**	0.96
1.2	-0.26 ± 0.02 **b**	0.82 ± 0.04 **B**	0.99
1.8	-0.28 ± 0.04 **b**	0.78 ± 0.05 **B**	0.98
2.4	-0.26 ± 0.03 **b**	0.78 ± 0.03 **B**	0.98

To better understand the effect of the thickness of the bacteria suspension on the transmission of UV-C, transmittance spectra through *E. coli* and *L. innocua* suspensions were determined. As a general trend, the transmission of light through the bacteria suspensions was smaller at shorter wavelengths. Fig. 2.3C shows the transmission of light in the spectral range that covers the emission of the UVC-LED source. Transmission over an expanded spectral range from 220 nm to 900 nm, is shown in Supplementary Fig. S1A. In Fig. 2.3C, the emission spectrum of the LEDs used was superimposed onto the transmittance spectra for direct comparison. Within the half width of the peak (i.e. 273 nm – 288 nm), transmittance (T) was lower than 4% at any given wavelength, even for the thinnest bacteria suspension tested (0.6 mm). T decreased significantly with the incremental increase in thickness, with: T< 0.4% for the 1.2 mm thick suspensions and T < 0.1% through the 1.8 mm and 2.4 mm thick suspensions.

The transmittance spectra provide insight into the availability of the bactericidal UV through the bacterial cell suspensions. To schematically represent this, a liquid film was virtually compartmentalized into 0.6 mm thick layers (Fig. 2.3D). In this representation, it was assumed that bacterial cells are uniformly distributed throughout the thickness of the liquid film. It should be noted that this is a simplification, as aggregates of cells can occur at the air-liquid interface, as discussed later. In case of the *L. innocua* suspensions, it was estimated that 2.7% of the incident 280 nm UV energy ($E_{\lambda=280nm}$) is still available after passing the first 0.6 mm of bacteria cells suspension, suggesting that 97.3% of the energy is lost due to the absorption by the *L. innocua* cells and the BPB medium. The transmittance of $E_{\lambda=280nm}$ through BPB alone was estimated to be responsible for absorption of only 0.4% of $E_{\lambda=280nm}$ (Supplementary Fig. S1), meaning

that the *L. innocua* cells in the suspension were responsible for more than 99% of the $E_{\lambda=280nm}$ absorbed. A schematic of the decrease in the available bactericidal energy $E_{\lambda=280nm}$ with increasing depth of the suspension is represented in Fig. 2.3D.

2.4.3 Inactivation of bacteria on stainless steel surfaces in wet and dry condition

Compared to the inactivation kinetics on air-dried SS surfaces, the presence of liquid droplets considerably reduced the level of inactivation for both *E. coli* (Fig. 2.4A) and *L. innocua* (Fig. 2.4B), especially within the first 60 s of exposure (cumulative fluence of 2.38 mJ/cm^2). This effect was more pronounced for *L. innocua*. However, the inactivation curves on dry SS (dashed lines) tend to reach a plateau earlier than on wet SS (solid lines), for both strains (Fig. 2.4A and 2.4B). This was also reflected in the smaller values of the Weibull shape parameters, which are indicative of concave inactivation curves, for the dry SS compared to the wet SS (Table 2.2). A crossover of the wet and dry inactivation curves for *E. coli* occurred at a cumulative dose of 7.13 mJ/cm^2 cumulative dosage (2 min treatment) and 22.18 mJ/cm^2 (7 min treatment) for *L. innocua*, respectively. Both the wet and the dry inactivation curves reached a plateau around 6 to 7 log reduction, after a cumulative UV-C fluence > 20 mJ/cm^2 (about 5 min of exposure); the plateau inactivation values were not significantly different between the wet and the dry conditions for either *E. coli* or *L. innocua* ($p > 0.05$).

The inactivation data was fitted using the Weibull model, and an excellent agreement between measured and predicted Log(N/N_0) values was obtained for the dry coupons for both strains, as evidenced by the very close agreement between nonlinear regression lines (dashed) and experimental data in Fig. 2.4A and 2.4B, as well as the overlapping of the fitted lines with the diagonal y = -x in Fig. 2.4C and 4D (R^2 = 1.00 and 0.99 for *E. coli* and *L. innocua*, respectively). It should be noted that in case of the wet coupons the Weibull model tended to over-estimate both the values for both the initial inactivation (dose < 2.38 mJ/cm^2) and the plateau (dose ≥ 39.60 mJ/cm^2), which resulted in a less strong model fit compared to the dry conditions (R^2 = 0.90 and 0.93 for *E. coli* and *L. innocua*, respectively). The Weibull model parameters are summarized

in Table 2.2. Some of the possible reasons for the weaker predictability of the inactivation data under wet conditions will be discussed next.

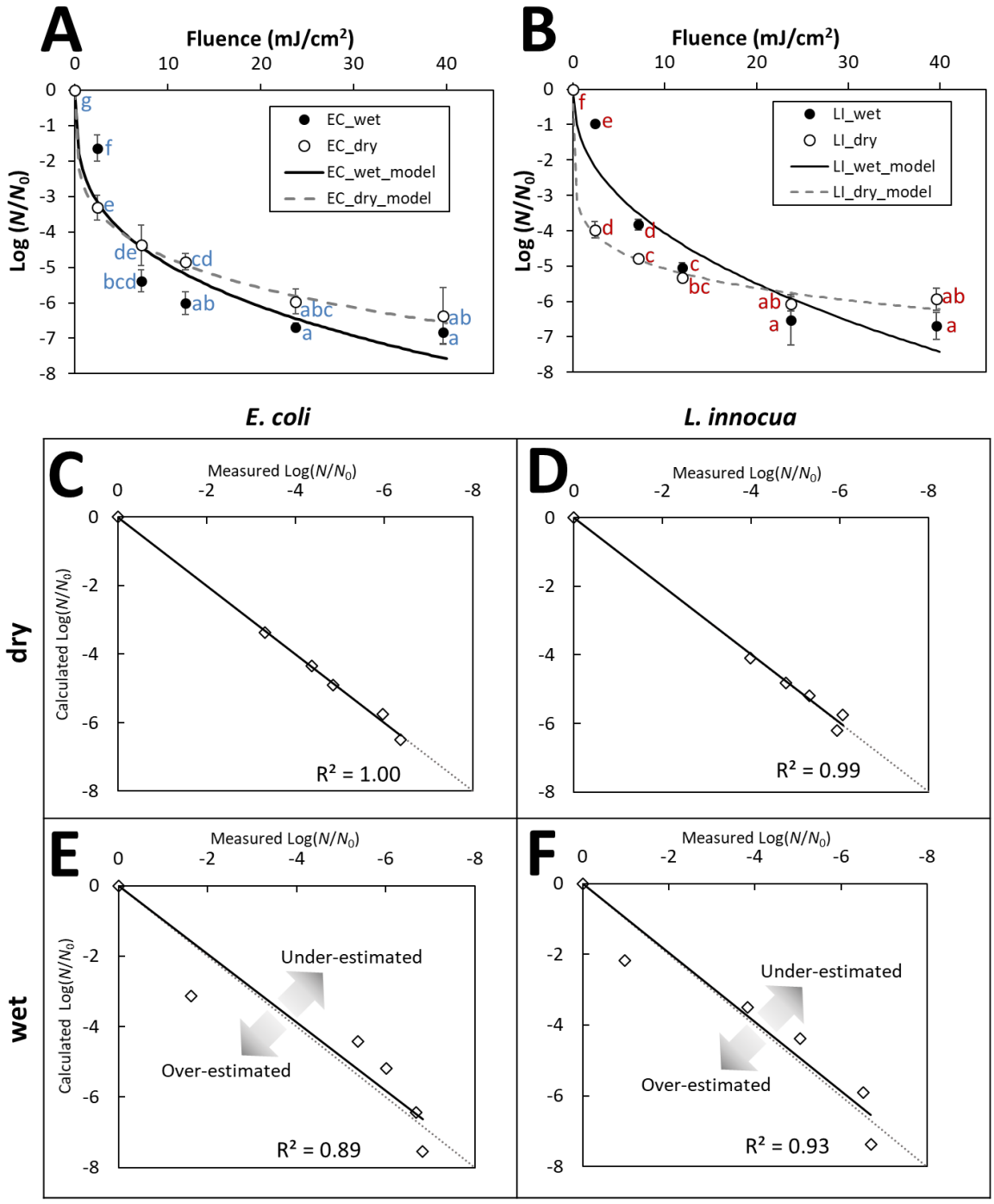

Figure 2.4. UV-C LED inactivation kinetics of *E. coli* (A) and *L. innocua* (B) on SS coupons in the wet and dry condition. Error bars represent standard deviations. Disconnected letters denote significant

differences ($p < 0.05$) (A and B were analyzed separately). Fitted vs. measured plots for *E. coli* and *L. innocua* in the dry (C and D) and the wet condition (E and F) were generated to evaluate the goodness-of-fit for each of the situations. Arrows represent the directions for over- and under-estimation by the Weibull model.

Table 2.2. Weibull model parameters for the UV-C LED inactivation kinetics of *L. innocua* and *E. coli* on stainless steel metal coupons in the wet and dry conditions

Bacteria	Substrate Conditions	Scale Parameter α	Shape Parameter β	R^2
E. coli	Wet	-2.40 ± 0.18 **b**	0.31 ± 0.03 **B**	0.89
E. coli	Dry	-2.76 ± 0.47 **b**	0.23 ± 0.06 **AB**	0.99
L. innocua	Wet	-1.50 ± 0.10 **c**	0.43 ± 0.03 **C**	0.92
L. innocua	Dry	-3.61 ± 0.24 **a**	0.15 ± 0.03 **A**	0.99

2.4.4 Distribution of bacterial cells at the liquid-air and solid-air interfaces

Confocal microscopy imaging of a quarter of a bacteria-containing droplet revealed that the distribution of bacterial in the radial direction is not uniform. As seen in Fig. 2.5A, within each horizontal plane of the 3D reconstruction of the droplet substantially higher fluorescence intensity, which corresponds to higher cell density, was found at the liquid-air interface of the droplet compared to the interior of the droplet. The gradual weakening of fluorescence intensity from the side of the droplet to its apex was likely an artifact caused by a combination of reduced laser power further away from the source and possibly photobleaching. To better visualize the details of the distribution of cells near the liquid-air interface, representative zoomed-in single-slice images in the x-y and x-z planes are shown in Fig. 2.5B. Strikingly, densely packed, multilayered bacteria cells of *E. coli* (left panel) and *L. innocua* (right panel) made up a dome-like outer shell at the liquid-air interface of the droplet, while the inner core of the liquid droplet contained planktonic cells. In Fig. 2.5B, the yellow panel shows images taken at the apex of the droplet, while the blue panel shows images taken at the side of the droplet. The horizontal slices in Fig. 2.5B revealed a smooth outward facing bacteria layer and a less defined, more diffuse appearance of this layer towards the liquid. This is particularly clear in the blue panel. This suggests that bacterial cells tend to preferentially align at the liquid-air interface. After 3 min of equilibration and less than 15 min of total imaging time, the average thickness of the resulting interfacial bacterial cell shells amounts to about 15 μm. Considering that the average length

of an *E. coli* cell is 2.22 μm and diameter 0.64 μm, and those of *L. innocua* cells are 1.26 μm and 0.52 μm, respectively (Supplementary Table S1), such a shell is estimated to consist of 10 to 20 layers of bacterial cells in its thickness. As shown in Fig. 2.3A and 2.3B, highly concentrated bacteria suspensions are extremely effective in dampening the incident UV-C irradiance. Therefore, it can be inferred that the high cell density of the outer shells of bacteria containing droplets is blocking UV-C and is effectively preventing the radiation from reaching the inner planktonic cells.

The thickness (up to 500 μm) of the liquid droplets forms a sharp contrast with the flat morphology of the dry bacteria pellets on SS surfaces, which are typically less than 20 μm thick (Fig. 2.5C). In the dry state scenario, both *E. coli* and *L. innocua* cell lawns exhibit rather homogenous distribution within the horizontal plane (Fig. 2.5D, top row) and dense packing in z direction (Fig. 2.5D, bottom row). The thickness of the bacteria pellet was estimated to contain 10-20 cells in the z direction, which is similar to the outer shell of droplets at the liquid-air interface in the wet scenario.

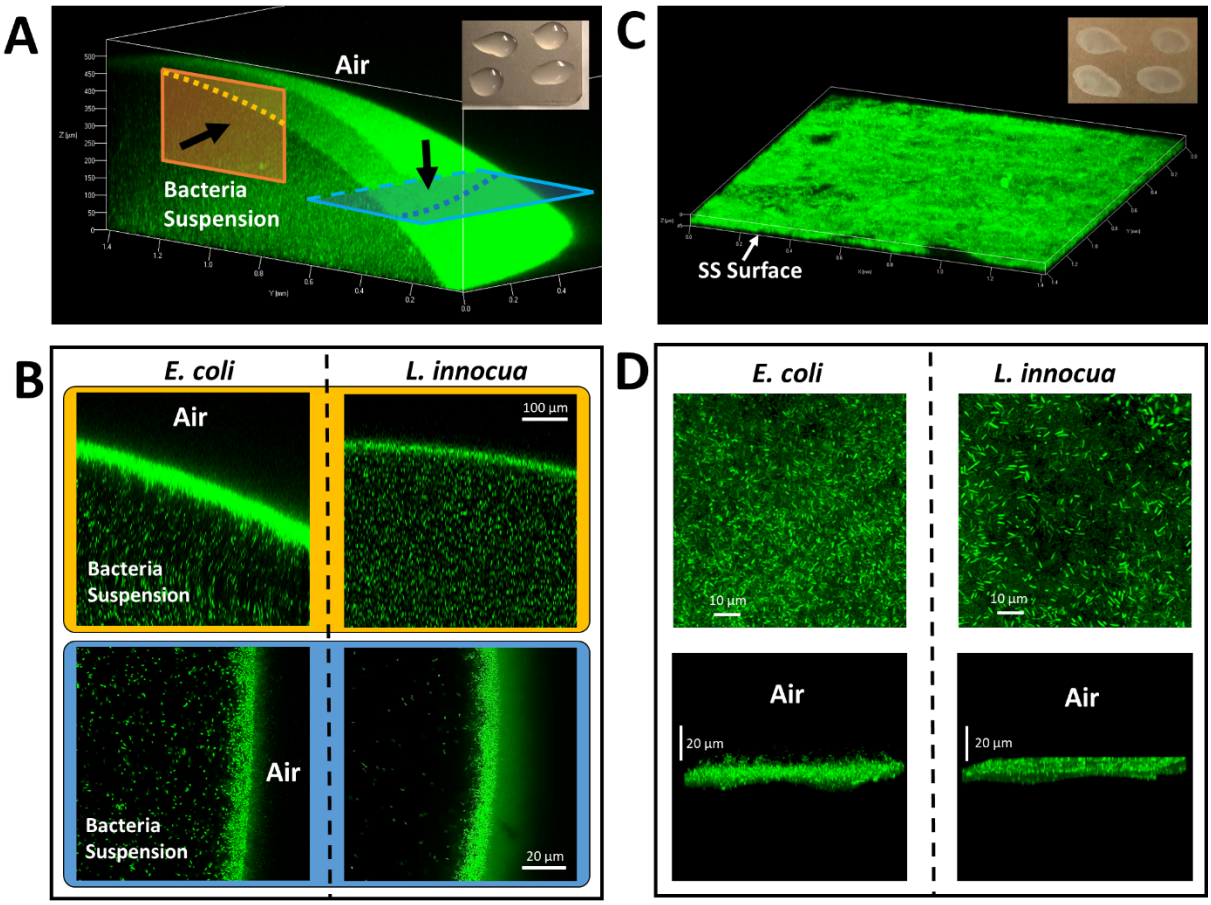

Figure 2.5. Distribution of untreated *L. innocua* and *E. coli* cells on SS coupons in the wet and the dry condition visualized using confocal microscopy. (A) and (C): typical macroscopic view of the fluorescent bacterial cells in the wet (A) and the dry (C) condition, with the insets showing the photos of the respective conditions. (B) Cross-sectional view of the top (yellow panel in (A)) and the side (blue panel) of typical bacteria-containing droplets on SS coupons in the wet condition. Black arrows denote the direction of observation. (D) Top-down view (top panel) and side view (bottom panel) of typical lawns of bacteria on SS coupons in the dry condition.

2.4.5 Effect of environmental conditions on the post-UV cell repair

To evaluate the potential repair of bacterial cells under environmental conditions representative of real-world applications, *L. innocua* on a SS coupon was first exposed to the UV-C LEDs, and subsequently subjected to various lighting and wetness conditions, and bacterial counts were determined after each treatment. Due to the large variability of the reactivation results, medians and interquartile range (depicted using a box-and-whisker plot) instead of means and standard deviations were used to represent the data, in order to avoid overall results being skewed by a few extreme values (Fig. 2.6). The experimental results

indicate that the median post-reactivation survival ratio (PRS) of *L. innocua* population was below 100%, regardless of the lighting and wetness conditions under which the reactivation process took place. It should be noted, however, that *PRS* > 100% did occur only rarely under certain reactivation conditions; more specifically: 3 out of the 11 biological replicates (i.e. 3/11) under the 'Dark'-'WET' condition, 3/11 under 'Amb'-'WET', 2/11 under 'Dark'-'DRY', and 1/8 under '405 H'-'DRY'. The '405 L' was the only lighting condition that did not result in *L. innocua* reactivation during the 6 h period in either the 'WET' (*PRS* range: 0.06% -30%) or 'DRY' (1% - 34%) conditions. This result is further substantiated by statistical analysis, which showed significantly lower *PRS* after reactivation under '405 L' than before ($p < 0.05$, Wilcoxon signed-rank test). The greatest variability in reactivation was observed under the 'Dark'-'Wet' conditions (*PRS* between 0.2% - 3556%). Because of the huge variability in data, no statistically significant differences among the medians from these eight reactivation conditions were found ($p = 0.25$, Kruskal-Wallis rank sum test).

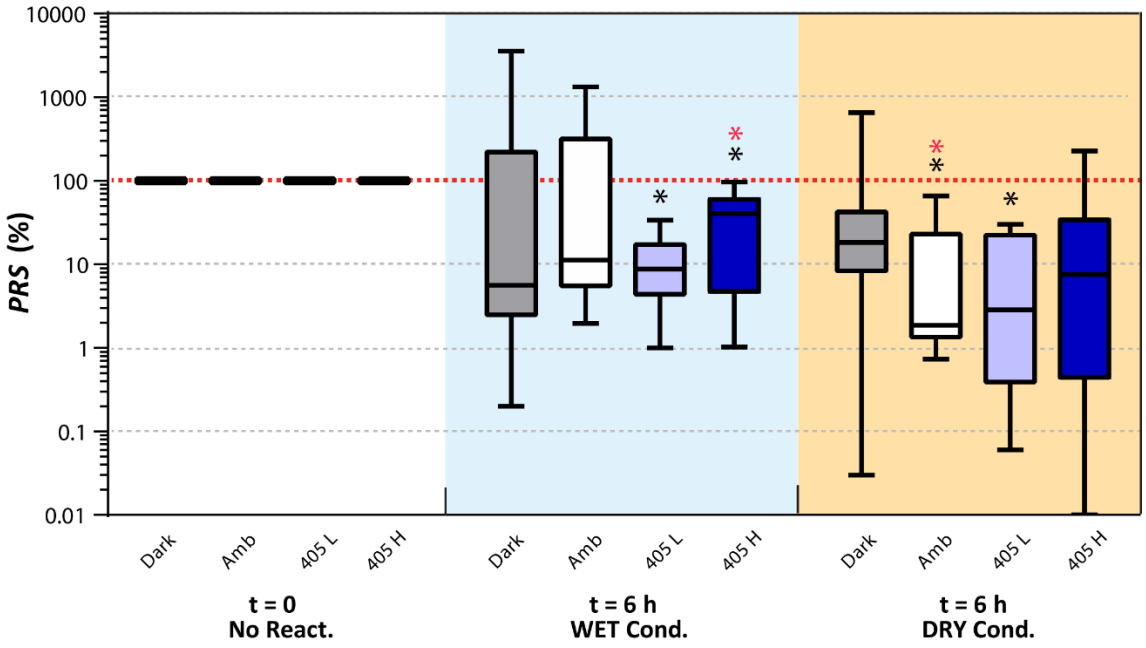

Figure 2.6. Post-reactivation survival rate of *L. innocua* in the dry or wet condition under various lighting conditions: dark, ambient light ('Amb'), low-intensity 405 nm LED ('405 L'), and high-intensity 405 nm LED ('405 H'). The lines dividing each box into two parts represent medians, top and bottom of the boxes represent upper and lower quartiles, and the upper and the lower whiskers represent the max and the min values, respectively. Black asterisks denote significant difference in PRS compared to '100%'

without adjusting for multiple comparison ($p < 0.05$); red asterisks denote significance after adjusting for multiple comparison ($p_{adj} < 0.05$).

2.5 Discussion

UV-C has been applied to reduce microbial load on many fresh food products, including fruits, vegetables, juices, water, other processed food products, and processing equipment surfaces (Akgün & Ünlütürk, 2017) (Sommers, Cooke, Fan, & Sites, 2009). Compared to traditional mercury UV lamps, UV-C LEDs were reported to accomplish higher levels of microbial inactivation at the same energy expenditure (Kim, Kim, & Kang, 2015). According to Kim et al., exposure to 266 nm UV-C LEDs resulted in over 5 log reduction in *E. coli* O157:H7 and *S.* Typhimurium, while only 1–2 log reductions were achieved using UV lamps at the same UV dose (Kim, Kim, & Kang, 2015). In this study, 5 log reduction of *E. coli* or *L. innocua* was achieved under a variety of surface conditions by exposure to UV-C fluence between 1 to 10 mJ/cm^2 (Fig. 2.2, Fig. 2.3 and Fig. 2.4). These values are comparable to inactivation levels reported previously for aqueous suspensions of bacteria of 6 -7 mm thickness, under constant stirring (Nyangaresi, 2018) (Rattanakul & Oguma, 2018). However, the fluence to achieve this level of inactivation was about 2 orders of magnitude higher than the fluence used to achieve similar inactivation values on agar surface by Kim *et al.* (Kim, Kim, & Kang, 2017). This difference could be caused by both the higher accessibility to UV-C of the bacteria on the smooth agar surface, and the lower bacterial cell concentration used by Kim *et al* compared to the current study.

When treating TLFs under static conditions, much higher inactivation efficiency was observed for the thinner TLFs than the thicker TLFs, at all fluence levels and for both microorganisms tested (Fig. 2.3B), which was attributed to the significant attenuation of UV-C irradiance by the thicker TLFs (Fig. 2.3D). Yet, despite the limited penetration depth of UV-C, up to 5 log reduction was achieved in the TLFs with thickness ≥1.2 mm (Fig. 2.3B). This suggests that there may be a constant movement of bacterial cells, either by passive diffusion or by active flagella propelled movement, which allows live cells to travel from the deep, low-exposure UV-C zone into the ‘deadly’ high-exposure zone. This can explain the high level of bacterial death within the thick, highly light-absorbing bacteria suspension.

One important insight provided by this data is that it is possible to tailor the UV-C treatment to improve its microbicidal efficiency, particularly for solid substrates. For instance, aqueous droplets tend to 'bead up' on hydrophobic surfaces, resulting in thick liquid morphologies that require high UV-C fluence for effective disinfection, particularly if the liquid is turbid. In such cases, removing the liquid before UV-C treatment, by drying or wiping the wet surface, can greatly improve the disinfection efficiency (Fig. 2.4). The caveat is that in the absence of liquid bacterial attachment to surfaces is enhanced, which may result in higher resistance to the UV-C treatment (Wong, Chung, & Yu, 2002) (Das, Bhakoo, Jones, & Gilbert, 1998).

Another important finding relates to cell repair after the UV-C treatment. It has been previously reported that photoreactivation of UV-C treated cells can occur after exposure to light in 300-500 nm wavelength range, due to repair of the UV damaged DNA (Harris, Dean Adams, Sorensen, & Curtis, 1987). In this study, there was no evidence of reactivation for cells exposed to 405 nm light post UV-C exposure, under either DRY and WET conditions (Fig. 2.6). It was previously reported that exposure to 280 nm UV LEDs significant repressed photoreactivation of *E. coli* (Li G. W., 2017) (Nyangaresi, 2018). In the present study, although both dark and light repair were observed for *L. innocua* exposed to 280 nm UV-C LEDs, the treatment caused irreversible damage to the bacterial cells. The 280 nm wavelength represents the peak absorbance for aromatic amino acids such as Tryptophan and Tyrosine (Stoscheck, 1990) (Felix Vajdos, Fee, Grimsley, & Gray', 1995). This allows 280 nm UV-C light to be absorbed by proteins, which eventually induces a higher level of deterioration of membrane proteins compared to shorter UV-C wavelengths (i.e. the traditional germicidal 254 nm) (Koutchma, Keller, Chirtel, & Parisi, 2004). In addition to DNA damage, 280 nm light can inflict ROS-mediated damage on multiple key bacterial targets, including membrane lipid peroxidation and respiratory enzyme activity (Kim & Dong-hyun, 2018), physical membrane destruction (Kim, Kim, & Kang, 2017), and loss of membrane potential (Kim, Kim, & Kang, 2017). All these lead to broad-target disruption and lower the likelihood of full restoration of all key cellular functions by light or dark reactivation reactions.

Another important finding of this work is that *E. coli* and *L. innocua* cells spontaneously form a shell-like structure at liquid-air interfaces that form when a droplet of bacterial suspension is deposited on a solid substrate (Fig. 2.5B), whereas after the removal of the suspending liquid the bacterial population is distributed homogenously onto the solid substrate (Fig. 2.5D, lower panels). These two distinct types of organization of bacterial community, along with the low penetration depth of UV-C in bacterial suspensions, as indicated by the sharp decline of $\boldsymbol{E}_{\lambda=280\text{nm}}$ in Fig. 2.3D, inevitably result in the very different UV-C irradiance distribution within a liquid droplet *vs* a liquid-less bacterial pellet. These in turn lead to substantial differences in inactivation kinetics in the two states for both *E. coli* (Fig. 2.4A) and *L. innocua* (Fig. 2.4B).

The deviation of inactivation kinetics on SS from the Weibull model under wet conditions, but not the dry conditions, for which an extremely good fit of the model was obtained (Fig. 2.4C and 2.4D), is rather intriguing. The Weibull model is well-suited for describing the inactivation kinetics of one bacterial population, with normally distributed susceptibility to a given stimulus (e.g. UV-C). (Peleg & Cole, 1998) In case of the wet SS coupons, the bacterial layers at the liquid-air interface function as a protective shell, effectively reducing the intensity of UV-C that is reaching the planktonic bacteria inside the liquid droplet. The co-existence of a population of packed cells exposed to high UV-C radiance, and a population of planktonic cells exposed to a much lower level of UV-C is likely the cause of the deviation of the experimental results on wet SS coupons from the predictions by the Weibull model (Fig. 2.4E and 2.4F). It should be noted that the agreement between the Weibull predictions and the results in TLFs is also very good (Table 2.1).

This study and previous studies prove the true potential of UV-C LEDs for bacterial inactivation, both in liquid and on solid substrates, and an exposure time of about 10 min is sufficient to achieve a 5-log reduction for the bacteria and disinfection scenarios tested here. Microbial contamination and growth are most problematic in certain hotspots where moisture and nutrients are readily accessible, and hence targeting UV-C treatment at these high-risk surfaces will be of highest practical advantage.

2.6 Conclusions

In this work, a proof-of-concept panel comprising an array of LEDs emitting UV-C of 280 nm wavelength was assembled, and its inactivation capability tested against surrogates for pathogenic *E. coli* and *L. innocua*, on substrate types frequently encountered in environmental, clinical, and food processing and handling environments. The tested UV-C LEDs demonstrated very promising surface disinfection efficiency in all the scenarios tested, with no detectable survivors for either strain after 5 min (or 11.9 mJ/cm^2) treatment on nutrient-rich surfaces, and 5-log reduction within 10 min (or 23.8 mJ/cm^2) on SS under both wet and dry conditions, and in TLFs of thickness less than 0.6 mm. UV-C inactivation of bacteria suspensions in liquid films thicker than 1.2 mm was much slower, due to the low penetration depth of UV-C through concentrated bacterial suspensions. Post UV-C treatment exposure to low-intensity 405 nm lighting provided consistent inhibition of reactivation.

This work also provides insights into how to select UV-C LED treatment parameters in order to achieve effective and efficient surface disinfection, with broad implications on the disinfection of both biotic and abiotic surfaces. With the advent of robotics and computer vision technologies, it is now possible to design LEDs-integrated robotics to deliver the appropriate level of UV-C energy to high-risk surfaces, in a targeted manner, which has the potential to be the more energy efficient and sustainable than traditional UV-C technology.

2.7 Acknowledgements

This work made use of the *Zeiss LSM 710 Confocal Microscope* at the Cornell University Biotechnology Resource Center Imaging Facility, supported by NIH S10RR025502. The authors would like to acknowledge support from *The* Cornell China Center for Innovations for funding the publication of this work. ASB would like to acknowledge COMEXUS for funding his research exchange program at Cornell University.

2.8 References

Abdul Karim Shah, N., Shamsudin, R., Abdul Rahman, R., & Adzahan, N. (2016). Fruit Juice Production Using Ultraviolet Pasteurization: A Review. *Beverages*, 3-22.

Akgün, M. P., & Ünlütürk, S. (2017). Effects of ultraviolet light emitting diodes (LEDs) on microbial and enzyme inactivation of apple juice. *Int. J. Food Microbiol.* , 65-74.

Amin, R., Bhayana, B., Hamblin, M., & Dai, T. (2016). Antimicrobial blue light inactivation of Pseudomonas aeruginosa by photo-excitation of endogenous porphyrins: In vitro and in vivo studies. *Lasers in Surgery and Medicine*, 562-568.

Bánáti, D. (2014). European perspectives of food safety. *Journal of the Science of Food and Agriculture*, 1941-1946.

Barnes, L.-M., Lo, M., Adams, M., & Chamberlain, A. (1999). Effect of milk proteins on adhesion of bacteria to stainless steel surfaces. *Applied and Environmental Microbiology*, 4543-4548.

Bhavya, M., & Hebbar, U. (2018). Efficacy of blue LED in microbial inactivation: Effect of photosensitization and process parameters. *International Journal of Food Microbiology*, 296-304.

Bintsis, T., Litopoulou-Tzanetaki, E., & Robinson, R. (2000). Existing and potential applications of ultraviolet light in the food industry - a critical review. . *Journal of the Science of Food and Agriculture*, 637-645.

Bjerkan, G., Witso, E., & Bergh, K. (2009). Sonication is superior to scraping for retrieval of bacteria in biofilm on titanium and steel surfaces in vitro. *Acta Orthop.*, 245-250.

Bower, C., McGuire, J., & Daeschel, M. (1996). The adhesion and detachment of bacteria and spores on food-contact surfaces. *Trends in Food Science & Technology*, 152-157.

Branas, C., Azcondo, F., & Alonso, J. (2013). Solid-state lighting: a system. *Industrial Electronics Magazine*, 6-14.

Chatterley, C., & Linden, K. (2010). Demonstration and evaluation of germicidal UV-LEDs for point-of-use water disinfection. . *J. Water Health* , 479–486 .

Chen, C.-J., Yao, J., Zhu, W., Chao, J.-H., Shang, A., Lee, Y.-G., & Yin, S. (2019). Ultrahigh light extraction efficiency light emitting diodes by harnessing asymmetric obtuse angle microstructured surfaces. *Optik*, 400-407.

Chen, C.-J., Yao, J., Zhu, W., Chao, J.-H., Shang, A., Lee, Y.-G., & Yin, S. (2019). Ultrahigh light extraction efficiency light emitting diodes by harnessing asymmetric obtuse angle microstructured surfaces. *Optik*, 400-407.

Cheng, Y., & Moraru, C. I. (2018). Long-range interactions keep bacterial cells from liquid-solid interfaces: Evidence of a bacteria exclusion zone near Nafion surfaces and possible implications for bacterial attachment. . *Colloids Surfaces B Biointerfaces* , 16-24.

Chmielewski, R. a., & Frank, J. F. (2003). Biofilm Formation and Control in Food Processing Facilities. . *Compr. Rev. Food Sci. Food Saf.*, 22-32.

Choudhary, R., & Bandla, S. (2012). Ultraviolet Pasteurization for Food Industry. *International Journal of Food Science and Nutrition Engineering*, 12-15.

Clancy, S. (2014). *DNA Damage & Repair: Mechanisms for Maintaining DNA Integrity*. Retrieved from Scitable by Nature Education: https://www.nature.com/scitable/topicpage/dna-damage-repair-mechanisms-for-maintaining-dna-344

D. L. Luthria, e. a. (2006). Content of total phenolics and phenolic acids in tomato (Lycopersicon esculentum Mill.) fruits as influenced by cultivar and solar UV radiation. *Journal of Food Composition and Analysis*, 771-777.

Dai T, G. A. (2013). Blue light rescues mice from potentially fatal Pseudomonas aeruginosa burn infection: efficacy, safety, and mechanism of action. *Antimicrobial Agents and Chemotherapy*, 1238–1245.

Dai, T., Gupta, A., Murray, C., Vrahas, M., Tegos, G., & Hamblin, M. (2012). Blue light for infectious diseases: Propionibacterium acnes, Helicobacter pylori, and beyond? *Drug resistance updates : reviews and commentaries in antimicrobial and anticancer chemotherapy*, 223-236.

Das, J. R., Bhakoo, M., Jones, M. V., & Gilbert, P. (1998). Changes in the biocide susceptibility of Staphylococcus epidermidis and Escherichia coli cells associated with rapid attachment to plastic surfaces. . *J. Appl. Microbiol.* , 852-858.

Donlan, R., & Costerton, J. (2002). Biofilms: Survival Mechanisms of Clinically Relevant Microorganisms. *Clinical Microbiology Review*, 167-193.

D'Souza, C., Yuk, H., Khoo, G. H., & Zhou, W. (2015). Application of Light-Emitting Diodes in Food Production, Postharvest Preservation, and Microbiological Food Safety. *COMPREHENSIVE REVIEWS IN FOOD SCIENCE AND FOOD SAFETY*, 719-740.

Eischeid, A., & Linden, K. (2011). Molecular indication of protein damage in adenoviruses after UV disinfection. *Applied Environmental Microbiology*, 1145-1147.

Enwemeka, C. W. (2009). Blue 470-nm light kills methicillin-resistant Staphylococcus aureus (MRSA) in vitro. *Photomedicine and Laser Surgery*, 221–226.

Faille, C. e. (2000). Influence of physicochemical properties on the hygienic status of stainless steel with various finishes. *Biofouling*, 261-274.

Felix Vajdos, ’. C., Fee, ’. L., Grimsley, ’. A., & Gray’, T. (1995). How to measure and predict the molar absorption coefficient of a protein. *Prorein Science* .

Feng, G., Cheng, Y., Wang, S.-y., Borca-Tasciuc, D. A., Worobo, R. W., & Moraru, C. (2015). Bacterial attachment and biofilm formation on surfaces are reduced by small-diameter nanoscale pores: how small is small enough? *npj Biofilms and Microbiomes*.

Feng, G., Cheng, Y., Wang, S.-Y., Hsu, L. C., Feliz, Y., Borca-Tasciuc, D. A., . . . Moraru, C. (2014). Alumina surfaces with nanoscale topography reduce attachment and biofilm formation by Escherichia coli and Listeria spp. *Biofouling: The Journal of Bioadhesion and Biofilm Research*, 1253-1268 .

Freitag, N., Port, G., & Miner, M. (2009). Listeria monocytogenes—from saprophyte to intracellular pathogen. *Nature Reviews Microbiology*, 623-628.

Ganz, R. A., Viveiros, Ahmad, Ahmadi, Khalil, Tolkoff, . . . Hamblin. (2005). Helicobacter pylori in patients can be killed by visible light. . *Lasers in Surgery and Medicine*, 260-265.

Gayán, E., Condón, S., & Álvarez, I. (2014). Biological Aspects in Food Preservation by Ultraviolet Light: a Review. *Food and Bioprocess Technology*, 1-20.

Ghate, V., Siang Ng, K., Zhou, W., Yang, H., Hoon Khoo, G., Yoon, W. B., & Yuk, H.-G. (2013). Antibacterial effect of light emitting diodes of visible wavelengths on selected foodborne pathogens at different illumination temperatures. *International journal of food microbiology*, 399-406.

Giuseppina, P., Sonia, B., Antonio, C., Lorenzo, M., Andrea, C., Ilaria, B., . . . Giorgio, G. (2019). Unraveling the Role of Red:Blue LED Lights on Resource Use Efficiency and Nutritional Properties of Indoor Grown Sweet Basil. *Frontiers in Plant Science* , 305.

Guffey, J. W. (2006). In vitro bactericidal effects of 405-nm and 470-nm blue light. . *Photomedicine and Laser Surgery*, 684–688.

Gupta, S. D., & Jatothu, B. (2013). Fundamentals and applications of light-emitting diodes (LEDs). *Plant Biotechnol Reports*, 211-220.

Hamblin, M. R., & Hasan, T. (2004). Photodynamic therapy: a new antimicrobial approach to infectious disease? *Photochemical & Photobiological Sciences*, 436-450.

Harris, G. D., Dean Adams, V., Sorensen, D. L., & Curtis, M. S. (1987). ULTRAVIOLET INACTIVATION OF SELECTED BACTERIA AND VIRUSES WITH PHOTOREACTIVATION OF THE BACTERIA. *Wat. Res* .

Held, G. (2009). Chapter 1: Introduction to LEDs. In: Introduction to Light Emitting Diode Technology and Applications. *Taylor & Francis Group, LLC*.

Hu, J., & Quek, P. (2008). Effects of UV radiation on photolyase and implications with regards to photoreactivation following low-and medium-pressure UV disinfection. . *Applied Environmental Microbiology*, 327-328.

Khan, M. S. (2005). III-nitride UV devices. *Janapense Journal of Applied Physics*, 7191-7206.

Kim, D., & Dong-hyun, K. (2018). Elevated Inactivation Efficacy of a Pulsed UVC Light-Emitting Diode System for Foodborne Pathogens on Selective Media and Food Surfaces. . *Food Microbiol.* , 1-14.

Kim, D., Kim, S., & Kang, D. (2017). Bactericidal effect of 266 to 279nm wavelength UVC-LEDs for inactivation of Gram positive and Gram negative foodborne pathogenic bacteria and yeasts. *Food research international*, 280-287.

Kim, S.-J., Kim, D.-K., & Kang, D.-H. (2015). Using UVC Light-Emitting Diodes at Wavelengths of 266 to 279 Nanometers To Inactivate Foodborne Pathogens and Pasteurize Sliced Cheese. *Applied and Environmental Microbiology*, 11-17.

Kondo, S., Tomiyama, H., Rodyoung, A., Okawa, K., Ohara, H., Sugaya, S., . . . Hirai, N. (2014). Abscisic acid metabolism and anthocyanin synthesis in grape skin are affected by light emitting diode (LED) irradiation at night. *Journal of plant physiology* , 823-829.

Koutchma, T., Keller, S., Chirtel, S., & Parisi, B. (2004). Ultraviolet disinfection of juice products in laminar and turbulent flow reactors. *Innov. Food Sci. Emerg. Technol.* , 179-189.

Li, G. W. (2017). Comparison of UV-LED and low pressure UV for water disinfection: Photoreactivation and dark repair of Escherichia coli. *Water Research*, 134-143.

Li, X., & Farid, M. (2016). A review on recent development in non-conventional food sterilization technologies. *Journal of Food Engineering*, 33-45.

Lobo, V. e. (2010). Free radicals, antioxidants and functional foods: Impact on human health. *Pharmacognosy reviews*, 118-126.

Maclean, M., MacGregor, S. J., Anderson, J. G., & Woolsey, G. (2008). High-intensity narrow-spectrum ligh inactivation and wavelength sensitivity of Staphylococcus aureus. *FEMS Microbiology Letters*, 227-232.

Maclean, M., MacGregor, S. J., Anderson, J. G., & Woolsey, G. (2009). Inactivation of Bacterial Pathogens following Exposure to Light from a 405-Nanometer Light-Emitting Diode Array. *APPLIED AND ENVIRONMENTAL MICROBIOLOGY*, 1932-1937.

Maclean, M., MacGregor, S., A. J., & Woolsey, G. (2008). The role of oxygen in the visible-light inactivation of Staphylococcus aureus . *Journal of Photochemistry and Photobiology B*, 180-184.

Minamata Convention on Mercury. . (2019, March 28). Retrieved from http://www.mercuryconvention.org/.

Moraru, C. I. (2009). Reduction of Listeria on Ready-to-Eat Sausages after Exposure to a Combination of Pulsed Light and Nisin. *AND*, 347-353.

Murdoch LE, M. M. (2012). Bactericidal effects of 405 nm light exposure demonstrated by inactivation of Escherichia, Salmonella, Shigella, Listeria, and Mycobacterium species in liquid suspensions and on exposed surfaces. *Scientific World Journal*, 1-14.

Nigro, F., & Ippolito, A. (2016). UV-C light to reduce decay and improve quality of stored fruit and vegetables: a short review. *Acta Horticulturae*, 293-298.

Nitzan, Y. M., Salmon-Divon, Shporen, E., & Malik, Z. (2004). ALA induced photodynamic effects on gram positive and negative bacteria. *Photochemical & Photobiological Sciences*, 430-435.

Nyangaresi, P. e. (2018). Effects of single and combined UV-LEDs on inactivation and subsequent reactivation of E . coli in water disinfection. *Water Research*, 331-341.

Pace, C. V. (1995). How to measure and predict the molar absorption coefficient of a protein. *Protein Science*, 2411-2423.

Park, S., & Kang, D. (2017). Influence of surface properties of produce and food contact surfaces on the efficacy of chlorine dioxide gas for the inactivation of foodborne pathogens. *Food Control*, 88-95.

Peleg, M., & Cole, M. B. (1998). Reinterpretation of microbial survival curves. . *Crit. Rev. Food Sci. Nutr.*, 353-380.

Proulx, J., Hsu, L., Miller, B., Sullivan, G., Paradis, K., & Moraru, C. (2015). Pulsed-light inactivation of pathogenic and spoilage bacteria on cheese surface. *Journal of Dairy Science*, 5890-5898.

Radetsky, L. C. (2018). *LED and HID Horticultural.* Troy: Lighting Research Center, Rensselaer Polytechnic Institute.

Rattanakul, S., & Oguma, K. (2018). Inactivation kinetics and efficiencies of UV-LEDs against Pseudomonas aeruginosa, Legionella pneumophila, and surrogate microorganisms. . *Water Research*, 31-37.

Richardson, C. (2008). Driving high-power LEDs in series-parallel. *National Semiconductor*, 45-49.

Sauer, A., & Moraru, C. I. (2009). Inactivation of Escherichia coli ATCC 25922 and Escherichia coli O157 : H7 in Apple Juice and Apple Cider , Using Pulsed Light Treatment. . *Journal of Food Protection*.

Shin, J., Kim, S., Kim, D., & Kang, D. (2016). Fundamental Characteristics of Deep-UV Light-Emitting Diodes and Their Application To Control Foodborne Pathogens. . *Appl. Environ. Microbiol.*, 2-10.

Sommers, C. H., Cooke, P. H., Fan, X., & Sites, J. E. (2009). Ultraviolet light (254 nm) inactivation of Listeria monocytogenes on frankfurters that contain potassium lactate and sodium diacetate. *J. Food Sci.* , 114-119.

Stoscheck, C. M. (1990). 50 GENERAL MEHODS FOR HANDLING PROTEINS AND ENZYMES. In *Quantitation of Protein. .*

SUDHIR K. SASTRY, A. K. (2000). Ultraviolet Light. In *Kinetics of Microbial Inactivation for Alternative Food Processing Technologies* (pp. 90-93). Journal of Food Science.

Takayoshi, T. e. (2017). Deep-ultraviolet light-emitting diodes with external quantum efficiency higher than 20% at 275 nm achieved by improving light-extraction efficiency. . *Appl. Phys. Express* .

Uesugi, A., Woodling, S., & Moraru, C. (2007). Inactivation kinetics and Factors of Variability in the Pulsed Light Treatment of Listeria innocua Cells. *Journal of Food Protection*, 2518-2525.

Venditti, T., & D'hallewin, G. (2014). Use of ultraviolet radiation to increase the health-promoting properties of fruits and vegetables. *Stewart Postharvest Review*, 10-13.

Vogler, E. (1998). Structure and reactivity of water at biomaterial surfaces. *Advances in Colloid and Interface Science*, 69-117.

Wang, Y., Wang, Y., Wang, Y., Murray, C., Hamblin, M., Hooper, D., & Dai, T. (2017). Antimicrobial blue light inactivation of pathogenic microbes: State of the art. . *Drug Resistance Updates*, 1-22.

Wong, H.-C., Chung, Y.-C., & Yu, J.-A. (2002). Attachment and inactivation of Vibrio parahaemolyticus on stainless steel and glass surface. . *Food Microbiol.* , 341-350.

Woodling, S. E., & Moraru, C. I. (2005). Influence of Surface Topography on the Effectiveness of Pulsed Light Treatment for the Inactivation of Listeria innocua on Stainless-steel Surfaces. . *J Food Sci* , 345-351.

World Health Organisation (WHO) Initiative for vaccine research. (2019). Retrieved from https://www.who.int/immunization/research/en/

Young, A. R. (2006). Acute effects of UVR on human eyes and skin. *Progress in Biophysics & Molecular Biology*, 80-85.

2.9 Supplementary Information

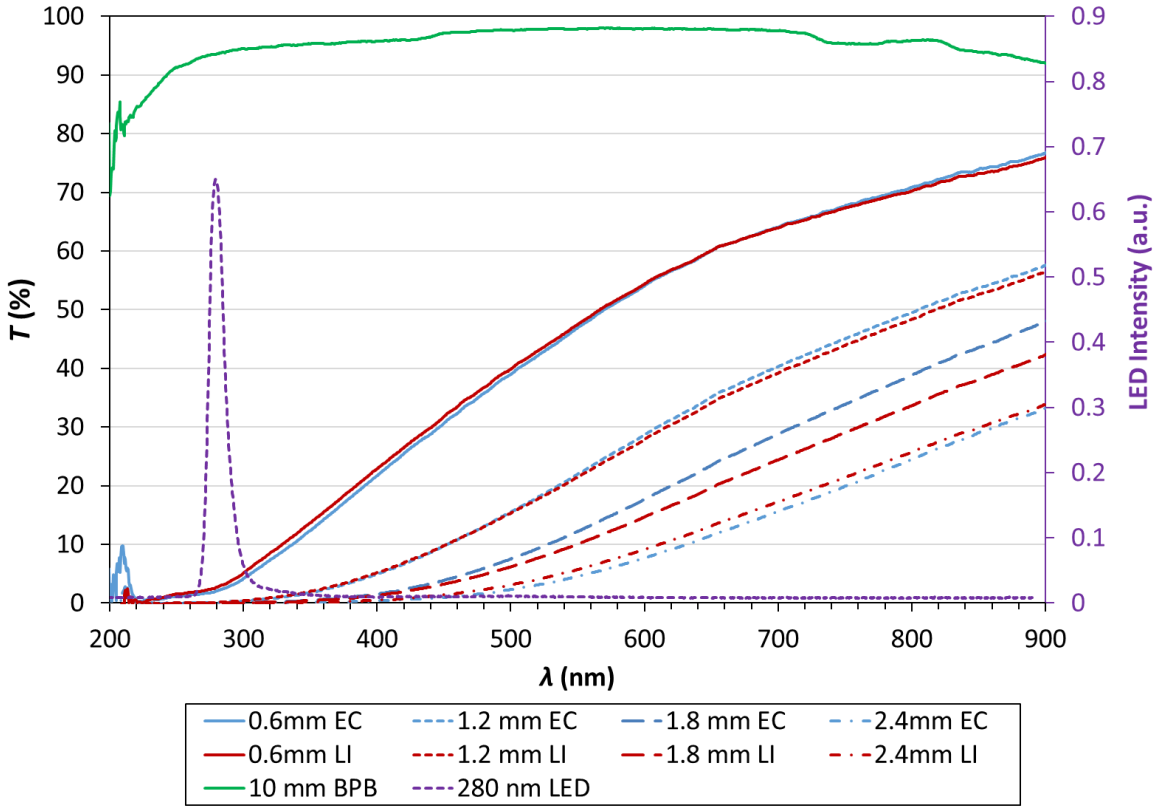

Figure S 1. Full transmittance spectra of *E. coli* (EC, blue) and *L. innocua* (LI, red) suspensions of various thickness, BPB medium, and the emission spectrum of the UV-C LED used in this work.

Table S 1. Summary of the bacterial cellular dimensions and contact angle values used in the thermodynamic model

Bacterial features	Mean ± SD for indicated bacteria strains		Reference
	E. coli ATCC 25922	*L. innocua* FSL C2-008	
Bacterial dimensions (μm) [a]			
Length - *l*	2.22 ± 0.29	1.26 ± 0.15	Hsu et al., 2013
Radius - *R*	0.32 ± 0.02	0.26 ± 0.02	
Contact angles (°) [b]			
Water	40.3 ± 1.1	46.5 ± 1.2	
Glycerol	70.7 ± 2.1	65.9 ± 2.3	Feng et al., 2014
Diiodomethane	56.9 ± 3.0	46.4 ± 1.7	

[a] Bacterial dimensions were measured on calibrated SEM images of cells on silica substrates

[b] Contact angles were measured on bacterial cell lawns collected on filter paper

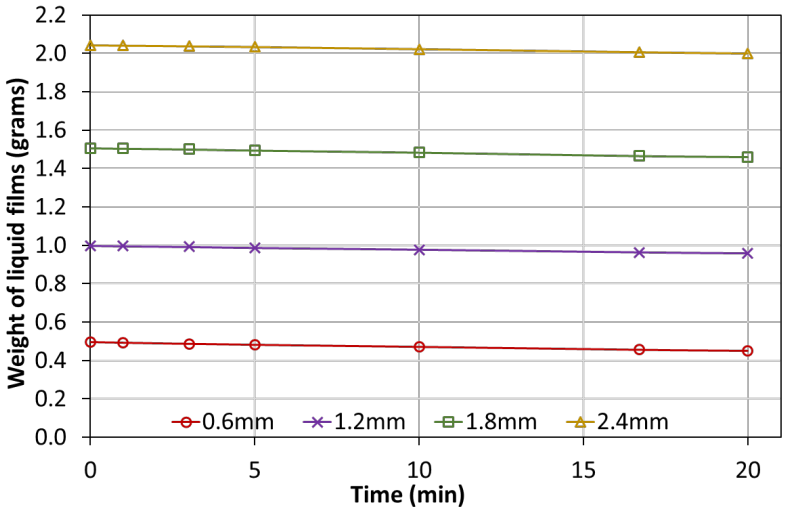

Figure S 2. Evaporation of thin liquid films of various thickness monitored as weight loss over time

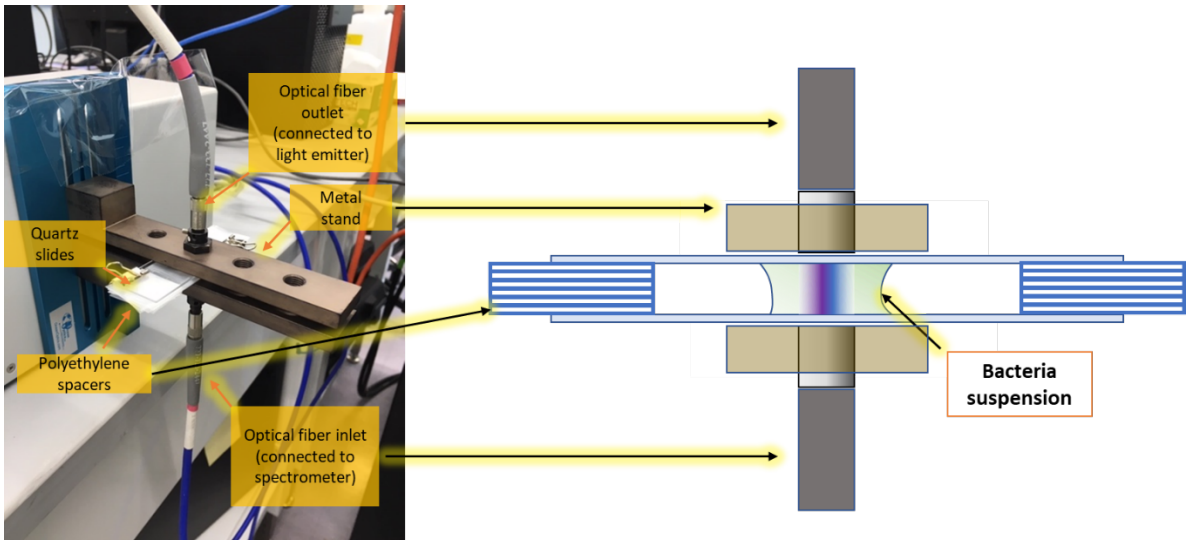

Figure S 3. Photographic and schematics illustration of the experimental setup for measuring UV-C transmittance. Thickness of the bacteria suspension was adjusted by changing the number of polyethylene spacers flanked by the quartz slides.

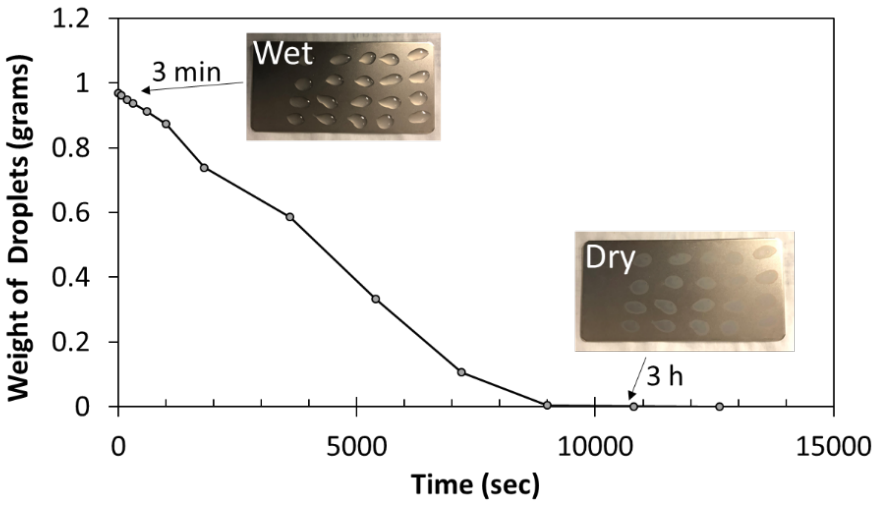

Figure S 4. Kinetics of drying of the inoculated SS coupons and selection of the dry and the wet conditions used for the UV-C LED inactivation experiments.

CHAPTER 3

Microbial inactivation by 405 nm blue light treatment

3.1 Abstract

Visible light of wavelengths centered around 405 nm has been reported to have antimicrobial effects, but the effectiveness under various substrate conditions is not fully unexplored. This study investigated the antimicrobial effectiveness of continuous 405 nm light emitting diode (LED) illumination against five food bacterial pathogens: *Escherichia coli* O157: H7, *Listeria monocytogenes*, *Pseudomonas aeruginosa, Salmonella* Typhimurium, and *Staphylococcus aureus* , both in thin liquid film (TLF) and on solid surfaces. Coupons of food grade stainless steel (SS), high density polyethene (HDPE), low density polyethene (LDPE), and borosilicate glass were used to mimic typical surfaces and disinfection scenarios encountered in food processing environments and clinical settings. Anodic aluminum oxide (AAO) coupons with different surface topography: nanosmooth, small nanopore (15nm), large nanopore (100nm) inoculated with bacteria were also exposed to 405 nm LEDs to evaluate the effect of surface modification on inactivation efficiency. All microbial inactivation curves followed non-linear kinetics, well represented by the Weibull model, The model better estimated inactivation on the solid surfaces, with $0.76 \leq R^2 \leq 0.99$ for TLF treatments and $0.89 \leq R^2 \leq 1.0$ for surface treatments. Exposure to 405 nm LED achieved over 5-log reduction of *P. aeruginosa* and *S. aureus* after 48h of exposure in TLF with a thickness of 1.2 mm. The fastest inactivation was observed on small nanopore (15nm) AAO coupons for *L. monocytogenes* and *S. aureus* after 12 h of treatment, indicating potential for inactivation enhancing properties of these surfaces. Besides demonstrating that 405 nm LEDs have great potential in inactivating diverse types of bacterial pathogens in liquid and on surfaces, this is the first study to investigate the effect of surface modification on antimicrobial efficacy of 405 nm LED treatment. The results of this work have immediate implications and demonstrates the potential of this technology for commercial applications in food processing and handling, domestic settings, as well as the and health care industry.

3.2 Introduction

Despite significant public and private investments mitigating bacterial transmission through foods, bacterial pathogens transmitted via certain foods, particularly raw foods, water, and various environmental sources remain a major cause of illness in both developed and developing countries. Ubiquitous gram-negative pathogenic bacteria such as *Escherichia*, *Salmonella*, and *Pseudomonas* continue to cause diarrheal and chronic infections worldwide (World Health Organisation (WHO) Initiative for vaccine research, 2019). Gram positive pathogens such as *Listeria monocytogenes* also has significant impact on health ; *L. monocytogenes* is particularly feared in the food sector since it can grow at low temperatures and cause illness in immunocompromised individuals (Freitag, Port, & Miner, 2009).

The methods commonly used for inactivation of pathogenic microorganisms include thermal treatments and use of antimicrobials for foods, or the use of sanitizers for food contact surfaces. While some of these treatments are effective, they also have limitations and may also have undesired effects on food quality and the environment. Considerable efforts have been put in recent years to develop novel approaches to prevent and/or mitigate contamination with pathogenic bacteria. Such efforts to find new methods of disinfection and decontamination are also made in hospital environments, where the occurrence of antibiotic / antimicrobial resistant bacterial strains has become a significant concern.

Such alternative methods of microbial inactivation include continuous Ultraviolet light (UV) and Pulsed Light (PL) treatments, both inducing DNA damage primarily as a result of UV absorption by bacterial DNA at wavelengths between 240 nm and 280 nm. However, limitations such as low efficiency of light sources, inability to design systems that offer three dimensional exposure of complex ad large objects, as well as low efficiency at refrigerated temperatures of the light sources and detrimental effects of UV to mammalian cells, restrict the use of these technologies (Kim, Kim, & Kang, 2015) (Young, 2006). Thus, there is a need for the development of a safe, non-UV, chemical-free decontamination technology for reducing or eliminating microbial contamination for applications in food industry and clinical environments.

In this contexts, light emitting diode (LED) emitting in the visible wavelength have been reported to have antimicrobial effect on a range of bacterial pathogens (Maclean M. , MacGregor, Anderson, & Woolsey, 2009). Particularly, blue light with wavelength ranging from 405 nm to 470 nm has been reported to have higher inactivation effects compared to other regions of visible light; light in this range stimulates endogenous microbial porphyrin molecules to produce oxidizing reactive oxygen species (ROS), predominantly singlet oxygen ($^1O_2$), which damage microbial cells, leading to their death (Ghate, et al., 2013) (Maclean M. , MacGregor, Anderson,, & Woolsey, 2008).

For example, previous work has demonstrated that *Staphylococcus aureus* can be photodynamically inactivated by 56 and 90% using 400 to 420 nm visible light, with a peak inactivation at 405 nm (Maclean M. , MacGregor, Anderson, & Woolsey, 2008). Blue LEDs have shown antimicrobial effect on both Gram-negative and Gram-positive bacteria, with a general trend showing Gram-positive species to be more susceptible than Gram-negative bacteria. Gram-positive *L. monocytogenes* reached 5-$\log_{10}$ reduction after exposure to a light dosage of 108 J/cm^2 while the Gram-negative *E. coli* reached similar reduction at a significantly higher light dosage of 288 J/cm^2 (Murdoch LE, 2012).

Scenarios of static, undisturbed liquids on various surfaces (e.g. droplets and/or thin layers of liquid) are ubiquitous in both food and health care industry, but knowledge of the effectiveness on blue LED on bacterial inactivation under such conditions is limited. To our best knowledge, no study has been conducted to explore the effect of surface condition and properties on the microbial inactivation efficiency of blue LED treatment. To address this gap, the present study investigates the effect of 405 nm LEDs exposure on several foodborne pathogens both in liquid suspensions and on various surfaces, at refrigerated temperatures. Inactivation data as a result of exposure to 405 nm LED treatment for both Gram-positive bacteria (*L. monocytogenes* and *S. aureus*) and Gram-negative bacteria (*E. coli, S.* typhimurium*, P. aeruginosa*) of relevance in food and healthcare industries was obtained and compared. The chosen substrates represent common food-contact materials with various physical properties. In addition, the effect of nanoscale surface modifications on treatment efficiency was also investigated.

3.3 Materials & Methods

3.3.1 Bacterial Cultures

The bacterial strains used in this study were *Listeria monocytogenes serotype 1/2a strain* 10493s*, Escherichia coli serotype* O157:H7 ATCC43895*, salmonella* Typhimurium *FSL S90123, Staphylococcus aureus* ATCC9144*,* and *Pseudomonas aeruginosa* ATCC15442. Prior to the experiments, all cultures were streaked onto tryptic soy agar (TSA) from the frozen stock (-80 ℃) and incubated for 24 h at 37 ℃. A single isolated colony was then transferred into 3mL of tryptic soy broth (TSB) for passage one (37 ℃, 24h). 30 μL of grown passage one culture was transferred to fresh 3mL TSB for passage two (37 ℃, 18h). Bacteria suspension in early stationary phase was centrifuged at 5000 RPM for 10 minutes at 21 ℃, and the pellet was resuspended in Butterfield Phosphate Buffer (BPB, pH=7.2) for three times total to ensure minimal remnants of TSB in the final bacteria suspension. The initial inoculum level was about 10^9 CFU/mL for all strains.

3.3.2 405nm LED Treatment Rig

All inactivation experiments were performed using a Vital Vio VVLD22® LED unit. This apparatus has a rectangular LED array that delivers monochromatic light with an output emission bandwidth at 405 nm (14 nm FWHM) . To prevent any heating of the tested samples by exposure to the LED source, and to mimic inactivation under refrigeration conditions, ,, the LED rig was kept in a 4 ± 2 ℃ low temperature incubator, at all times. The rectangular LED array (60.3 cm x 8.48 cm) was set in a fixed position 27.5 cm directly above the target surfaces to provide a good balance between intensity of irradiance and the homogeneity of the light distribution. The LED unit was powered by a DC power supply (120-277 V), giving an approximate irradiance of 0.5 mW/cm^2 at the targeted surfaces. Several treatment durations were chosen to deliver different cumulative dosage of 405 nm light: 4h, 8h, 12h, 24, 36h, 48h, corresponding to cumulative fluences of 7.2 mJ/cm^2, 14.4 mJ/cm^2, 21.6 mJ/cm^2, 43.2 mJ/cm^2, 64.8 mJ/cm^2, and 86.4 mJ/cm^2, respectively.

3.3.3 Bacterial Inactivation by 405nm LED on Various Substrates

3.3.3.1 Inactivation in thin liquid films

To mimic contaminated standing water in food processing environments, 1mL of bacteria suspension was transferred into Nunc Lab-Tek™ II 1 well Chamber Slide™ (17 mm x 48 mm, Fisher Scientific, Rochester, NY), in the form of a thin liquid film. Prior to use these chambers were soaked in 70% ethyl alcohol for 24 h for decontamination, followed by 2 h of drying in a biosafety cabinet to evaporate the remaining ethyl alcohol. The bacteria suspensions were allowed to equilibrate for 3 min prior to the 405 nm light exposure. To reduce the effect of excess drying on inactivation efficiency, all chambers were sealed with transparent, non-light absorbing Low Density Polyethylene (Uline, Waukegan, IL) during the light treatment. The inactivation kinetics of 405 nm LED treatment on *E. coli, L. monocytogenes, S. aureus, P. aeruginosa,* and *S.* Typhimurium were all investigated by exposing 1 mL of bacteria containing liquid film (thickness = 1.2 mm) for the durations specified previously, excluding the 8h duration. The survivors from both 405 nm light treated, and untreated control samples were enumerated using the standard plate counting method on TSA agar. Plates were incubated at 37 ℃ for 24 h, after which the survivors were enumerated, and results reported as CFU/mL. Log reduction was calculated using the following equation:

$$Log\ Reduction = Log_{10}N/N_0 \qquad \text{Eqn. 3.1}$$

Where N_0 and N are bacterial cunts (in colony forming units per mL of suspension) before and after 405 nm light treatment, respectively. The detection limit for all strains in TLF experiments was 10 CFU/mL of bacteria suspension. All 405 nm LED treatments were performed in triplicate, with independently grown bacterial cultures.

3.3.3.2 Treatment of solid food contact surfaces

Rectangular (1 x 2.5 cm) coupons of the following materials were used: high density polyethylene (HDPE) (6.45 mm thickness; Regal Plastics, Dallas, TX), low density polyethylene (LDPE) (0.14 mm thickness, Uline, Waukegan, IL), food-grade soda-lime glass (0.96 mm thickness, Fisher Scientific, Rochester, NY), food-grade stainless steel with glass bead blast finish (SS) (1.45 mm thickness, Fountain Valley, CA). Prior

to inoculation, all coupons were sequentially sonicated (40 kHz, Branson 1210 Ultrasonic Cleaner, Branson Ultrasonics, Danbury, CT) in acetone (95%, Fisher Scientific, Rochester, NY), ethyl alcohol (95%), and deionized water, for 15 min at each step to remove surface contaminants and potential microbial contamination. The cleaned coupons were then rinsed with sterile deionized water and dried at room temperature in a biosafety cabinet. A total of 1 µL bacteria suspension was aliquoted on the coupon surfaces. The inoculated coupons were placed in sterile polystyrene Petri dishes (Fisher brand, Pittsburgh, PA) and left in the laminar flow hood (23 ℃, hood humidity = 17%) for 3 hours to equilibrate and reach a constant weight without excessive drying. During the 405 nm light treatment, all coupons were covered with 405 nm light transmitting Low Density Polyethylene of 0.14 mm thickness (Uline, Waukegan, IL) to prevent excessive drying.

To recover the bacteria from treated surfaces, all treated coupons were individually placed in sterile Whirl-Pak bags with 10 mL BPB and sonicated for 5 min at 40 kHz (Branson 1210 Ultrasonic Cleaner, Branson Ultrasonics, Danbury, CT). Samples were then taken from the resulting BPB. The same recovery procedure was also used for the control groups. Log reduction results were calculated using Eq. 3.1. The detection limit of the inactivation experiments on all coupon surfaces was 100 CFU per coupon for all strains. Technical duplicates were performed on each coupon and all LED treatments were performed in triplicate, with independently grown bacterial cultures.

3.3.3.3 Treatment of anodic aluminum oxide coupons

Nanoporous anodic aluminum oxide (AAO) surfaces with pore diameters of 15 and 100 nm were prepared by two-step anodization of high purity aluminum (99.99%, Alfa Aesar, Ward Hill, MA), as described before (Feng G. , et al., 2014). The Al substratum was first subjected to mechanical and electrical polishing, with an intermediate annealing step to release internal stresses. The Al substratum was then immersed in an etchant to remove the alumina layer formed during the electrochemical polishing. The first anodization step was then carried out in room temperature using a setup similar to the one used for electrochemical polishing. The voltage and anodizing mixture depended on the pore size. The first porous alumina layer was etched

away, and the second anodization procedure was performed, during which pore growth was initiated from dents left over by the nanopores in the first layer, resulting in regular surface features. Nanosmooth aluminum oxide surfaces of 1 x 2.5 x 0.5 mm (Alfa Aesar) were used as control here. It is also important to note that aluminum oxide (alumina) is a generally recognized safe (GRAS) material.

3.3.4 Modelling of inactivation kinetics

The kinetics of microbial inactivation by the 405nm LED treatment was modelled using the Weibull model (Uesugi, Woodling, & Moraru, 2007):

$$\log_{10}(N/N_0) = \alpha t^{\beta} \qquad \text{Eqn. 3. 2}$$

Where N/N_0 represents the ratio of survivors after treatment over the initial population, α is the scale parameter and β is the shape factor, which describes the concavity or convexity of the inactivation curves.

3.3.5 Physical property analysis of the coupons

To measure surface hydrophobicity, water contact angle measurements were performed using a Ramé-Hart 500 Advanced Goniometer/Tensiometer (Ramé-Hart Inc., Succasunna, NJ) with reagent grade deionized water at room temperature on cleaned and sterilized coupons, as described before (Proulx, et al., 2015). The data was analyzed using the instrument's DROPimage software. All measurements were performed in triplicate and average values of contact angles were used as a measure of surface hydrophobicity. Contact angle values smaller than 65° indicate a hydrophilic surface, and values larger than 65° indicate a hydrophobic surface (Vogler, 1998). This measurement of hydrophobicity was used to evaluate the tendency for surface spreading of the liquid inoculum.

Surface roughness of all substrates was measured using a Keyence VK-X260 Laser-Scanning profilometer at the Cornell Center for Materials Research (Ithaca, NY). The following roughness parameters were determined: S_a, the extension of R_a (arithmetical mean height of a line) to a surface, which expresses the average roughness, and represents the difference in height of each point compared to the arithmetical mean; and S_z, the sum of the largest peak height value and the largest pit depth value within the defined area.

Measurements were conducted on a 5 mm length of the sample, which was scanned with an applied stylus force of 4.47 mg. Triplicate measurements were performed for each material.

3.3.6 Statistical analysis

Mean values of data were obtained from three independent trials, with technical duplicates. Analyses of variance and post hoc Tukey's HSD were used evaluate differences in log reduction, Weibull kinetic parameters, and physical properties among materials and different treatment levels. A confidence level of 95% was adopted for all statistical tests. All statistics analyses were performed using Minitab software release 19.

3.4 Results

3.4.1 Inactivation of bacteria in thin liquid films

Liquid bacterial suspensions, each with an initial population density of 10^9 CFU/mL, were exposed to 405 nm LED treatments at an irradiance of 0.5 mW/cm^2 for time periods of up to 48 h (86.4 J/cm^2). The inactivation kinetics of *E. coli*, *L. monocytogenes*, *S.* Typhimurium, *S. aureus* and *P. aeruginosa* with TLF thickness of 1.2 mm were determined and used to compare the responses of Gram-positive and -negative bacteria to 405 nm LED treatment. As shown in Fig.3.1, the overall results demonstrate that the viability of all tested pathogens treated with 405 nm LEDs decreased nonlinearly with treatment time. A 48h exposure time to blue LED resulted in 1.3- to 5.8-log reduction inactivation, with *E. coli* being the least susceptible and *P. aeruginosa* being the most susceptible strain to the treatment. The reductions of all five strains were similar for a cumulative dose of less than 7.2 J/cm^2 (4h) ($p>0.05$). At higher cumulative doses, *S. aureus* and *P. aeruginosa* became significantly more susceptible to the 405 nm LED treatments, eventually reaching 5-log reduction and 5.8-log reduction, respectively. No significant difference in inactivation kinetics was observed among *E. coli*, *L. monocytogenes*, and *S.* Typhimurium for cumulative dose of 64.8 J/cm^2 (4h) and less. *L. monocytogenes* showed higher inactivation during the last 12h of exposure, and eventually reached a higher log reduction than the other strains. Significant differences in log-reduction values between any two strains were found at fluence levels of 21.6 J/cm^2 and higher ($p < 0.05$).

Among TLFs with the thickness of 1.2 mm, *E. coli* was the least susceptible to 405 nm LED treatments than the other strains, at any fluence level. This result was further corroborated by the Weibull model parameters (Table 3.1), with the shape parameter of the *E. coli* inactivation curve being the smallest among the rest. Overall, the TLF experimental data showed a good fit with the Weibull model, with : $0.76 \leq R^2 \leq 0.99$.

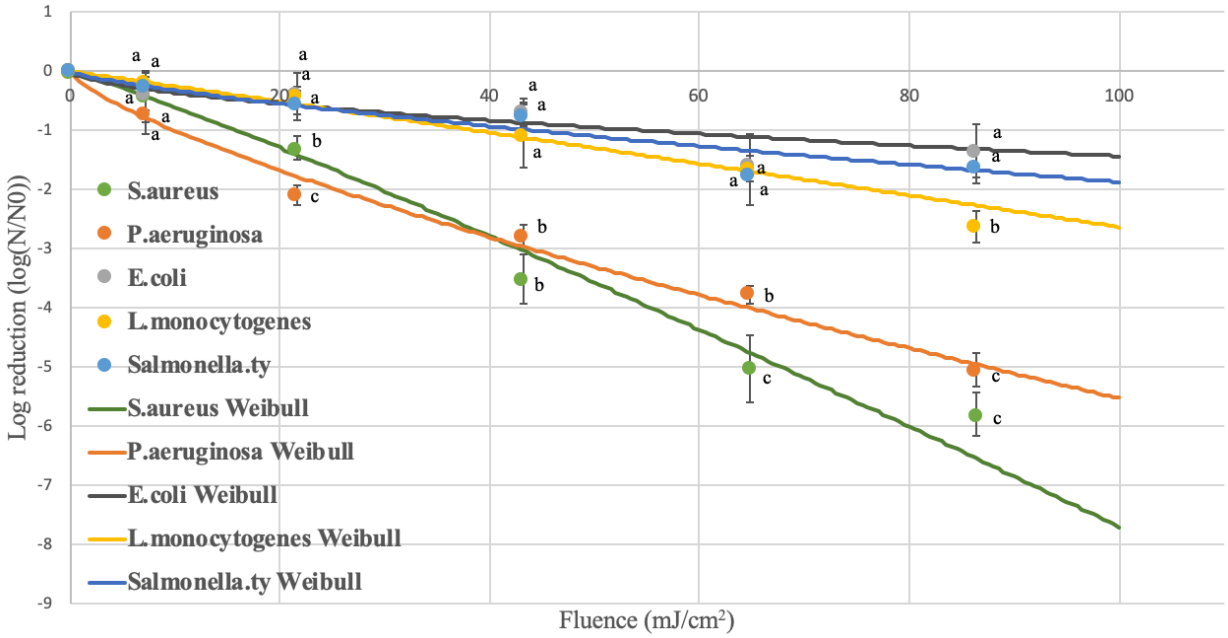

Figure 3. 1. Inactivation of *E. coli, L.monocytogenes, S.* Typhimurium*, P. aeruginosa, S. aureus* in liquid suspension by exposure to continuous 405 nm LEDs of an irradiance of approximately 0.5 mW/cm^2 *. *Values within the same treatment level followed by the same letter are not significantly different from each other ($p>0.05$).

Table 3. 1. Weibull model parameters for the 405 nm LED inactivation kinetics of *E. coli*, *L. monocytogenes*, *S.* Typhimurium, *S. aureus* and *P. aeruginosa* suspended in thin liquid film of 1.2 mm thickness. Values represent means ± standard deviations from three replicates.

Bacterial Strain	Scale Parameter, α	Shape Parameter, β	R^2
E. coli	0.09±0.09	0.60±0.39	0.77
L. monocytogenes	0.02±0.02	1.02±0.33	0.98
S. Typhimurium	0.06±0.06	0.76±0.35	0.94
S. aureus	0.05±0.06	1.11±0.48	0.99
P. aeruginosa	0.18±0.12	0.74±0.19	0.98

3.4.2 Inactivation of bacteria on solid substrates

Results of the 405 nm LED inactivation of *E. coli* and *L. monocytogenes* spread onto various solid substrates are reported in Fig.3.2 and Fig.3.3. Significant reduction of both *E. coli* and *L. monocytogenes* was obtained on all materials, at each applied fluence level ($p < 0.05$). In the case of *E. coli*, the bacterial population counts were reduced below the limit of detection (100 cells/coupon) after 86.4 J/cm^2 cumulative dose (48h exposure), on all substrates. The reduction for *E. coli* suspended on AAO coupons experienced fast initial inactivation within the first 43.2 J/cm^2 (24h) of exposure, followed by a gradual plateau up to 86.4 J/cm^2 cumulative dose (48h exposure). *E. coli* on 100 nm AAOs had the lowest overall log reduction (3-log$_{10}$ CFU/mL at 86.4 J/cm^2 fluence level) and the inactivation curve tapered off earlier than on 15nm and NS AAOs. This was also reflected by the smaller Weibull shape and scale parameters (Table 3.2). For *E. coli* spread on SS, HDPE, LDPE, and glass surfaces, the reduction by blue LED was fast, resulting an almost linear trend; no visible plateau was detected within the treatment period.

The exposure to blue LED resulted 3- to 5.5-log reduction of *E. coli* on solid substrates, with susceptibility decreasing in the following order: SS > LDPE > HDPE > Glass > NS AAO > 15nm AAO > 100nm AAO. The highest treatment susceptibility of SS is also reflected by the highest Weibull shape parameter on this substrate (Table 3.2). Nonlinear regression of calculated vs values predicted using the Weibull model for *E. coli* on solid substrates showed good conformity: $0.93 \leq R^2 \leq 0.99$.

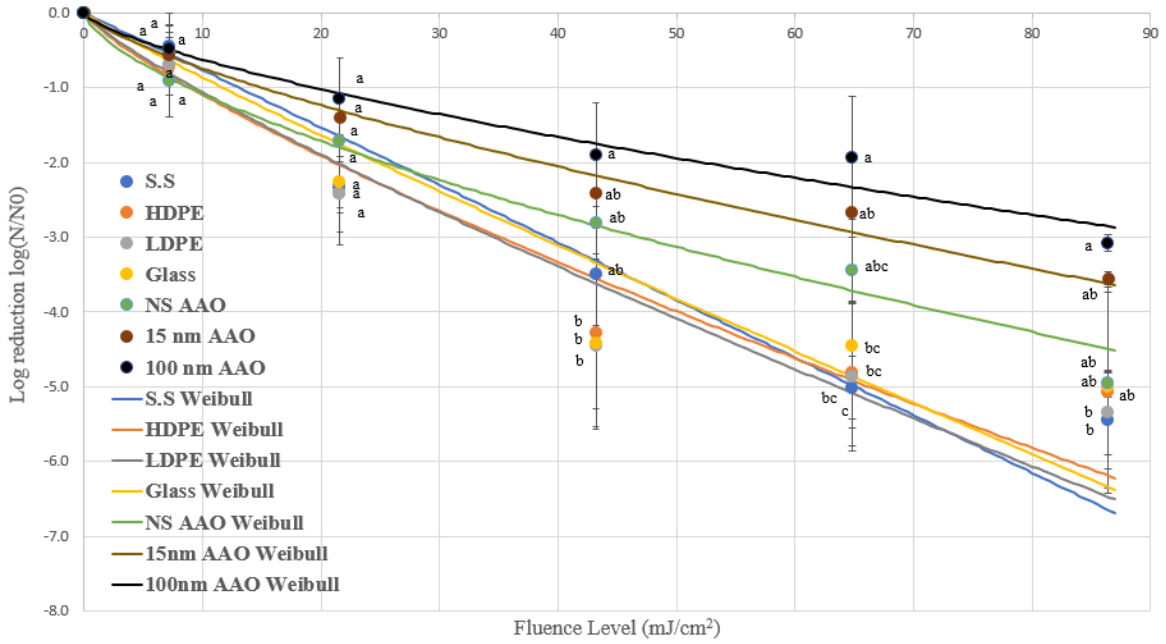

Figure 3. 2. Inactivation of *E. coli* spread on solid substrates by exposure to continuous 405 nm LEDs of an irradiance of approximately 0.5 mW/cm^2. Substrates include stainless steel (SS), high density polyethene (HDPE), low density polyethene (LDPE), food-grade borosilicate glass (Glass), and anodic aluminum oxide with different nanotopograohy: nanosmooth (NS AAO), small nanopore (15nm AAO), large nanopore (100nm AAO) *. *Values within the same treatment level followed by the same letters are not significantly different (p>0.05).

Table 3. 2. Weibull model parameters for the 405 nm LED inactivation kinetics of *E. coli* spread on various solid substrates. Values represent means ± standard deviations from three replicates.

Solid Substrates	Scale Parameter, α	Shape Parameter, β	R^2
SS	0.08±0.27	1.00±0.31	0.95
HDPE	0.17±0.16	0.80±0.24	0.95
LDPE	0.15±0.32	0.84±0.59	0.95
Glass	0.10±0.14	0.92±0.48	0.93
NS AAO	0.24±0.05	0.66±0.06	0.99
15nm AAO	0.14±0.08	0.73±0.16	0.99
100nm AAO	0.12±0.11	0.70±0.21	0.97

Compared to *E. coli*, the inactivation of *L. monocytogenes* suspended on solid substrates experienced a much faster decrease under exposure to blue LED. The bacterial population counts were reduced below the limit of detection (100 cells/coupon) after 21.6 J/cm^2 cumulative dose (12h exposure), on all substrates. Exposure to 405 nm LEDs resulted 2.7- to 5.0-log reduction of *L. monocytogenes* on solid substrates, with

the susceptibility decreasing in the following order: 15nm AAO > Glass > NS AAO > 100nm AAO > HDPE > SS > LDPE. The inactivation curves for *L. monocytogenes* on SS, HDPE, LDPE have showed a concave down trend, with a slower inactivation for cumulative dose of 14.4 J/cm^2 (8h) and lower, followed by a fast reduction, eventually reaching ~3-log reduction at 21.6 J/cm^2 cumulative dose (12h exposure). Glass and AAO surfaces showed almost linear reduction, and the inactivation of *L. monocytogenes* on these four substrates reached 4.5-log$_{10}$ reduction and no visible plateau within duration of the treatment. For inactivation of *L. monocytogenes* on solid substrates, small nanopore AAO (15nm) is shown to be the most susceptible substrate to the 405 nm LED treatment within the 12h treatment period. The inactivation kinetics of *L. monocytogenes* on solid substrates was successfully modeled (0.89≤ R^2≤1.0) by nonlinear regression using the Weibull model (Table 3.3), and the the Weibull model predicted further linear reduction for an extended treatment time..

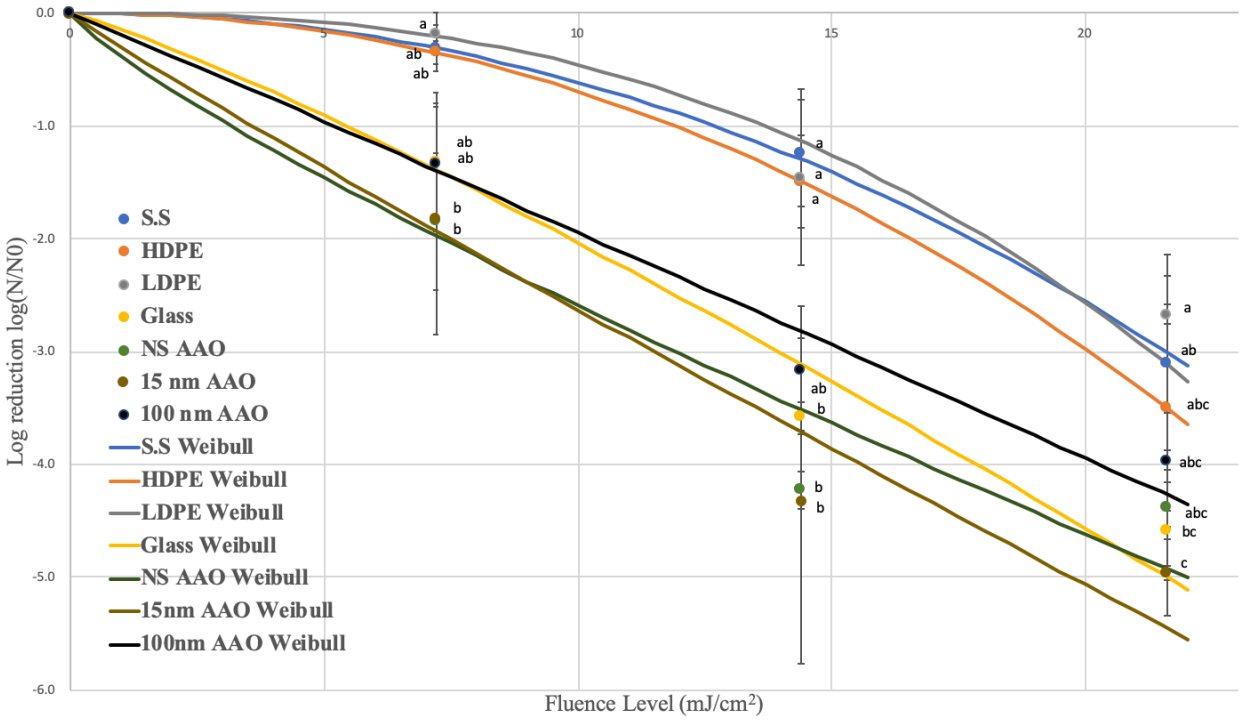

Figure 3. 3. Inactivation of *L. monocytogenes* on solid substrates by exposure to continuous 405 nm LEDs of an irradiance of approximately 0.5 mW/cm^2. Substrates include stainless steel (SS), high density polyethene (HDPE), low density polyethene (LDPE), food-grade borosilicate glass, and anodic aluminum oxide with different nanotopograohy: nanosmooth (NS AAO), small nanopore (15nm AAO), large

nanopore (100nm AAO) *. *Values for the same treatment level followed by the same letters are not significantly different ($p>0.05$).

Table 3. 3. Weibull model parameters for the 405 nm LED inactivation kinetics of *L. monocytogenes* on various solid substrates. Values represent means ± standard deviations from three replicates.

Solid Substrates	Scale Parameter, α	Shape Parameter, β	R^2
SS	0.01±0.01	2.07±0.60	1.00
HDPE	0.01±0.01	2.11±0.61	1.00
LDPE	0.00±0.00	2.49±1.31	0.98
Glass	0.14±0.16	1.17±0.60	0.97
NS AAO	0.38±0.35	0.83±0.43	0.89
15nm AAO	0.30±0.53	0.95±0.40	0.94
100nm AAO	0.19±0.28	1.02±0.41	0.97

Inactivation of *S. aureus* suspended on anodic aluminum oxide (AAO) coupons was also investigated. Like *L. monocytogenes*, the bacterial population counts of *S. aureus* were reduced below the limit of detection (100 cells/coupon) after 21.6 J/cm^2 cumulative dose (12h exposure), on all substrates. The inactivation curve of *S. aureus* showed a concave down trend, also reflected by an Weibull shape parameter $\beta > 1$ for all tested AAO surfaces (Table 3.4). The inactivation of *S. aureus* on all AAO surfaces experienced a slower reduction within the first 7.2 J/cm^2 cumulative dose, followed by fast reduction. A 12 h exposure to 405 nm LED treatment (21.6 J/cm^2 cumulative dose) resulted in 4.5- to 5.4-log reduction on AAO surfaces with different pore sizes. The nonlinear regression of the data using the Weibull model presented excellent conformity: $0.94 \leq R^2 \leq 0.99$.

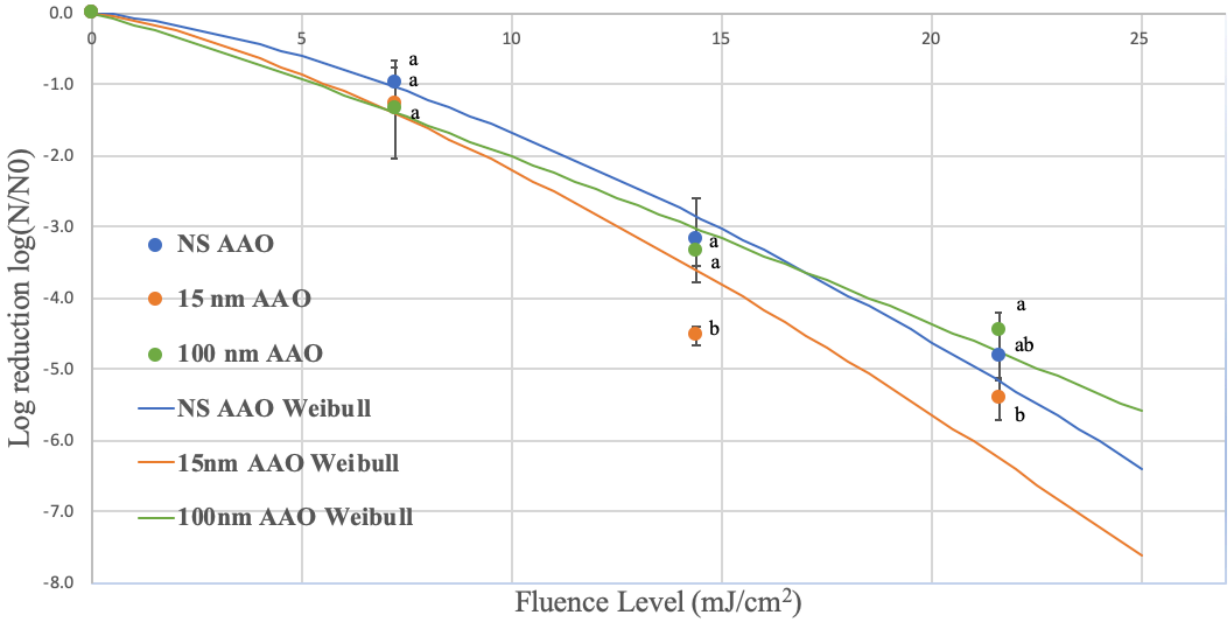

Figure 3. 4. Inactivation of *S. aureus* on solid substrates by exposure to continuous 405 nm LEDs of an irradiance of approximately 0.5 mW/cm^2. Substrates include anodic aluminum oxide with different nanotopograohy: nanosmooth (NS AAO), small nanopore (15nm AAO), large nanopore (100nm AAO) *. * Values followed by the same letters within the same treatment level are not significantly different ($p>0.05$).

Table 3. 4. Weibull model parameters for the 405 nm LED inactivation kinetics of *S. aureus* on anodic aluminum oxide (AAO) substrates. Values represent means ± standard deviations from three replicates.

Solid Substrates	Scale Parameter, α	Shape Parameter, β	R^2
NS AAO	0.06±0.03	1.46±0.22	0.99
15nm AAO	0.10±0.01	1.36±0.06	0.94
100nm AAO	0.16±0.34	1.11±052	0.98

Among the small nanopore, large nanopore, and nanosmooth AAO surfaces, *L. monocytogenes* and *S. aureus* had significantly higher rate of reduction on 15nm pore surfaces, for the entire time span of the treatment. *E. coli* displayed a slightly different trend, with bacteria on the nanosmooth surface being the most susceptible within the treatment span. However, no statistically significant difference in log reduction was observed at any cumulative dose ($p<0.05$) except at 64.8 J/cm^2 fluence level (36h exposure, $p>0.05$). For treatment on large nanopore surfaces (100nm), f *E. coli*, *L. monocytogenes*, and *S. aureus* experienced significantly lower rate of reduction at all fluence levels of blue light ($p>0.05$).

3.4.3 Effect of physical properties of substrates on microbial inactivation

Table 3.4 shows the surface roughness parameters of inert solid substrate including stainless steel (SS), high density polyethylene (LDPE), low density polyethylene (LDPE), borosilicate glass (glass), anodic aluminum oxide (AAO) with modified nanopores: nanosmooth (NS AAO), small pore (15nm AAO), large pore (100nm AAO). S_a and S_q values of HDPE showed the highest values (1.31 and 13.59 μm), followed by SS (1.04 and 11.27 μm), 15nm AAO (0.84 and 9.61 μm), 100nm AAO (0.76 and 9.91 μm), NS AAO (0.60 and 8.78 μm), LDPE (0.21 and 4.72 μm), and glass (0.0205 and 0.457 μm). The roughness parameters differed significantly among materials ($p<0.05$).

Contact angles of the solid substrate surfaces are presented in Table 3.5. All water contact angles measured were smaller than 90°, and decreased in the following order: HDPE (89.56°) > LDPE (87.63°) > 100nm AAO (59.16°) > Glass (57.74°) > NS AAO (48.83°) > 15nm AAO (44.58°) > SS (31.02°). Significant differences in water contact angles were observed among materials ($p<0.05$).

Table 3. 5. Surface roughness parameters of solid substrates. Substrates include stainless steel (SS), high density polyethylene (LDPE), low density polyethylene (LDPE), borosilicate glass (Glass), anodic aluminum oxide (AAO) with modified nanopores: nanosmooth (NS AAO), small pore (15nm AAO), large pore (100nm AAO). * Data represent means ± standard deviations from three replicates. Values followed by the same letters within columns are not significantly different ($p>0.05$).

Solid Substrates	Surface roughness parameters* (μm)	
	S_a	S_q
SS	1.04±0.09 *b*	11.27±0.50 *ab*
HDPE	1.31±0.07 *a*	13.59±1.04 *a*
LDPE	0.21±0.15 *e*	4.72±0.916 *c*
Glass	0.0205±0.0006 *f*	0.457±0.084 *d*
NS AAO	0.60±0.06 *d*	8.78±1.78 *b*
15nm AAO	0.84±0.08 *c*	9.61±1.74 *b*
100nm AAO	0.76±0.06 *cd*	9.91±0.55 *b*

Table 3. 6. Water contact angle analysis of solid substrates. Substrates include stainless steel (SS), high density polyethylene (LDPE), low density polyethylene (LDPE), borosilicate glass (glass), anodic aluminum oxide (AAO) with modified nanopores: nanosmooth (NS AAO), small pore (15nm AAO), large pore (100nm AAO) *. *Data represent means ± standard deviations from three replicates. Values followed by the same letters within columns are not significantly different ($p>0.05$).

Solid Substrates	Water contact angle* (°)

SS	31.02±6.59 *d*
HDPE	89.56±2.93 *a*
LDPE	87.63±4.34 *a*
Glass	57.74±3.88 *b*
NS AAO	48.83±4.00 *bc*
15nm AAO	44.58±3.83 *c*
100nm AAO	59.16±3.02 *b*

3.5 Discussion

This data demonstrates that 405 nm LED treatment has a significant bactericidal effect on several foodborne pathogens. The results show that the most susceptible bacterium in liquid suspension was *S. aureus*, which was inactivated by 5.7-$\log_{10}$ CFU/mL at a cumulative dose of 86.4 J/cm^2 (48h), much higher than the log reduction of the most resistant bacterium *E. coli* at the same dose. At a cumulative dose of 86.4 J/cm^2 (48h exposure), *S*. Typhimurium was inactivated by 1.7-$\log_{10}$ CFU/mL, *L. monocytogenes* by 2.6-$\log_{10}$ CFU/mL, and *P. aeruginosa* by 5.0-$\log_{10}$ CFU/mL, respectively. The inactivation curves shown in Fig 3.1 are consistent with those obtained in earlier studies (Murdoch LE, 2012) (Maclean M. , MacGregor, Anderson, & Woolsey, 2008). The results from liquid suspension experiments in the current study show that gram-positive bacteria require lower dosage of 405 nm LED light for inactivation than gram-negative bacteria, which is also in agreement with previous studies (Murdoch LE, 2012) (Maclean M. , MacGregor, Anderson, & Woolsey, 2009). An exception is *P. aeruginosa*, which was found highly sensitive to antimicrobial blue light, likely due to the production of coproporphyrin III and/or uroporphyrin III (Amin, Bhayana, Hamblin, & Dai, 2016). Visible light inactivation has been credited to the photostimulation of endogenous intracellular porphyrins by visible light in the wavelength range of 200 nm to 460 nm and, more specifically, 400 nm to 420 nm in for optimal inactivation (Ganz, et al., 2005). Stimulation of these porphyrins leads to the production of reactive species, predominantly singlet delta oxygen ($^1O_2$), which is a well-recognized trigger of cell death (Hamblin & Hasan, 2004). A study done by Nitzan *et al* demonstrated that the predominant porphyrin produced in both *S. aureus* and *Staphylococcus epidermidis* was coproporphyrin, whereas there was no predominant porphyrin produced in the gram-negative *E. coli*, *Acinetobacter*,

and *Aeromonas* strains. The amount of coproporphyrin produced by the staphylococcal strains was two to three times higher than in the gram-negative strains (Nitzan, Salmon-Divon, Shporen, & Malik, 2004). This agrees with the present results (Fig.3.1), where *S. aureus* was observed to be far more susceptible to 405 nm LEDs than *E. coli*.

When spread onto solid substrates, *L. monocytogenes* proved to be more readily inactivated compared to *E. coli*, with near complete inactivation achieved after a cumulative dose above 21.6 J/cm^2 (12h exposure). On the other hand, at the same a cumulative dose of 86.4 J/cm^2 (48h exposure), *E. coli* suspended on solid substrates showed far higher reduction rate compared to that the reduction in liquid suspension. This is possibly due to differences in the experimental arrangements and exposure conditions. Under the surface test conditions, uniform exposure of a spot of isolated bacterial inoculum was achieved, whereas for the liquid suspension tests, light irradiance may have been partially blocked by the corners of the rectangularly shaped chamber, therefore shielding bacteria from the antimicrobial light.

To understand the possible correlation between physical properties of material surfaces and the inactivation kinetics, surface roughness parameters and water contact angles were measured. The correlation between roughness values of material surfaces and bactericidal effect seems to be inconsistent in literature. Several previous researchers have reported that surfaces with lower roughness values tend to be more hygienic (Bower, McGuire, & Daeschel, 1996) (Faille, 2000) while an unclear relationship exists between roughness and adhesion or removal of microorganisms (Park & Kang, 2017) (Barnes, Lo, Adams, & Chamberlain, 1999). In this study, no strong correlation between surface roughness and inactivation of bacterial pathogens was observed. The highest inactivation of *E. coli* and *L. monocytogenes* was observed on SS and small pore AAO (15 nm) surfaces respectively, while the lowest surface roughness parameter was measured on glass surface. This is possibly because hydrophobicity of surfaces also influenced the distribution and subsequent inactivation of bacterial pathogens on solid materials. Surfaces with greater than 65° water contact angle are considered hydrophobic (Vogler, 1998); HDPE and LDPE surfaces used in this study were found to be hydrophobic because their contact angles were greater than 65°. This property led to different distributions

of bacterial aggregations on surfaces, so that dense stacking structures of cells developed and the possibility of shading effect increased. The inoculum on hydrophilic SS surface can spread over a largerer area compared to that on hydrophobic HDPE surface, increasing the possibility of a uniform light exposure. This is further corroborated by the inactivation results: the highest inactivation of *E. coli* and *L. monocytogenes* were observed on SS and 15nm AAO surfaces, which are the two most hydrophilic surfaces used in this study; the lowest inactivation of *E. coli* and *L. monocytogenes* were found on near-hydrophobic 100nm AAO and hydrophobic LDPE surfaces.

Surface modification has been reported as an emerging strategy for preventing biofilm formation on abiotic surfaces. Previous studies have demonstrated that bacterial attachment and subsequent biofilm formation are significantly impacted by surface nanotopography (Feng G. , et al., 2014) (Feng G. , et al., 2015). Surfaces with topographic features of dimensions much smaller than microbial cells, in the submicrometric or nanometric range, have been reported to inhibit attachment by reducing the contact area between bacteria cells and the surface. Additionally, surface nanotopography can create energetic situations unfavorable for bacterial attachment, and induce repulsive surface-bacteria interaction forces that impair attachment and subsequent biofilm formation (Feng G. , et al., 2015). Specifically, nanoporous surfaces with surface diameters of 15 and 25 nm were able to effectively minimize attachment by *E. coli* spp. And *Listeria* spp. (Feng G. , et al., 2014). However, effect of surface nanotopography on subsequent inactivation of bacterial pathogens remain unknown. The results of the current study demonstrate that the modification of nanoporous topography achieved an additive or enhancing effect in controlling L. monocytogenes and *S. aureus* on solid surfaces with 405 nm LED treatment (Fig. 3.3). Small nanopore (15nm) AAO showed significantly higher inactivation rate at all light doses compared to nanosmooth and large nanopore surfaces. This finding is extremely meaningful from a practical perspective, because it can be used to design hurdle systems with antifouling surfaces and blue light disinfection applications for food processing, as well as dentistry or biomedical application.

3.6 Conclusions

This study demonstrates that 405 nm LEDs have great potential for antimicrobial treatments in the food industry, but disinfection success depends on bacterial species, substrate, and environmental conditions. Bactericidal effect was demonstrated quantitatively both in liquid suspension and on exposed solid surfaces. The light treatment of bacterial pathogens suspended on modified anodic aluminum oxide surfaces provides important insight on the effect of surface nanotopography on the inactivation kinetics of bacterial pathogens, which is particularly significant for practical applications in the food and healthcare industries, where cross-contamination from environmental contact surfaces and equipment is a problem. The non-toxicity of 405 nm light and the nonrequirement for photosensitizing agents provide this antimicrobial method with unique benefits that could support its further development as a potential alternative to UV light-based systems. Further work to assess the treatment potential of 405 nm light on the inactivation of more diverse types of bacteria on actual food product, as well as on bacterial biofilms, will be important to fully assess the potential of this inactivation technology for applications in the food and healthcare industries.

3.7 Acknowledgements

This work made use of the Keyence VK-X260 Laser-Scanning Profilometer in the Cornell Center for Materials Research (CCMR) Shared Facilities which are supported through the NSF MRSEC program (**DMR-1719875**). The authors would like to thank Vital Vio for providing the LED unit used for the treatments.

3.8 References

Abdul Karim Shah, N., Shamsudin, R., Abdul Rahman, R., & Adzahan, N. (2016). Fruit Juice Production Using Ultraviolet Pasteurization: A Review. *Beverages*, 3-22.

Akgün, M. P., & Ünlütürk, S. (2017). Effects of ultraviolet light emitting diodes (LEDs) on microbial and enzyme inactivation of apple juice. *Int. J. Food Microbiol.* , 65-74.

Amin, R., Bhayana, B., Hamblin, M., & Dai, T. (2016). Antimicrobial blue light inactivation of Pseudomonas aeruginosa by photo-excitation of endogenous porphyrins: In vitro and in vivo studies. *Lasers in Surgery and Medicine*, 562-568.

Bánáti, D. (2014). European perspectives of food safety. *Journal of the Science of Food and Agriculture*, 1941-1946.

Barnes, L.-M., Lo, M., Adams, M., & Chamberlain, A. (1999). Effect of milk proteins on adhesion of bacteria to stainless steel surfaces. *Applied and Environmental Microbiology*, 4543-4548.

Bhavya, M., & Hebbar, U. (2018). Efficacy of blue LED in microbial inactivation: Effect of photosensitization and process parameters. *International Journal of Food Microbiology*, 296-304.

Bintsis, T., Litopoulou-Tzanetaki, E., & Robinson, R. (2000). Existing and potential applications of ultraviolet light in the food industry - a critical review. . *Journal of the Science of Food and Agriculture*, 637-645.

Bjerkan, G., Witso, E., & Bergh, K. (2009). Sonication is superior to scraping for retrieval of bacteria in biofilm on titanium and steel surfaces in vitro. *Acta Orthop.*, 245-250.

Bower, C., McGuire, J., & Daeschel, M. (1996). The adhesion and detachment of bacteria and spores on food-contact surfaces. *Trends in Food Science & Technology*, 152-157.

Branas, C., Azcondo, F., & Alonso, J. (2013). Solid-state lighting: a system. *Industrial Electronics Magazine*, 6-14.

Chatterley, C., & Linden, K. (2010). Demonstration and evaluation of germicidal UV-LEDs for point-of-use water disinfection. . *J. Water Health* , 479–486 .

Chen, C.-J., Yao, J., Zhu, W., Chao, J.-H., Shang, A., Lee, Y.-G., & Yin, S. (2019). Ultrahigh light extraction efficiency light emitting diodes by harnessing asymmetric obtuse angle microstructured surfaces. *Optik*, 400-407.

Chen, C.-J., Yao, J., Zhu, W., Chao, J.-H., Shang, A., Lee, Y.-G., & Yin, S. (2019). Ultrahigh light extraction efficiency light emitting diodes by harnessing asymmetric obtuse angle microstructured surfaces. *Optik*, 400-407.

Cheng, Y., & Moraru, C. I. (2018). Long-range interactions keep bacterial cells from liquid-solid interfaces: Evidence of a bacteria exclusion zone near Nafion surfaces and possible implications for bacterial attachment. . *Colloids Surfaces B Biointerfaces* , 16-24.

Chmielewski, R. a., & Frank, J. F. (2003). Biofilm Formation and Control in Food Processing Facilities. . *Compr. Rev. Food Sci. Food Saf.*, 22-32.

Choudhary, R., & Bandla, S. (2012). Ultraviolet Pasteurization for Food Industry. *International Journal of Food Science and Nutrition Engineering*, 12-15.

Clancy, S. (2014). *DNA Damage & Repair: Mechanisms for Maintaining DNA Integrity*. Retrieved from Scitable by Nature Education: https://www.nature.com/scitable/topicpage/dna-damage-repair-mechanisms-for-maintaining-dna-344

D. L. Luthria, e. a. (2006). Content of total phenolics and phenolic acids in tomato (Lycopersicon esculentum Mill.) fruits as influenced by cultivar and solar UV radiation. *Journal of Food Composition and Analysis*, 771-777.

Dai T, G. A. (2013). Blue light rescues mice from potentially fatal Pseudomonas aeruginosa burn infection: efficacy, safety, and mechanism of action. *Antimicrobial Agents and Chemotherapy*, 1238–1245.

Dai, T., Gupta, A., Murray, C., Vrahas, M., Tegos, G., & Hamblin, M. (2012). Blue light for infectious diseases: Propionibacterium acnes, Helicobacter pylori, and beyond? *Drug resistance updates : reviews and commentaries in antimicrobial and anticancer chemotherapy*, 223-236.

Das, J. R., Bhakoo, M., Jones, M. V., & Gilbert, P. (1998). Changes in the biocide susceptibility of Staphylococcus epidermidis and Escherichia coli cells associated with rapid attachment to plastic surfaces. . *J. Appl. Microbiol.* , 852-858.

Donlan, R., & Costerton, J. (2002). Biofilms: Survival Mechanisms of Clinically Relevant Microorganisms. *Clinical Microbiology Review*, 167-193.

D'Souza, C., Yuk, H., Khoo, G. H., & Zhou, W. (2015). Application of Light-Emitting Diodes in Food Production, Postharvest Preservation, and Microbiological Food Safety. *COMPREHENSIVE REVIEWS IN FOOD SCIENCE AND FOOD SAFETY*, 719-740.

Eischeid, A., & Linden, K. (2011). Molecular indication of protein damage in adenoviruses after UV disinfection. *Applied Environmental Microbiology*, 1145-1147.

Enwemeka, C. W. (2009). Blue 470-nm light kills methicillin-resistant Staphylococcus aureus (MRSA) in vitro. *Photomedicine and Laser Surgery*, 221–226.

Faille, C. e. (2000). Influence of physicochemical properties on the hygienic status of stainless steel with various finishes. *Biofouling*, 261-274.

Felix Vajdos, ’. C., Fee, ’. L., Grimsley, ’. A., & Gray’, T. (1995). How to measure and predict the molar absorption coefficient of a protein. *Prorein Science* .

Feng, G., Cheng, Y., Wang, S.-y., Borca-Tasciuc, D. A., Worobo, R. W., & Moraru, C. (2015). Bacterial attachment and biofilm formation on surfaces are reduced by small-diameter nanoscale pores: how small is small enough? *npj Biofilms and Microbiomes*.

Feng, G., Cheng, Y., Wang, S.-Y., Hsu, L. C., Feliz, Y., Borca-Tasciuc, D. A., . . . Moraru, C. (2014). Alumina surfaces with nanoscale topography reduce attachment and biofilm formation by Escherichia coli and Listeria spp. *Biofouling: The Journal of Bioadhesion and Biofilm Research*, 1253-1268 .

Freitag, N., Port, G., & Miner, M. (2009). Listeria monocytogenes—from saprophyte to intracellular pathogen. *Nature Reviews Microbiology*, 623-628.

Ganz, R. A., Viveiros, Ahmad, Ahmadi, Khalil, Tolkoff, . . . Hamblin. (2005). Helicobacter pylori in patients can be killed by visible light. . *Lasers in Surgery and Medicine*, 260-265.

Gayán, E., Condón, S., & Álvarez, I. (2014). Biological Aspects in Food Preservation by Ultraviolet Light: a Review. *Food and Bioprocess Technology*, 1-20.

Ghate, V., Siang Ng, K., Zhou, W., Yang, H., Hoon Khoo, G., Yoon, W. B., & Yuk, H.-G. (2013). Antibacterial effect of light emitting diodes of visible wavelengths on selected foodborne pathogens at different illumination temperatures. *International journal of food microbiology*, 399-406.

Giuseppina, P., Sonia, B., Antonio, C., Lorenzo, M., Andrea, C., Ilaria, B., . . . Giorgio, G. (2019). Unraveling the Role of Red:Blue LED Lights on Resource Use Efficiency and Nutritional Properties of Indoor Grown Sweet Basil. *Frontiers in Plant Science* , 305.

Guffey, J. W. (2006). In vitro bactericidal effects of 405-nm and 470-nm blue light. . *Photomedicine and Laser Surgery*, 684–688.

Gupta, S. D., & Jatothu, B. (2013). Fundamentals and applications of light-emitting diodes (LEDs). *Plant Biotechnol Reports*, 211-220.

Hamblin, M. R., & Hasan, T. (2004). Photodynamic therapy: a new antimicrobial approach to infectious disease? *Photochemical & Photobiological Sciences*, 436-450.

Harris, G. D., Dean Adams, V., Sorensen, D. L., & Curtis, M. S. (1987). ULTRAVIOLET INACTIVATION OF SELECTED BACTERIA AND VIRUSES WITH PHOTOREACTIVATION OF THE BACTERIA. *Wat. Res* .

Held, G. (2009). Chapter 1: Introduction to LEDs. In: Introduction to Light Emitting Diode Technology and Applications. *Taylor & Francis Group, LLC*.

Hu, J., & Quek, P. (2008). Effects of UV radiation on photolyase and implications with regards to photoreactivation following low-and medium-pressure UV disinfection. . *Applied Environmental Microbiology*, 327-328.

Khan, M. S. (2005). III-nitride UV devices. *Janapense Journal of Applied Physics*, 7191-7206.

Kim, D., & Dong-hyun, K. (2018). Elevated Inactivation Efficacy of a Pulsed UVC Light-Emitting Diode System for Foodborne Pathogens on Selective Media and Food Surfaces. . *Food Microbiol.* , 1-14.

Kim, D., Kim, S., & Kang, D. (2017). Bactericidal effect of 266 to 279nm wavelength UVC-LEDs for inactivation of Gram positive and Gram negative foodborne pathogenic bacteria and yeasts. *Food research international*, 280-287.

Kim, S.-J., Kim, D.-K., & Kang, D.-H. (2015). Using UVC Light-Emitting Diodes at Wavelengths of 266 to 279 Nanometers To Inactivate Foodborne Pathogens and Pasteurize Sliced Cheese. *Applied and Environmental Microbiology*, 11-17.

Kondo, S., Tomiyama, H., Rodyoung, A., Okawa, K., Ohara, H., Sugaya, S., . . . Hirai, N. (2014). Abscisic acid metabolism and anthocyanin synthesis in grape skin are affected by light emitting diode (LED) irradiation at night. *Journal of plant physiology* , 823-829.

Koutchma, T., Keller, S., Chirtel, S., & Parisi, B. (2004). Ultraviolet disinfection of juice products in laminar and turbulent flow reactors. *Innov. Food Sci. Emerg. Technol.* , 179-189.

Li, G. W. (2017). Comparison of UV-LED and low pressure UV for water disinfection: Photoreactivation and dark repair of Escherichia coli. *Water Research*, 134-143.

Li, X., & Farid, M. (2016). A review on recent development in non-conventional food sterilization technologies. *Journal of Food Engineering*, 33-45.

Lobo, V. e. (2010). Free radicals, antioxidants and functional foods: Impact on human health. *Pharmacognosy reviews*, 118-126.

Maclean, M., MacGregor, S. J., Anderson, J. G., & Woolsey, G. (2008). High-intensity narrow-spectrum ligh inactivation and wavelength sensitivity of Staphylococcus aureus. *FEMS Microbiology Letters*, 227-232.

Maclean, M., MacGregor, S. J., Anderson, J. G., & Woolsey, G. (2009). Inactivation of Bacterial Pathogens following Exposure to Light from a 405-Nanometer Light-Emitting Diode Array. *APPLIED AND ENVIRONMENTAL MICROBIOLOGY*, 1932-1937.

Maclean, M., MacGregor, S., A. J., & Woolsey, G. (2008). The role of oxygen in the visible-light inactivation of Staphylococcus aureus . *Journal of Photochemistry and Photobiology B*, 180-184.

Minamata Convention on Mercury. . (2019, March 28). Retrieved from http://www.mercuryconvention.org/.

Moraru, C. I. (2009). Reduction of Listeria on Ready-to-Eat Sausages after Exposure to a Combination of Pulsed Light and Nisin. *AND*, 347-353.

Murdoch LE, M. M. (2012). Bactericidal effects of 405 nm light exposure demonstrated by inactivation of Escherichia, Salmonella, Shigella, Listeria, and Mycobacterium species in liquid suspensions and on exposed surfaces. *Scientific World Journal*, 1-14.

Nigro, F., & Ippolito, A. (2016). UV-C light to reduce decay and improve quality of stored fruit and vegetables: a short review. *Acta Horticulturae*, 293-298.

Nitzan, Y. M., Salmon-Divon, Shporen, E., & Malik, Z. (2004). ALA induced photodynamic effects on gram positive and negative bacteria. *Photochemical & Photobiological Sciences*, 430-435.

Nyangaresi, P. e. (2018). Effects of single and combined UV-LEDs on inactivation and subsequent reactivation of E . coli in water disinfection. *Water Research*, 331-341.

Pace, C. V. (1995). How to measure and predict the molar absorption coefficient of a protein. *Protein Science*, 2411-2423.

Park, S., & Kang, D. (2017). Influence of surface properties of produce and food contact surfaces on the efficacy of chlorine dioxide gas for the inactivation of foodborne pathogens. *Food Control*, 88-95.

Peleg, M., & Cole, M. B. (1998). Reinterpretation of microbial survival curves. . *Crit. Rev. Food Sci. Nutr.*, 353-380.

Proulx, J., Hsu, L., Miller, B., Sullivan, G., Paradis, K., & Moraru, C. (2015). Pulsed-light inactivation of pathogenic and spoilage bacteria on cheese surface. *Journal of Dairy Science*, 5890-5898.

Radetsky, L. C. (2018). *LED and HID Horticultural.* Troy: Lighting Research Center, Rensselaer Polytechnic Institute.

Rattanakul, S., & Oguma, K. (2018). Inactivation kinetics and efficiencies of UV-LEDs against Pseudomonas aeruginosa, Legionella pneumophila, and surrogate microorganisms. . *Water Research*, 31-37.

Richardson, C. (2008). Driving high-power LEDs in series-parallel. *National Semiconductor*, 45-49.

Sauer, A., & Moraru, C. I. (2009). Inactivation of Escherichia coli ATCC 25922 and Escherichia coli O157 : H7 in Apple Juice and Apple Cider , Using Pulsed Light Treatment. . *Journal of Food Protection*.

Shin, J., Kim, S., Kim, D., & Kang, D. (2016). Fundamental Characteristics of Deep-UV Light-Emitting Diodes and Their Application To Control Foodborne Pathogens. . *Appl. Environ. Microbiol.*, 2-10.

Sommers, C. H., Cooke, P. H., Fan, X., & Sites, J. E. (2009). Ultraviolet light (254 nm) inactivation of Listeria monocytogenes on frankfurters that contain potassium lactate and sodium diacetate. *J. Food Sci.* , 114-119.

Stoscheck, C. M. (1990). 50 GENERAL MEHODS FOR HANDLING PROTEINS AND ENZYMES. In *Quantitation of Protein.* .

SUDHIR K. SASTRY, A. K. (2000). Ultraviolet Light. In *Kinetics of Microbial Inactivation for Alternative Food Processing Technologies* (pp. 90-93). Journal of Food Science.

Takayoshi, T. e. (2017). Deep-ultraviolet light-emitting diodes with external quantum efficiency higher than 20% at 275 nm achieved by improving light-extraction efficiency. . *Appl. Phys. Express* .

Uesugi, A., Woodling, S., & Moraru, C. (2007). Inactivation kinetics and Factors of Variability in the Pulsed Light Treatment of Listeria innocua Cells. *Journal of Food Protection*, 2518-2525.

Venditti, T., & D'hallewin, G. (2014). Use of ultraviolet radiation to increase the health-promoting properties of fruits and vegetables. *Stewart Postharvest Review*, 10-13.

Vogler, E. (1998). Structure and reactivity of water at biomaterial surfaces. *Advances in Colloid and Interface Science*, 69-117.

Wang, Y., Wang, Y., Wang, Y., Murray, C., Hamblin, M., Hooper, D., & Dai, T. (2017). Antimicrobial blue light inactivation of pathogenic microbes: State of the art. . *Drug Resistance Updates*, 1-22.

Wong, H.-C., Chung, Y.-C., & Yu, J.-A. (2002). Attachment and inactivation of Vibrio parahaemolyticus on stainless steel and glass surface. . *Food Microbiol.* , 341-350.

Woodling, S. E., & Moraru, C. I. (2005). Influence of Surface Topography on the Effectiveness of Pulsed Light Treatment for the Inactivation of Listeria innocua on Stainless-steel Surfaces. . *J Food Sci* , 345-351.

World Health Organisation (WHO) Initiative for vaccine research. (2019). Retrieved from https://www.who.int/immunization/research/en/

Young, A. R. (2006). Acute effects of UVR on human eyes and skin. *Progress in Biophysics & Molecular Biology*, 80-85.